Coherent scattering of pulsatile flow

Nemati, Mahsa

DOI
10.4233/uuid:518c6610-8614-4863-80a0-a888f40c3165

Publication date
2016

Document Version
Final published version

Citation (APA)
Nemati, M. (2016). *Coherent scattering of pulsatile flow*. [Dissertation (TU Delft), Delft University of Technology]. https://doi.org/10.4233/uuid:518c6610-8614-4863-80a0-a888f40c3165

Coherent Scattering of Pulsatile Flow

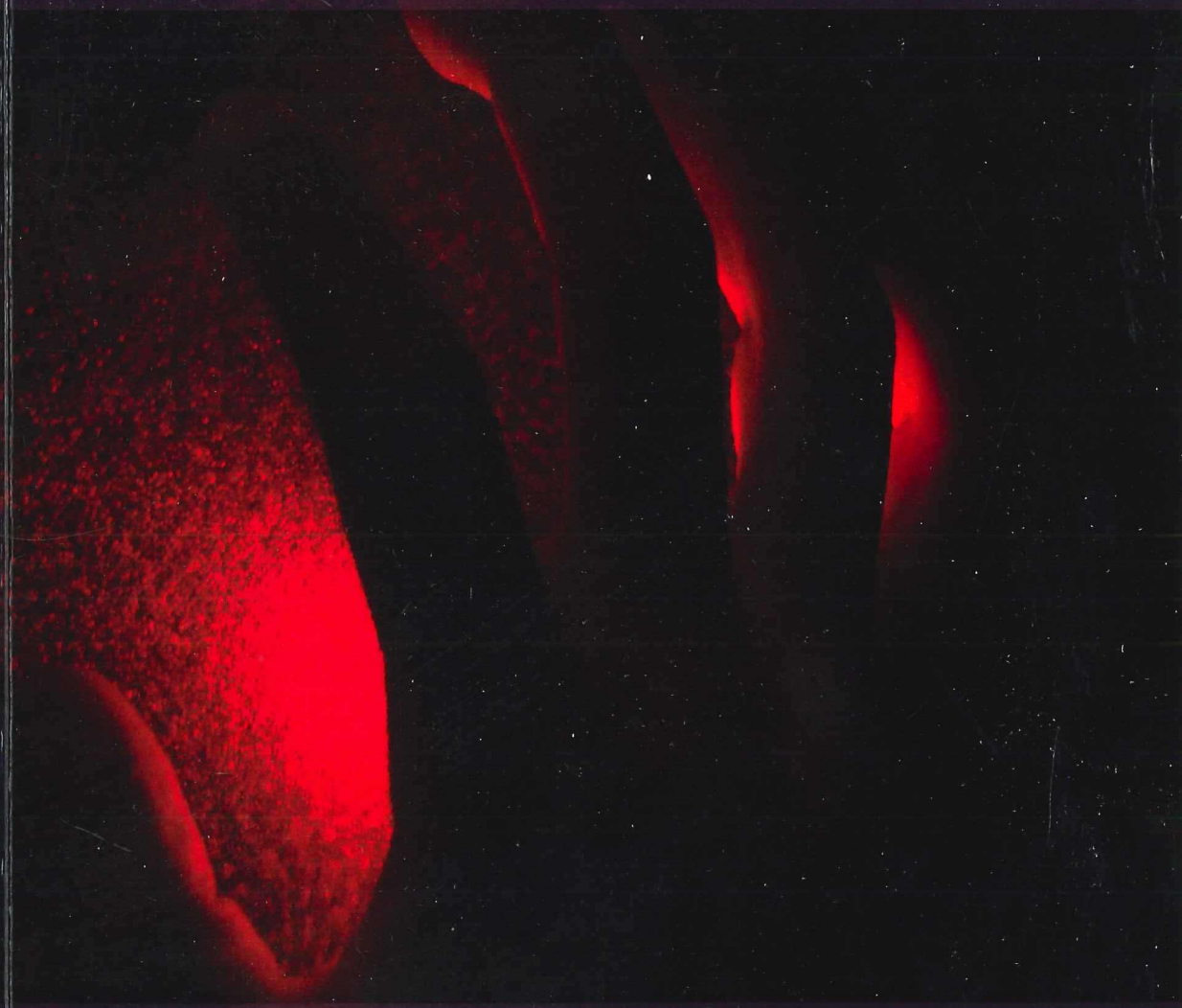

Mahsa Nemati

Propositions

accompanying the Ph.D. thesis:

Coherent scattering of pulsatile flow

To be defended on Thursday, June 16th 2016 at 15:00 in Delft by

Mahsa Nemati

1. Blood flow measurements can be performed in the presence of motion artifacts.
2. Laser speckle is a sensible tool for monitoring dynamic changes in flow, however it is unable to distinguish its direction.
3. The spatial distribution of a speckle pattern can be studied using a fractal dimension, where the dimension changes can be directly related to the dynamic behavior of the sample.
4. Different analysis methods when applied to speckle patterns reveal complementary characteristics of the studied sample.
5. The properties of a complex system are better understood if we start with a simple benchmark.
6. Systematic characterization experiments are time consuming, but provides much better insight.
7. A new research result can seem like magic till one masters it, after which it becomes mundane.
8. The course of one's life is out of one's control when society regulates people based on outdated beliefs.
9. Bureaucratic regulation can in many cases go against common sense and logic.
10. Change is an inherent feature of living organisms.

These propositions are regarded as opposable and defendable, and as such have been approved by the promotor prof. dr. H. P. Urbach.

Stellingen

behorende bij het proefschrift:

Coherente verstrooiing van pulserende stromen

te verdeligen op Donderdag 16 Juni 2016 om 15:00 te Delft door

Mahsa Nemati

1. Bloedstromingsmetingen kunnen worden uitgevoerd de aanwezigheid van artefacten ten gevolge van bewegingen.
2. Laser speckle is een zinnig gereedschap voor het waarnemen van dynamische stromingsveranderingen, echter het is niet in staat richting te onderscheiden.
3. De ruimtelijke verdeling van een specklepatroon kan worden bestudeerd door gebruik te maken van de fractale dimensie, waar verandering direct gerelateerd is aan het dynamisch gedrag van het monster.
4. Diverse analyse methoden toegepast op specklepatronen, onthullen complementaire eigenschappen van het bestudeerde monster.
5. De eigenschappen van een complex system zijn beter inzichtelijk te maken door gebruik te maken van een eenvoudig referentie systeem.
6. Systematisch experimenteel werk is tijdrovend maar geeft een veel beter inzicht.
7. Een nieuwe onderzoeksresultaat kan ongelofelijk lijken, maar als het verklaard is wordt het alledaags.
8. De loop van het leven is niet meer in eigen hand indien de gemeenschap voorschriften oplegt gebaseerd op verouderde opvattingen.
9. Bureaucratische regelgeving druist in veel gevallen in tegen gezond verstand en logica.
10. Verandering is een inherente eigenschap van levende organismen.

Deze stellingen worden opponeerbaar en verdedigbaar geacht en zijn als zodanig goedgekeurd door de promotor prof. dr. H. P. Urbach.

COHERENT SCATTERING OF PULSATILE FLOW

Proefschrift

ter verkrijging van de graad van doctor
aan de Technische Universiteit Delft,
op gezag van de Rector Magnificus prof. ir. K.C.A.M. Luyben,
voorzitter van het College voor Promoties,
in het openbaar te verdedigen op donderdag 16 june 2016 om 15:00 uur

door

Mahsa NEMATI

Master of Science in Biomedical Engineering,
Delft University of Technology, Delft, The Netherlands,
geboren te Ahvaz, Iran.

The dissertation has been approved by the

promotor: Prof.dr. H.P. Urbach
copromotor: Dr.N. Bhattacharya

Composition of the doctoral committee:

Rector Magnificus,	voorzitter
Prof.dr. H.P. Urbach	Technische Universiteit Delft, promotor
Dr.N. Bhattacharya	Technische Universiteit Delft, copromotor

Independent members:

Prof. dr. ir. L.J. van Vliet	Technische Universiteit Delft
Prof.dr.ir. J.W.M. Bergmans	Technische Universiteit Eindhoven
Prof.dr. R.M. Aarts	Technische Universiteit Eindhoven
Prof.dr.ir. W.Steenbergen	Universiteit Twente
Prof.dr.ir. P. Kruit	Technische Universiteit Delft, reserve member

This work was supported by the IOP Photonic Devices programme of NL-Agency of the Dutch Ministry of Economic Affairs (Project number IPD 083359) and by Stichting voor Technise Wetenschappen (STW).

An electronic version of this dissertation is available at
http://repository.tudelft.nl/dissertations.

Contents

Summary

Modern society has an increasing demand for technologies for better diagnosis and treatment. This is driven by the growth of health awareness and a shift in population demographics to the aged. The concept of continuous health monitoring is one of the key factors towards healthier life style, improving the healthcare services and to provide a better monitoring of chronic diseases. A new market research has predicted a dramatic increase in the number of portable health monitoring devices which can be used for medical diagnostics or for health and wellness monitoring. Cardiovascular disease is one of the most prevalent diseases nowadays and this is why developing techniques to monitor vital signs are of great interest. However, there is still a potential need in the market to address the expensive healthcare equipment and worldwide inequality in access to it, through a cost efficient technology. In this regard, optics based solutions are seen to be a growing field which can influence the health care industry.

One of the well known and clinically established devices is the pulse oximeter. It is a non-invasive optical based method which measures the volumetric changes due to arterial expansion and contraction. By monitoring the amplitude variation, the instrument can measure the pulsation rate. The main working principle is due to light absorption. When a vessel expands due to the heart beat, the volume of the blood flow increases, eventually leading to a lower measured signal due to more absorption of light. By playing with different light absorption properties, two wavelength settings are capable of measuring the oxyhemoglobin level in the blood. However, these devices are only sensitive to periodic signals and therefore can not provide an indication of tissue blood flow. Additionally, these devices suffer from a lack of required precision and repeatability of signals when it comes to scenarios with motion artifacts. To have clinically reliable measurements, these devices require a steady environment and contact with the patient's body. To address the challenges of designing non-contact methods and signal attenuation due to motion artifacts, we have demonstrated another optical technique. Laser speckle imaging is a low cost method which can bring a new dimension to compliance and treatment, by monitoring the hemodynamic properties remotely. This method uses coherent properties of light to illuminate the sample and as the blood propagates the spatial distribution of light in tissue changes, which can be then monitored. This method was initially developed to measure blood flow in the retina. However, in this thesis we report several measurements, to address not only results from phantoms but also from different regions of the body such as finger nail or neck.

Further experiments using this technology are presented, which provide a broader range of applications and different configurations. These studies are a step forward towards the potential of using laser speckle techniques for assessing some of the common clinical situations.

This thesis reports the possibility of using laser speckle for monitoring pulsatile flow where it investigates its feasibility in case of motion artifacts. We have studied, designed and implemented different experimental flow and optical setups to study laser speckle dynamics. Laser speckle dynamics is based on measuring intensity fluctuation caused by temporal changes in speckle patterns. The principle is rather similar to the technique of laser Doppler, where there is a frequency shift from a moving scatterer which is used to monitor the changes in the sample. For laser speckle, the changes can be recorded directly using these interference patterns. These are however different techniques where the same theoretical principle of dynamic light scattering is applied. This has been originally studied for single scattering particles and was extended later on to highly scattering medium. Laser speckle has shown potential advantages over laser Doppler due to faster acquisition. In this approach a very high spatial and temporal resolution blood flow map can be obtained using single images, where the changes in flow can be quantified based on spatial blurring of them.

The thesis begins with a brief introduction to the light-tissue interaction along with different numerical modeling techniques which are commonly used to retrieve tissue optical properties. We address the theory of laser speckle and how they are created. Furthermore, different analysis methods for the speckle pattern data are described. Since speckle is random in nature, we first need to introduce the statistical tools. In this chapter, we focus on laser speckle contrast analysis, correlation and fractals which have been used in the rest of thesis as the main analytical tools.

The laser speckle imaging has a simple experimental setup yet a powerful technique. The setup mainly consists of a laser to illuminate the sample and generate the reflected speckle which are recorded through the imaging system. However, the study of flow dynamics is rather a complex problem. The complex behavior of the flow can be due to complexity in the geometry, or the fluid dependent properties itself. We showed that laser speckle imaging is able to measure the changes in flow which may arise due to various physiological/experimental conditions. In order to be able to compare and understand the influence of different parameters individually, a series of experiments using different experimental setups have been conducted. These experiments have been done to monitor the changes in a systematic way, so initially the measurements were done for steady flow and then pulsatile flow. For each experiment, the laser speckle patterns have been further processed to retrieve the required information. We also provide a description over different experimental components and phantoms with different geometries.

To extract maximum information from the flow dynamics, we introduced an alternative but complimentary method to study flow properties in chapter 4. Particle image velocimtery (PIV) is a gold standard technique when it comes to study flow dynamics. The novelty and great advantage of this technique are its high resolution flow velocity vector of the whole plane in the flow. By adapting the optics of the illuminating system and applying image-processing algorithms, we

reported the result for both PIV and laser speckle method. In this chapter, we report our measurements and data analysis for two different geometries of cylindrical and carotid artery based phantoms. The preliminary results demonstrated the efficacy of combining these two technique for simultaneous full-field imaging of flow dynamics.

To broaden the scope of thesis, we used the concept of fractals to study the changes in speckle data. Fractal is a quantitative tool for understanding the chaos and complex shapes in nature. Fractal analysis has been often used to characterize randomness in a series of data. There is a correlated randomness in the dynamics changes of speckle data that can be interpreted by fractals. We show that fractal dimension is able to reveal pulsation features in a highly scattered medium. We have reported a comparison analysis between laser speckle contrast and fractal dimension measured using differential box counting method. These measurements have been done for a uniform flow channel in a cylindrical phantom and also for a more complex flow through a patient-specific carotid artery phantom.

We have further reported a different speckle behavior through a layered structure containing static scatterers. For this reason, we have further investigated the concept of fractal dimension to study the so called 'speckled speckle' patterns. Fractal analysis has been used to characterize irregular time data series in non-linear systems. Therefore, we extended our analysis to study the non-linear effect detected in flow pulsation caused by the secondary reflection of speckle. We suggest that fractal dimension can give a better description of reality. A possible application of this is to use laser speckle to investigate a wide variety of pathological skeletal conditions for instance, by measuring the changes of flow dynamics inside a bone.

In the last part of the thesis, we study the effect of induced motion artifacts using laser speckle images. These results have shown for the first time the use of laser speckle against motion artifacts. We initiated the measurements to study the influence of motion induced artifacts using laser speckle contrast analysis. To further exploit these results, the measurements have been extended to a larger range of motion and we also reported a comparison between laser speckle contrast and correlation based analysis. By the end of this chapter, to show the possibility of having a more compact device development based on laser speckle, the feasibility of using only few pixels has been demonstrated.

In summary, this thesis has addressed experimentally, several of the challenges which are faced in case of developing a portable health monitoring device. Although work for this thesis has been carried out specifically for health care monitoring, the studied methods are not limited to biomedical applications and can be further applied to flow dynamics in different cases.

Samenvatting

In de moderne samenleving bestaat een toenemende vraag naar technologien voor een betere diagnose en behandeling. Dit wordt ingegeven door de groei van het gezondheidsbewustzijn en de toenemende vergrijzing. Het concept om gezondheid voortdurend te monitoren is n van de belangrijkste factoren voor een gezondere levensstijl, verbetering van de gezondheidszorg en een betere controle van chronische ziekten. Een nieuw marktonderzoek heeft een forse toename voorspeld van het aantal mobiele gezondheidtesters die kunnen worden toegepast voor medische diagnose of monitoring van gezondheid en welzijn. Hart en vaatziekten zijn wereldwijd volksziekte nummer n en daarom is het van groot belang om technieken te ontwikkelen die de vitale functies kunnen controleren. Er is ook behoefte aan meer betaalbare technologie om zo de wereldwijde ongelijkheid in de beschikbaarheid van dure gezondheidsapparatuur aan te pakken. In dit opzicht vormen oplossingen gebaseerd op fotometrie een toenemende veld voor ontwikkelingen in ten behoeve van de gezondheidszorg.

De Pulse-oximeter is een bekend en klinisch bewezen instrument. Het is een op fotometrie gebaseerde non-invasieve methode, waarmee volume veranderingen in de aders door uitzetting en contractie worden gemeten. Doordat het signaal in sterkte varieert met de vulling van de slagaders, kan het instrument berekenen wat de frequentie van de hartslag is. De werking is gebaseerd op het principe van lichtabsorptie. Bij uitzetting van een bloedvat door een hartslag wordt er meer bloed in het bloedvat gestuwd; daardoor neemt de lichtabsorptie toe en wordt er een lager signaal gemeten. Door het toepassen van verschillende absorptie-eigenschappen kan met twee golflengtes de hoeveelheid oxyhemoglobine in het bloed worden gemeten. Deze apparatuur is echter alleen gevoelig voor periodieke signalen en levert daardoor geen indicatie van weefseldoorbloeding. Bovendien heeft dit type apparatuur last van verminderde precisie en reproduceerbaarheid van signalen als gevolg artefacten die door beweging worden veroorzaakt. Voor klinisch betrouwbare metingen is dan ook een stabiele omgeving en contact met de patint vereist. Ten einde de uitdagingen aan te gaan een contactloze methode te ontwerpen en signaalverzwakking door beweging te vermijden, hebben we een alternatieve optische techniek gedemonstreerd.

Laser speckle imaging is een goedkope methode, die een nieuwe dimensie kan brengen in toepassing en behandeling bij op afstand monitoren van de hemodynamische eigenschappen. Bij deze methode wordt coherent licht toegepast om het lichaamsdeel te belichten ; tijdens het stromen van het bloed verandert de licht-

verdeling in het weefsel, wat vervolgens kan worden gemonitord. Deze methode werd oorspronkelijk ontwikkeld om de bloedstroom in het netvlies te meten. Echter, in dit proefschrift rapporteren wij verscheidene metingen waarbij niet alleen resultaten van fantomen, maar ook van lichaamsdelen zoals vinger, nagel of hals worden gebruikt. Er worden meerdere experimenten gepresenteerd waarbij van deze techniek gebruik is gemaakt, waarmee een breder scala van toepassingen en van verschillende configuraties wordt geboden. Deze studies zijn een stap voorwaarts voor de inzetbaarheid van laser speckle technieken in sommige gebruikelijke klinische situaties. In dit proefschrift wordt de mogelijkheid beschreven om 'laser speckle' toe te passen om pulserende stromen te monitoren. Het onderzoek gaat over de toepasbaarheid bij bewegingsartefacten. Er zijn verschillende experimentele stromen en optische opstellingen bestudeerd, ontworpen en gemplementeerd om dynamische eigenschappen van 'laser speckle' te bestuderen. De dynamische eigenschappen van 'laser speckle' worden bepaald door het meten van intensiteitsveranderingen te meten, die worden veroorzaakt door temporele fluctuaties in speckle patronen. Het principe is vergelijkbaar met de laser Doppler techniek, waarbij er een frequentieverschuiving plaatsvindt door een bewegende verstrooier die wordt gebruikt om de veranderingen in het specimen te meten. Voor 'laser speckle' kunnen deze veranderingen direct worden vastgelegd door gebruik te maken van deze inteferentiepatronen. Dit zijn echter verschillende technieken waarin dezelfde theoretische principes van dynamische lichtverstrooiing worden toegepast. Dit is oorspronkelijk onderzocht voor enkelvoudige deeltjes; later werd dit uitgebreid tot een sterk verstrooiend medium. 'Laser speckle' heeft potentile voordelen laten zien ten opzichte van de Laser Doppler methode, met name door de snellere data-acquisitie. Bij deze benadering kan een een bloedstroomkaart met zeer hoge ruimtelijke en temporele resolutie worden verkregen met behulp van afzonderlijke beelden, waarbij de veranderingen in de stroming kunnen worden gekwantificeerd op basis van ruimtelijke vervaging. Het proefschrift begint met een korte introductie van interactie tussen licht en weefsel tezamen met verschillende numerieke modelleringstechnieken, die gewoonlijk worden gebruikt voor het bepalen van de optische eigenschappen van weefsel. Vervolgens beschrijven we de theorie van 'laser speckle' en hoe dit fenomeen ontstaa. Daarna worden de verschillende analysemethoden voor de speckle patroon data beschreven. Aangezien speckle van origine willekeurig is, moeten we eerst de statistische methodes beschrijven. In dit hoofdstuk richten we ons op 'laser speckle' contrast-analyse, correlatie en fractals die zijn gebruikt in de rest van het proefschrift als belangrijkste analytische methodes. De opstelling die gebruikt is voor 'laser speckle' imaging is erg eenvoudig, omdat deze voornamelijk bestaat uit een laser voor het belichten van het specimen en het genereren van het gereflecteerde speckle patroon dat wordt opgenomen met een camera. De studie van stromingsdynamica is complex. Het complexe gedrag van de stroming kan worden veroorzaakt door de complexiteit van de geometrie of door de vloeistofspecifieke eigenschappenzelf. We hebben aangetoond dat met 'laser speckle' imaging de veranderingen in de stroming kunnen worden gemeten die kunnen ontstaan door verschillende fysiologische / experimentele omstandigheden. Om de invloed van de verschillende parameters te kunnen vergelijken en te kunnen begrijpen, is een serie experimenten uitgevoerd met een aantal ver-

schillende opstellingen. Deze experimenten zijn gedaan om op een systematische manier de veranderingen te monitoren. In eerste instantie voor een continue stroming en vervolgens voor een pulserende. Voor elk experiment zijn de laser speckle patronen verder verwerkt om de gevraagde informatie te verkrijgen. We bieden ook een beschrijving voor verschillende experimentele componenten en fantomen met verschillende geometrien. In hoofdstuk 4 introduceren we een alternatieve en complementaire methode om de eigenschappen van de stroming te bestuderen, teneinde zoveel mogelijk informatie uit de dynamische eigenschappen te verkrijgen. 'Particle image velocimetry' (PIV) is een gouden standaard techniek als het gaat om bestudering van de dynamische eigenschappen van stromingen. De vernieuwing en het grote voordeel van deze techniek is de hoge-resolutie stroomsnelheidsvector van het gehele vlak in de stroom. Door aanpassing van de optiek van het belichtingssysteem en het toepassen van beeldverwerkingsalgoritmes, beschrijven we het resultaat van zowel PIV als de 'laser speckle methode'. In dit hoofdstuk beschrijven we onze metingen en gegevensanalyse voor twee verschillende geometrien van cilindrische en op de halsslagader gebaseerde fantomen. De voorlopige resultaten demonstreren de mogelijkheid om deze twee technieken te combineren voor gelijktijdige full-field imaging van dynamische stromingseigenschappen. Om de reikwijdte van het proefschrift te verbreden, hebben we gebruik gemaakt van het begrip fractals om de veranderingen in speckle data te bestuderen. Fractals worden gebruikt voor het begrijpen van chaos en complexe vormen in de natuur. Fractale analyse wordt vaak gebruikt om de willekeur in een reeks van data te karakteriseren. Er is sprake van een gecorreleerde willekeur in de dynamische veranderingen van speckle gegevens die kunnen worden genterpreteerd door fractals. We tonen aan dat met behulp van fractale dimensie pulsatiemetingen in een zeer verstrooiend medium kunnen worden uitgevoerd. We rapporteren een vergelijkende analyse tussen laser speckle contrast en gemeten fractale dimensie met behulp van de 'differential box counting' methode. Deze metingen zijn gedaan voor een uniform stroomkanaal in een cilindrisch fantoom en ook voor een meer complexe stroming door een patintspecifiek halsslagader fantoom. Voorts hebben we een ander specklegedrag beschreven, veroorzaakt door een gelaagde structuur met statische verstrooiers. Mede hierom hebben we het begrip fractale dimensie verder onderzocht om de zogenaamde gespikkelde speckle patronen te bestuderen. Fractale analyse is gebruikt om onregelmatige tijdgegevensreeksen te karakteriseren in niet-lineaire systemen. Daarom hebben we onze analyse uitgebreid om het niet-lineaire effect te bestuderen dat kan worden waargenomen in stroompulsaties, ontstaan door secundaire reflectie van speckle. Wij stellen vast dat fractale dimensie een meer nauwkeurige weergave oplevert van de werkelijkheid. Een mogelijke toepassing hiervan is om 'laser speckle' te gebruiken voor het onderzoeken van een grote variatie van pathologische skeletcondities, bijvoorbeeld door het meten van de veranderingen in stromingsdynamica binnen een bot. In het laatste deel van het proefschrift, bestuderen we het effect van genduceerde bewegingsartefacten, met behulp van 'laser speckle' beelden. Deze resultaten toonden voor het eerst het gebruik van 'laser speckle' in aanwezigheid van bewegingsartefacten. We zijn de metingen gestart om de invloed van bewegingsartefacten te bestuderen door het gebruik van 'laser speckle' contrast-analyse. Om deze resultaten verder te

onderzoeken, zijn de metingen uitgebreid naar een groter bewegingsbereik en rapporteerden we ook een vergelijking tussen analyse van laser speckle contrast en op correlatie gebaseerde analyse. Aan het einde van dit hoofdstuk laten we zien dat het haalbaar is een compacter apparaat op basis van 'laser speckle' ontwikkelen, als gebruik wordt gemaakt van een beperkt aantal pixels. Samengevat zijn in dit proefschrift diverse uitdagingen waarmee men geconfronteerd wordt bij het ontwikkelen van mobiele gezondheidtesters, experimenteel behandeld. Alhoewel het proefschrift specifiek voor monitoring in de gezondheidszorg is uitgevoerd, beperken de bestudeerde methodes zich niet tot biomedische toepassingen; ze kunnen ook worden toegepast bij stroomdynamica in andere disciplines.

Chapter

1 Introduction

If you can't explain it simply, you don't understand it well enough.

Albert Einstein

Continuous monitoring of physiological signals has been a topic of increasing importance in modern society. An increasing demand for personal healthcare services, due to factors such as aging population, changes in lifestyle or the individual pursuit of health and wellness [1] creates a need for reliable, continuous and non-invasive devices for the measurement of physiological signals. In order to address this increasing demand for ambulatory monitoring and services surrounding it, technology has been leaning towards a new era of health monitoring devices. The usage of such devices can potentially reduce the costs associated with regular health assessment measurements performed by health professionals and reduce the stress associated with hospital visits, allowing the patient to remain connected to their home environment. The continuous monitoring of physiological signals is motivated by several factors, such as demographic changes (aging population), changes in lifestyle which reflect upon population health and an increased conscience and desire towards a healthier lifestyle. Regular monitoring devices can help people track their daily activities and improve their lifestyles. Within this target group the main demand is for monitoring vital signs such as blood flow, pressure, oxygenation and heart rate. Although such devices are currently used in regular clinical practice based on different techniques like angiography [2], ultrasound [3], magnetic resonance imaging [4] or laser Doppler imaging [5], it is challenging to apply these techniques in a non-controlled environment, where the individual follow its *normal* life.

One key challenge is the ability to create devices which can be used without direct clinical supervision while being comfortable, unnoticeable and with no side

effects for the user. Due to it's non-invasive nature, optical methods have been regarded as a promising approach towards this end. These techniques have been applied in medical settings for diagnostics and monitoring applications [6, 7]. A very common example of such a device is the pulse oximeter. Its working principle is based on the photoplethysmogram (PPG) which quantifies volumetric changes in blood flow [8]. The device illuminates the skin and measures the changes in light absorption at each cardiac cycle. These devices can be applied to different sites of the body using either reflection or transmission designs. However, despite the frequent use of these devices, they require very steady measuring conditions as the technique suffers from motion artifacts. The main measurement errors are due to sensor movement with respect to skin. Also repetitive motion induces sloshing of venous blood which can create a different pulsation compared to arterial blood. In addition, vasomotion or the vessel diameter variations due to movement lead to errors [9, 10].

In the framework of research the main focus is on developing a non-invasive method which monitors the behavior of cardiovascular system. The vital parameters which need to be quantified in diagnosis are revealed by measuring pulsation characteristics of flow. In this thesis, we target on the research challenges in developing a non-invasive, motion robust, portable device for blood flow sensing. For this purpose we explore the use of a laser speckle based solution.

1.1 Laser speckle for physiological signal measurements

Similar to laser Doppler imaging techniques, laser speckle can monitor microvascular blood flow or tissue perfusion [11]. However, laser speckle has the advantage of a simple and inexpensive setup which has shown promising results in biomedical applications [12]. The initial use of laser speckle was in imaging the blood flow in retina [13]. Its biomedical application has been further expanded for skin [14], brain [15] and the interior of teeth known as pulp [16]. Laser speckle can be further used as an ambulatory monitoring device, as the current optical methods (PPG based) are highly susceptible to motion artifacts. For such application, the most common sources of motion artifacts are caused by both the relative body and sensor position variations and the absolute body motion.

Laser speckle is created as coherent light scatters from diffuse or rough surfaces. Due to optical path differences of the scattered light, constructive or destructive interference takes place. This signal is collected using an intensity detector with a finite aperture and recorded as a granular pattern of dark and bright spots. Any movement in the media, such as evolution of cell or movement of red blood cells, causes the speckle patterns to change. This high sensitivity of speckle to minor changes can be a powerful tool for studying the dynamics of fluctuation in the blood flow. The importance of blood flow monitoring can be observed in studying the heart valve dynamics, or in diagnosing variations in blood vessel

stiffness which typically is a sign of cardiac disease: changes in the stiffness of arteries and veins, creates a different range of speed of dilatation waves and that eventually results in an irregular range of flow speed. The laser speckle technique has both a temporal and a spatial characteristic, as temporal and spatial intensity variation of the speckle pattern contain information over the dynamic properties. This method provides a two dimensional map of localized blood flow dynamics. To explore the advantages of this technique, we have used laser speckle as the main tool to measure pulsatile flow.

To study the flow dynamics, we started by building a laser speckle experimental setup to monitor the pulsatile flow. Given the importance of characterizing the required features of the device when ultimately it's applied in practice, we constructed an experimental setup on a simplified model of the real situation. In collaboration with LifeTec Group, we have developed an *in-vitro* model of a blood channel with different channel depths in a medium which mimics the skin scattering properties. Obviously, care must be taken in interpreting the result as the human body is a complex system and differences in *in-vivo* behavior should be expected. This complexity originates from variation in micro-vascular structure of each individual and different vessel geometry. The difference in blood rheology is another factor as any aggregation of red blood cells can change the optical properties of the blood flow and influences the laser speckle measurements [17]. Moreover, with non-invasive monitoring we do not have direct access to blood flow since this is accessed through a layered skin structure. Due to such factors, laser speckle can only report blood flow changes rather than absolute values. In order to come up with a solid platform, the *in-vitro* measurements can provide a good reference of the blood flow principle as an initial step.

In addition to the above studies, we studied the combination of laser speckle techniques with direct imaging ones, such as particle image velocimetry (PIV). Using PIV, we can measure the complementary parameters of the flow dynamics as it can accurately compute the flow velocity using tracing particles. Both laser speckle and PIV have the ability to capture entire optical field for the flow measurement and combination of these two techniques can provide a better insight into flow dynamics. These experiments were reported for the study of pulsatile flow using ventricular assist device in a patient-specific carotid artery phantom. This was done to also cross reference the technique in the same phantom.

The analysis of dynamic speckle patterns can be quantified using laser speckle contrast, which is defined as the ratio of standard deviation over the average of intensity fluctuations. This can be calculated for each random distributions of bright and dark patterns. In order to study dynamics of the physical problem, more additional measures need to be done where we capture a time sequence of images and calculate the speckle contrast for each pattern. Furthermore, we introduced an additional approach to measure the time fluctuation dynamics of speckle images based on fractal analysis. These measurements have been performed in comparison with laser speckle analysis and for different experimental configurations. The multiscale analysis of speckle data using fractal based techniques provides a deeper

insights into the system. To demonstrate that, the fractal analysis has been applied to a different scattering configuration where the scattered wavefront of the pulsatile flow has been propagated through a layered structure.

In this thesis, we emphasize on the importance of having a flow measurement setup in the first place which allows to simulate the various *real-life* conditions under which the system is intended to be used. Motion artifact is a key challenge in any portable application as it distorts the data and reduces the signal quality significantly, therefore influencing its applicability in (optical based) health monitoring devices. There already have been many attempts to deal with this problem based on both hardware and software approaches. Such approaches introduce the use of additional sensors such as trackers and accelerometers [18, 19], piezo and pressure [20], or combinations of the above [21] to be applied as a noise reference signal. The second approach is mainly using software based techniques for reducing the motion artifacts, aim at improving the signal quality, using different techniques such as the wavelet transform [22], adaptive noise cancellation, least mean square [23,24] and other non-linear methods [25]. In most cases, these methods help to decrease the number of false alarms but not to remove the influence of artifacts totally.

To study the influence of motion artifacts, we performed both phantom based and *in-vivo* experiments. To look into the initial problem of motion artifacts, we artificially simulated the induced motion artifacts in a controlled lab environment. This allowed us to deepen the understanding of the parameter range under which laser speckle could be applied. The *in-vivo* measurements provided us with a validation of the approach.

1.2 Research project settings

The project started as a collaboration between Optics Research Group of Delft University of Technology (TU Delft) and Eindhoven University of Technology, Philips Research and LifeTec Group, Eindhoven. This project has been performed in close collaboration with Philips as an industry partner. This enables a clear focus on the problems faced by current devices in the market and to narrow the research to market gap. The contributions from the academic side have been focused on researching the usage of laser speckle based techniques to retrieve data in real-world continuous monitoring situations.

1.3 Thesis structure

This thesis is focused on laser speckle analysis created from a pulsatile flow, and it is organized as follows:

Chapter 2: We start with an introduction to light tissue interaction. The physical study and numerical approaches for processing data. This is followed with a

brief survey over laser speckle techniques. Finally, different data analysis methods, useful in the context of subsequent chapters are introduced.

Chapter 3: This chapter provides a general understanding over different parameters which have a major influence in monitoring pulsatile flow. The time dependent analysis of speckle patterns was used to study the influence of different parameters, such as particle concentration or volume of fluid and influence of static particles due to bone and tissue for instance. The different experimental setups and phantoms are described.

Chapter 4: This chapter introduces the combination of laser speckle contrast analysis (LASCA) with another known method in fluid dynamics, particle imaging velocimetry (PIV). These full-field optical techniques have both been used to study flow and extract complementary parameters. LASCA can provide a quick study of signal fluctuations over time so that transient phenomena can be recorded and observed. PIV can be used for a detailed study of the cause of the phenomena. This is perhaps also very useful for studying geometries with flow instability. A preliminary comparative measurement between PIV and LASCA to study pulsatile flow using ventricular assist device in a patient-specific carotid artery phantom is reported.

Chapter 5: In this chapter, a different approach towards data processing of acquired speckle data is introduced. The fractal nature of speckle is explored. Moreover, same set of experimental data which was discussed in the previous chapter, was analyzed with this technique. This was used to compare the fractal analysis with the standard analysis used for laser speckle patterns.

Chapter 6: This chapter addresses the problems of acquiring and analyzing flow data in the presence of multi-layered medium. We report a comparison on the acquired data using laser speckle and fractal analysis.

Chapter 7: Finally, a key requirement for portable, continuous monitoring devices is addressed in this chapter. The measurement of flow in presence of motion artifacts. We address using the speckle dynamics for measuring a pulsatile flow in a noisy environment.

We conclude the thesis with a chapter discussing the contributions of the thesis and concluding this manuscript.

CHAPTER

2 Theory and analytical methods for flow measurement

It is the theory which decides what can be observed.

Albert Einstein

Coherent light scattered from diffuse media can reveal the underlying phenomenon active in the media. Dynamic light scattering is the study of the decay rate of the autocorrelation function of the scattered light as a result of scatterer motion. Laser speckle imaging (LSI) together with laser Doppler flowmetry [26] or diffusing wave spectroscopy (DWS) [27] are techniques that have evolved from the principle of dynamic light scattering (DLS). The laser speckle imaging has the advantage of evaluating the sample without scanning and images a wide field of view with a simple and inexpensive apparatus. The objective of this thesis is to apply this method for the case of studying flow. For this application, it is essential to understand the light propagation in the sample. The propagation of light through a diffused sample and how the light will be scattered is mainly defined by material properties. As in this study we explicitly aims to measure the blood flow *in-vivo*, we provide an overview of light and tissue interaction. This chapter is intended to provide a brief introduction to understand the background of the studied phenomena and overview of the main terms which will be used in the rest of this thesis. It introduces, the tissue optical properties along with diffuse light transport regimes. These regimes are important when quantitative measurements are of interest. There are certain approximations that are applied at each regimes, in order to describe light distribution accurately. By applying these theorems with some prior knowledge, for instance the separation distance between the illumination source and detector, we can retrieve tissue optical properties from different propagation models. In section 2.1.1 some of the commonly used models and approximation will be mentioned. Then, we introduce what speckles are and how

they are created. As the phenomenon which leads to the generation of speckles is random, statistical techniques are mainly used in studying and parameterizing them. The data analysis which have been used to study laser speckle images are mentioned by the end of this chapter.

2.1 Light tissue interaction

Biological samples are generally optically turbid and highly absorbing when studied *in-vivo*. The structure can be rather inhomogeneous and have a refractive index higher than air (assuming most of the body is water). When light illuminates a diffuse media like tissue the electromagnetic radiation is absorbed, scattered and reflected. It is useful to note that in the absorption process, long wavelength photons deposit lower energy compared to short wavelength photons. For the case of low intensity laser light interaction with tissue, the illuminated light is incident along a certain direction, but soon the direction is lost due to reflection and scattering in the sub-layers. The light that penetrates the tissue undergoes multiple scattering till it is eventually absorbed. Chromophores are the main absorbers and the most common ones known in skin are hemoglobin, melanin and water in different absorption wavelengths. The probability of absorption varies by the concentration of absorbers which is expressed in terms of the absorption coefficient. The absorption coefficient (μ_a) is defined as the sum of contributions from all absorbing chromophores within the tissue, which is expressed as [28]:

$$\mu_a = \ln(10) \sum_i C_i \varepsilon_i \tag{2.1}$$

where C_i is the absorber concentration of the chromophore, $[M]$, and ε_i is the molar extinction coefficient $[M^{-1}cm^{-1}]$ at the specific wavelength. The product of these two factors is in $[cm^{-1}]$ unit which indicates the wavelength dependency of the absorption coefficient. The changes in optical absorption as a function wavelength is shown in Fig. 2.1 for a variety of important chromophores, including melanin, oxy-(HbO_2) and deoxyhemoglobin (Hb). The light absorption in blood is dependent on the oxygenated (HbO_2) and deoxygenated (Hb) hemoglobin, where the difference in their absorption spectra can be seen in this plot. The tissue optical window is referring to a low absorbing range where the light penetration in the tissue is at its maximum.

Nevertheless, scattering is the dominant phenomenon which originates due to refractive index inhomogeneities within the tissue. Scattering influences the depth of light penetration by spreading it out. There are two kinds of (elastic) scattering processes known as Rayleigh and Mie scattering (dependent on the laser wavelength and size of the scatterers). When the objects are of the same size or smaller than the incident wavelength, then Rayleigh scattering occurs where the intensity of scattered light is proportional to λ^{-4}. However, for objects that are larger than the incident wavelength Mie scattering occurs with the intensity of

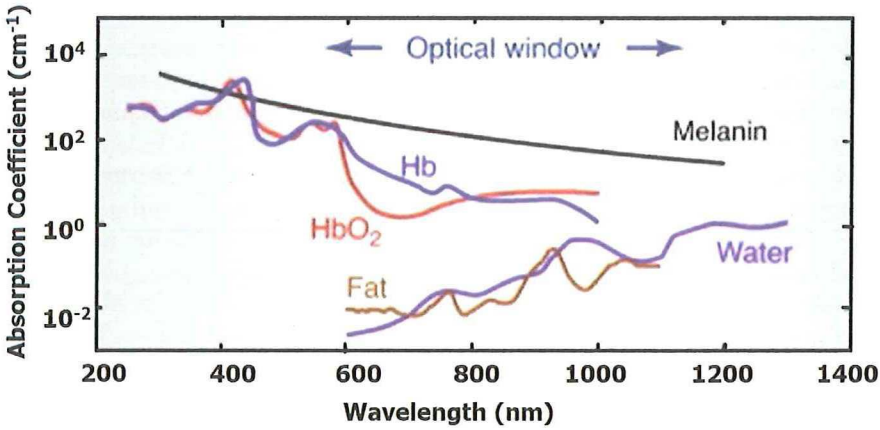

Figure 2.1: Absorption spectra of some of the important chromophores in the body, adapted from [29].

scattering light is proportional to λ^{-2}. In case of visible light, for most of the tissues, a combination of both, Rayleigh and Mie scattering takes place, although Mie scattering is dominant. This is mainly due to different cell size (lysosomes, vesicles, mitochondria) and cell spacing. All other sub-cellular components and molecules lead to Rayleigh scattering [30,31]. In contrast to absorption where light travels into the tissue and loses its energy, light diffuses due to scattering. Elastic scattering can be considered as process of photon absorption and re-emission without loss of energy but possibly associated with a change in photon direction. The main properties of tissue are described in terms of absorption coefficient (μ_a), scattering and reduced scattering coefficients (μ_s, μ_s') and anisotropy factor (g). However, the structural composition of tissue with different material properties, requires a new definition of transport coefficient which is the sum of reduced scattering (μ_s') and absorption (μ_a) coefficient: $\mu_t = \mu_s' + \mu_a$. The term μ_s' is including the anisotropy (g) factor which is a directionally dependent. These parameters can be estimated using an inverse method, where through an iteration method these parameters are initiated and applied in a light propagation model [32]. These parameters need to be continuously adjusted till the reflection or transmission values are the sames as the ones required from measurements. One of the method is using thin slices of different thicknesses and a narrow beam geometry, so in this case the absorption in tissue is based on the Lambert-Beer Law, so the intensity measured at a certain depth (z) is:

$$I(z) = (1 - R)I_0 \exp(-kz) \tag{2.2}$$

where R is the Fresnel reflection coefficient which is known from the refractive indices, the incoming angle and the reflection angle. I_0 is the intensity of the incident light and k is the attenuation coefficient which is sum of the coefficient of absorption and loss due to scattering. In this approach, the scattering is ne-

glected as we only considered thin slices of sample. In the case of thick samples, the multiple scattering effect need to be taken into consideration. Moreover, the reliability of this method is dependent on the numerical aperture set in the measurements. In case of having small recording angle, it can be assumed that all the scattered light will not be measured by the detector [33]. Another common technique to extract optical properties is using the Integrating Sphere method. This approach is often used for tissue phantoms where the μ_s, μ_a and g parameters can be extracted. The integrating sphere is made of highly reflecting material, so that the light passing through the sample will be scattered highly till it reaches the detector. However due to inconvenient sample preparation, for the *in-vivo* cases is more common to use the time or spatially resolved techniques. These are based on measuring the diffuse reflectance or transmittance from the medium where a known source detector separation is used [34, 35].

In time-resolved measurements, a series of short pulses, in picoseconds range, is applied so the temporal point spread function can be measured at a certain distance from the source [36]. In this case the shape of detected pulse measured with absolute intensity value, carries the information about the optical interaction coefficients. In the spatially resolved technique, diffused reflectance is measured versus different separation distance between source and detector, so that each time light probes different volumes and different depths. The optical properties can be calculated by fitting the transmittance or reflectance values measured from any of this approaches into a numerical modeling. These models will be addressed shortly, since it is essential to first introduce different scattering regimes where these models can be applied.

In the interest of introducing different scattering regimes and how photons are transported in the medium, we need to use transport mean free path. This is defined as the reciprocal of reduced scattering coefficient, $l'_s = \frac{1}{\mu'_s}$. This path can be realized as a length that photons forgets its initial orientation. The regime where photons experience no scattering event is called the ballistic regime, while in case of few scattering the term quasi-ballistic will be used. In this case, few scattering happens and photons will be deflected but still they have a strong memory of their initial orientation, which is about 1 to 10 transport mean free path. In the ballistic regime, mean free path ($l_s = 1/\mu_s$) is an important factor to describe the mean distance between the successive scattering event. If number of scattering events goes high, beyond 10 transport mean free path, photons experience many scattering events and they have no memory about their original orientation [37]. So in this case, the distance between successive collision is of no importance. As multiple scattering happens, we need to take into account the influence of scattering angle and transport mean free path. For instance, in diffusion regime, photons are scattered in all directions so the amount of light reaching the detection plane is proportional to the measuring solid angle while in case of ballistic, photons still retain their original direction [38]. In case of diffused light, energy in the ballistic component drops exponentially as it goes deeper in the sample, and energy in the scattered components increases. This is a common problem when it comes to direct imaging. In direct imaging, the spatial origin of the ballistic component is of

interest. Since monitoring this information is rather difficult for these applications, scattered light is mainly treated as noise and suppressing it can further improve the results. However, we are using the method of laser speckle imaging, where we are monitoring mainly the scattered components. The scattered light from a certain traveled depth in the sample, creates diffuse scattering and this is the main source of information in speckle patterns.

2.1.1 Numerical modeling

In order to have an accurate modeling of light propagation in tissue, an exact description of spatial and size distribution of tissue structure with their exact optical properties would be required which in case of real tissue would be rather impractical. This is the reason why mostly a tissue phantom is used and tissue is modeled as a bulk material with absorbing properties and randomly positioned scatterers. The numerical modeling gives the possibility to predict and simulate optical behavior in such a structure. There exist several models for light propagation in tissue, where we provide a summary of these models in the Fig. 2.2.

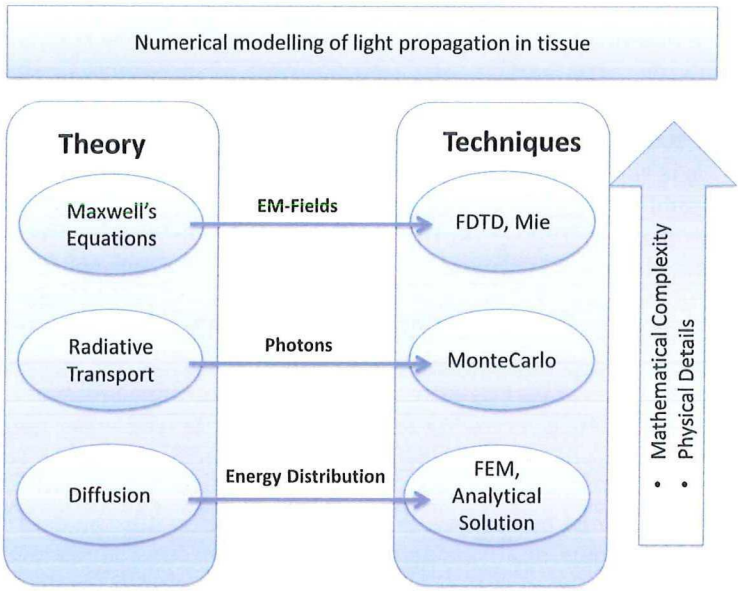

Figure 2.2: An overview of numerical models used for light propagation in tissue.

There are three categories which are most widely used to model light distribution in tissue, based on: Maxwell's equation, radiative transport and diffusion theory.

Light is considered as electromagnetic field and the study of light propagation is well described by Maxwell's equations. Although electromagnetic theory conserves the wave properties of light and can be applied for describing light propagation in the tissue, it introduces extra complication. On the microscopic level, Maxwell's equations can be solved numerically, for which different methods are implemented. One of the most important analytical solution is based on the Mie theory, which calculate the scattered field for homogeneous spherical objects. Although this approach is limited by geometrical approximation, it is often used as a reference method. Moreover, being computational fast, made it to be a suitable platform to be used in flow studies. This work has been initiated in our group and has been applied in an existing computational fluid dynamics code by Kevin van As [39]. This is mainly applied for a collection of particles, for instance red blood cells (RBCs) which heavily scatters light. To model the propagation of light in tissue, light scattering is influenced as the result of changes in refractive indices, and also the size, shape and orientation of objects. To consider the non-spherical geometry, other methods such as finite-difference time-domain (FDTD) [40] or T-matrix methods [41] need to be considered.

Essentially, in order to consider multilayerd and inhomogeneity of tissue, it would be more common to use the application of radiative transport theory. The main difference between transport theory and electromagnetic theory is that, in transport theory the wave properties of light are not considered and light propagation is described as superposition of energy fluxes rather than electromagnetic fields [42, 43]. The radiative transfer equation is derived from the Boltzmann's equation and states the conservation of energy in terms of the specific intensity and as a function of position in the random medium [44]. The specific intensity of radiation is the energy flux per unit time, unit frequency, unit solid angle and unit area normal to the direction of propagation. This is the theory of how radiation and matter interact based on the particle description of light. To further develop this point, the possible approaches can be divided in two groups of deterministic or statistical methods. Deterministic methods are based on the radiative transport theory require solving the radiative transport equation [45]. One of the commonly used numerical solution is the adding-doubling method for layered media. The doubling was introduced to solve the radiative transport equation in a slab based geometry [46], where doubling refers to finding the reflection and transmission matrices for two layers with identical optical properties rather than individual layers [47]. So in this case, measuring the properties of a slab with a certain thickness has been done by repeatedly doubling the layers till the desired thickness is achieved. The main disadvantages of this technique are the assumption that each layer has homogeneous optical properties and has uniform irradiation [48].

On the other hand, statistical methods are more flexible to handle complex geometries and non-homogeneous properties. Monte Carlo and random walk are the common examples of this method. These models are based on tracing the path of photon bundles. The principal idea of photon propagation is based on probability distributions to define random variable sampling. This method can be summarized in few steps as describe here. The photons are generated with a weight

of unity at a known medium and they illuminate the sample with a defined angle of incident. At first, the distance to first collision need to be determined. This is defined using a random number, being uniformly distributed between 0 and 1, and the extinction coefficient (sum of absorption and scattering coefficients). As the photon packets start to move then they will be scattered with a deflection and azimuthal angle which are sampled statistically. The scattering angles are shown in the Fig. 2.3(a). The azimuthal angle, ϕ, is sampled based on another independent random number. The deflection angle, θ, which is deflection from the original incident direction is given by a probability distribution of the cosine of deflection angle, and is defined based on Henyey-Greenstein phase function:

$$p(\cos\theta) = \frac{1 - g^2}{2(1 + g^2 - 2g\cos\theta)^{\frac{3}{2}}} \tag{2.3}$$

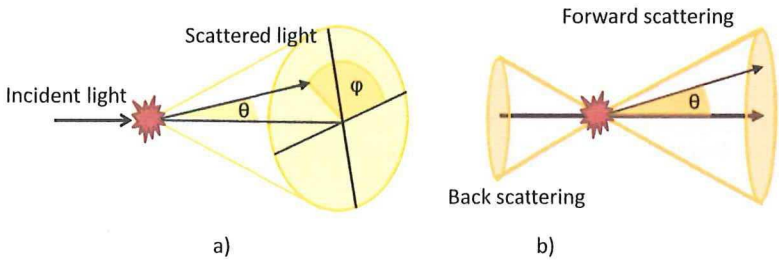

Figure 2.3: a) The scattering event causes the change of direction of the incident light shown by the scattering angles: ϕ and θ b) The amount of forward and back scattering is controlled by anisotropy factor in the Henyey-Greenstein phase function.

This function is dependent on g, the anisotropy factor, and it is the controlling parameter in defining the amount of forward and backward scattering as it is shown in the Fig. 2.3(b). The anisotropy factor is measured as the mean cosine of the scattering angle, $g =< cos\theta >$, (value between -1 and 1). The value of $g = 1$ indicates forward scattering, while a measured value of $g = 0$ means uniform scattering. For biological sample, the re-emission has a high probability to be in the forward direction for each scattering event and a typical value for human tissue is around 0.95 [37, 49]. Once the angles are sampled, a new propagation path of photon packet is defined. The photon weight will be decreased along the path due to absorption and when the weight of the photon has passed a threshold then the photon will be eliminated. The whole procedure will be repeated till the photon escape the volume or its weight reaches the defined value. Otherwise, the trajectory of the photon path will be followed till it reaches the detection plane. The final value of interest is averaged over many photon histories [50,51]. Although this method handles different optical inhomogeneities and geometries, being a statistical method requires a large number of commutation to provide meaningful

results and at the end random errors can not be avoided due to practical finite sampling.

The solutions to radiative transport theorems are computationally expensive and for a medium like biological tissue, where light interaction can be dominated by scattering [52] then diffusion approximation can be applied. Diffusion model is an approximation for obtaining the analytical solution of the radiation transport equation [53, 54]. This model has its own limitation as it can not model the light propagation close to the collimated light sources and boundaries [55]. Diffusion theory can be then a useful tool to describe the light propagation over millimeter range and further for visible wavelength (one mean free path distance in visible range is less than 1 or 2 mm), [56]. This theory is mainly applied for visible and near infrared regions, as it is not an accurate model for a tissue model where, $\frac{\mu_s'}{\mu_a} << 10$, meaning that there is a high absorption [57].

2.2 Physics behind speckle

The origin of speckle goes back to the arrival of a coherent source, laser, as this mottled pattern appears every time when laser illuminates a diffuse surface. The reflected or transmitted light creates such a structure as a result of interference of many scattered waves having a random phase. The occurrence of speckles can not be avoided as the random phase occurs due to roughness and scattering nature of diffuser. This changes the spatial coherence in the near field and creates a grainy pattern in far field distribution of diffuser.

The speckle patterns are generally generated in two main categories of subjective and objective pattern. In free space geometry, by shining a laser beam on an optically rough surface, the light will be freely propagated on a screen far away and the so called objective speckle is produced on the observation plane. This is shown in Fig. 2.4(a). However, a different kind of speckle pattern can be created if this scattered light is imaged through a lens, as shown in Fig. 2.4(b). This is called subjective speckle pattern, where the observation plane is the focal plane of the lens [58].

The term subjective is used as the limit of spatial frequencies of the recorded speckles is dependent on the numerical aperture of the used lens system. On the contrary, the scattered wavefront being collected directly, through a photosensitive material for instance, would result in a larger spectrum. In case of an interference due to the superposition of two scattering points separated by the distance, d , the spatial frequency of such a pattern recorded at a distance z is calculated as: $\frac{d}{\lambda z}$. The maximum spatial frequency is dependent on the size of the scattering surface and corresponds to the minimum periodicity in the interference pattern. Based on the Rayleigh's resolution criterion, a minimum distance between two neighboring maximum intensity points is defined as the minimum speckle size. For the objective speckle, the speckle size, both longitudinal size d_z and lateral size d_s will be dependent on the section of free space [60]. The illuminated area,

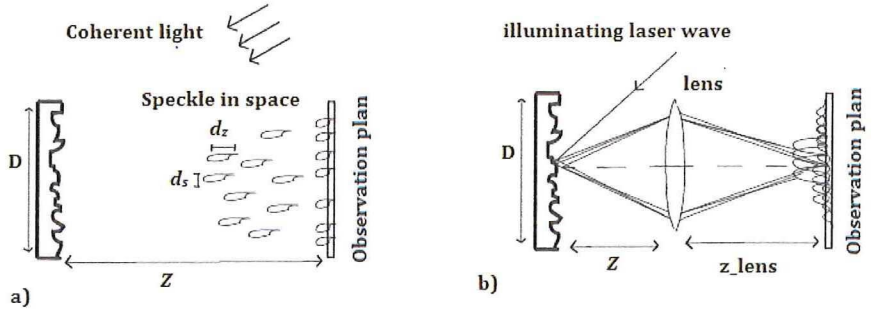

Figure 2.4: a) Objective speckle pattern and b) Subjective speckle pattern [59].

D, after being a z distance propagated in free spaces create the spatial extent of the speckle, as:

$$\begin{aligned} d_s &= \lambda \frac{z}{D} \\ d_z &= \lambda (2\frac{z}{D})^2 \end{aligned} \tag{2.4}$$

This results in usually a larger value for the longitudinal size of the speckle which explains why the speckles are referred to as cigar-shaped and they become more elongated by increasing z. The irradiance at a single point in the observation plane perpendicular to the scattering direction, would be the result of large number of waves with random phases. The average speckle size is introduced as $d_{av} = 1.22\lambda\frac{z}{D}$. The size of subjective speckle pattern can be calculated in a similar manner. In this case, using a lens changes the number of speckles locating at the image plane, given by the ratio of the lens diameter to the lateral size of speckle $\frac{d_{lens}}{d_s}$. The image has a diameter of $D\frac{z_{lens}}{z}$ which is dependent on the focal length of the lens. By knowing the number of speckles in this image area, the speckle size can be calculated as:

$$d_s = D(\frac{z_{lens}}{z})(\frac{d_s}{d_{lens}}) = \lambda \frac{z_{lens}}{d_{lens}} \tag{2.5}$$

This is more or less similar to the objective speckle, except for the fact that now the scattered light is imaged into the screen through a lens. For the calculation, in this case we need to use the lens properties. It is more common, to use the average term as $d_{av} = 1.22\lambda(1+M)F$, where F is the F-number expressed as the ratio of the imaging distance and lens aperture $\frac{z_{lens}}{d_{lens}}$ and M is the magnification factor. An example of the speckle pattern measured with different camera setting is shown in the Fig. 2.5. In this set of images, it can be seen that decreasing the aperture size (or increasing F-number), a larger speckle pattern can be expected. This is shown for three different camera F-number of 2.8, 22 and 32.

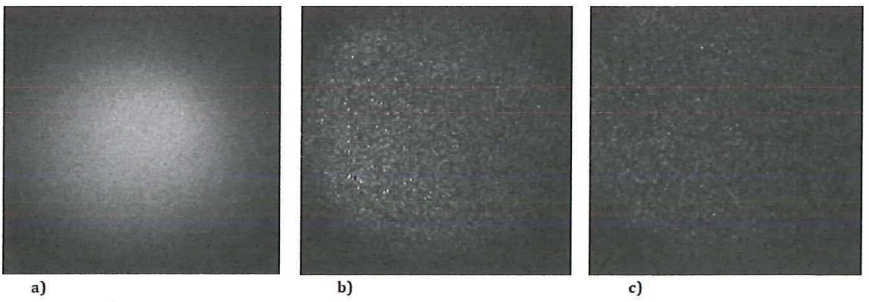

Figure 2.5: The measured speckle pattern with the camera F-number setting of : a) 2.8 b) 22 and c) 32.

The important concepts behind the physics of speckle based on their statistical properties, was first introduced by Goodman [61] and Dainty [62]. This is based on the random phasor sum to describe the complex amplitude of the field at each point in space. So in case of illuminating a medium with monochromatic and polarized light, the total field at a point can be expressed as the superposition of many scattered waves. Each of these waves has a random amplitude and phase. The output electric field complex amplitude can be studied using the phasor sum model, or the complex amplitude of the scattered field arriving at an observation point, as:

$$\vec{A} = \frac{1}{\sqrt{N}} \sum_{k=1}^{N} a_k \exp\left(-j\phi_k\right) \tag{2.6}$$

where a_k is the amplitude and ϕ_k is the phase of the k_{th} scattering wave. The field in a single speckle is the sum of all the contributions from a large number of light paths and when all these light paths are considered to be random and independent. This resultant phasor sum, $\vec{A}$, can be rewritten in the form of $\vec{A} = R + jI$ for which the real, $Re\{\vec{A}\}$ and imaginary $Im\{\vec{A}\}$ parts are derived as:

$$\begin{aligned} R = Re\{\vec{A}\} &= \frac{1}{\sqrt{N}} \sum_{k=1}^{N} a_k \cos(\phi_k) \\ I = Im\{\vec{A}\} &= \frac{1}{\sqrt{N}} \sum_{k=1}^{N} a_k \sin(\phi_k) \end{aligned} \tag{2.7}$$

To understand how the speckle patterns behave, we need to measure the probability density function. This function contains the information of how different intensities in the speckle patterns are distributed. In order to find the probability density function of speckle patterns certain assumption are made:

(1) The a_k and ϕ_k are statistically independent which means the knowledge of a phasor's amplitude does not provide the knowledge of the same phasor's phase and vice versa.

(2) The amplitude and phase for each element k and p where $k \neq p$ are statistically independent meaning that knowledge of one phasor's amplitude or phase does not provide any knowledge for another phasor's amplitude or phase.

(3) The phase ϕ_k is uniformly distributed over $[-\pi, \pi]$ which means that all phase values are equally probable. This is mainly valid when the surface roughness is greater than a wavelength.

Based on these assumption, this model is a random walk in the complex plane where the magnitude of each step is independent of its direction and there is an equal probability of taking step in any direction. Following the last assumption the expectation values of $\cos(\phi_k)$ and $\sin(\phi_k)$ are zero which means the mean value for R and I are also zero, $E[R] = E[I] = 0$. Here, $E[]$ is the expected value of a random variable. In this case, the variance of the real and imaginary parts of the resultant phasor is calculated as:

$$\begin{aligned} \sigma_R^2 = E[R^2] = \frac{1}{N} \sum_{k=1}^{N} \frac{E[a_K^2]}{2} \\ \sigma_I^2 = E[I^2] = \frac{1}{N} \sum_{k=1}^{N} \frac{E[a_K^2]}{2} \end{aligned} \tag{2.8}$$

Here $E[R^2]$ and $E[I^2]$ are the second moment of the real and imaginary parts of the resultant phasor, which are equal to their variances as the means are zero. These two variance values are identical, which is shown be a common value of $\sigma^2 = \sigma_R^2 = \sigma_I^2$. Knowing the variance of the real and imaginary parts of the resultant phasor, now we calculate the correlation coefficient between them. The correlation coefficient ρ is related to the covariance, Γ:

$$\rho = \frac{\Gamma_{R,I}}{\sigma_R \sigma_I} \tag{2.9}$$

where σ_R, σ_I is the standard deviation of real and imaginary parts of the resultant phasor respectively. It can be seen that $\rho \propto \Gamma_{R,I} = E[RI] = 0$ as $E[R] = E[I] = 0$

Assuming that the number of phasor components is large, N, the central limit theorem can be applied. The statistics of the sum of N independent random variables is asymptotically Gaussian as $N \to \infty$ [63]. In order to derive the joint probability density function of the real and imaginary part of the speckle field [64]:

$$p_{R,I}(R, I) = \frac{1}{2\pi\sigma^2} \exp\big(-\frac{R^2 + I^2}{2\sigma^2}\big) \tag{2.10}$$

From here, we can see that the joint probability density function of the length A and phase θ is then:

$$p_{A,\theta}(A, \theta) = \frac{A}{2\pi\sigma^2} \exp\big(-\frac{A^2}{2\sigma^2}\big) \tag{2.11}$$

for $A \geq 0$ and $-\pi \leq \theta \leq \pi$, otherwise it results in zero. By knowing the joint distribution of A and θ, now we need to find the marginal statistics of each of

them individually, which is defined by integrating Eq. (2.11):

$$p_A(A) = \int_{-\pi}^{\pi} p_{A,\theta}(A,\theta)d\theta = \frac{A}{\sigma^2} exp(-\frac{A^2}{2\sigma^2}) \tag{2.12}$$

for $A \geq 0$, this result is known as the Rayleigh density function. Now, by integrating the Eq. (2.11) with respecting to amplitude, we find the density function of phase $p_\theta(\theta)$:

$$p_\theta(\theta) = \int_0^{\infty} p_{A,\theta}(A,\theta)dA = \frac{1}{2\pi} \tag{2.13}$$

for $-\pi \leq \theta \leq \pi$. Here the fact that the integral of the Rayleigh density function is unity, has been used. Furthermore, in most of the experiments the direct measured variable is intensity, the amplitude A is related to measured intensity I, as $I = A^2$. From a fundamental result of probability theory [63], the probability density function $p_V(\upsilon)$ of υ can be related to the probability density function for a random variable υ related to another random variable u by:

$$p_V(\upsilon) = p_U(f^{-1}(\upsilon))\left|\frac{du}{d\upsilon}\right| \tag{2.14}$$

It can be seen that, knowing the probability density function $p_A(A)$ we can find the probability density function for the intensity through:

$$p_I(I) = p_A(\sqrt{I})\left|\frac{dA}{dI}\right| = \frac{1}{2\sqrt{I}} p_A(\sqrt{I}) \tag{2.15}$$

By using Eq. (2.12) and applying the transformation law of Eq. (2.15) we see that it obeys negative exponential statistics so that its probability density function is:

$$p_I(I) = \frac{1}{2\sigma^2} \exp(\frac{-I}{2\sigma^2}) \tag{2.16}$$

As it has been mentioned earlier, the probability distribution is an important feature of speckle pattern as it can describe how likely is to observe a bright or dark spot at a given point. One important feature of the assumption of Gaussian distribution for speckle patterns is that standard deviation is equal to its mean. This is known as fully developed speckle pattern, an example of which is shown in the Fig. 2.6. This speckle pattern is the result of a perfect ground glass diffuser which has Gaussian surface height variation and being illuminated with a coherent light. This kind of speckle results in a maximum variation in one speckle pattern and has been a speckle contrast value of 1. The speckle contrast, ratio of standard deviation to mean value, with value less than one indicates a partially developed speckle pattern. This is the result of weak diffuser with smoother surfaces [65].

However, the sum of many independent speckle patterns has a different behavior. As the number of these patterns increases the probability distribution plots tends to a Gaussian distribution. This has been shown to be the case for biological tissue where the light penetrates and as a result of multiple scattering, the probability

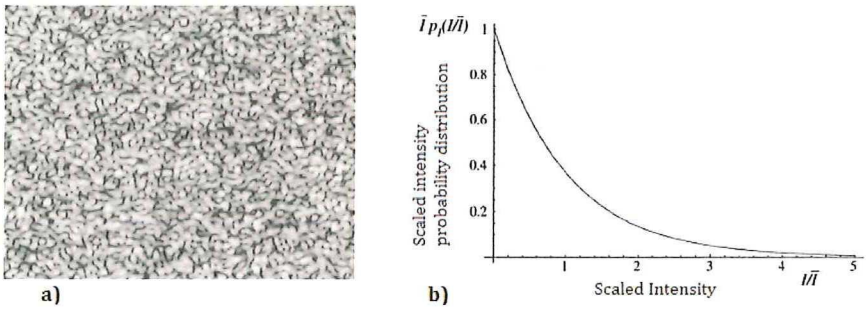

Figure 2.6: a) Fully developed speckle pattern and b) Probability distribution plot [63].

distribution function will not follow a negative exponential relation as in Fig. 2.7 but it would be more of combination of different speckle fields. Also time integration will change the distribution function [66].

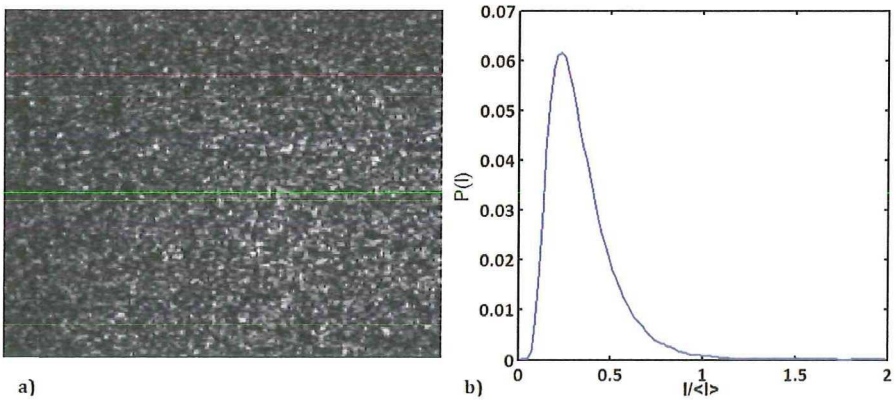

Figure 2.7: a) Speckle pattern measured from human finger and b) its probability distribution.

This is referred to as low coherence speckle pattern, which is not the result of surface scattering but volume scattering. Here the recorded back scattered speckle can be considered as the combination of many speckle patterns [67,68] and creates speckle contrast value of less than one. In some experimental configurations, these assumptions may not be valid anymore and non-Gaussian speckle distribution are created. This can be due to a weak scattering medium, having a non uniform phase distribution [69], or in case of having cascade of thin diffusers [70]. An experimental example of the last case will be discussed in chapter 6.

2.3 Time varying speckle

The recorded speckle pattern from a steady object results in a stationary speckle pattern. If the sample moves, for a small displacement in the sample, the speckle pattern will retain its shape but move with the sample. In this case, the movement of the sample can be measured using the double exposure photograph. In this method, double exposure photograph is taken after and before the movement happens. By illuminating the photograph with a laser beam, the interference fringes will be observed from each speckle pair. The distance between fringes, contains information about the speckle displacement which is eventually a measure of the movement in the sample [71]. However, for larger movement of the object the speckle will be decorrelated and a totally different speckle pattern will be recorded. A similar effect can happen when there is a motion of many small moving particles in the sample, such as in fluid. The movement in the illuminated sample, creates a new formation of speckle patterns, which are called dynamic speckle or bio-speckle. This is the case of tissue with underlying flow. The difference between static and dynamic speckle pattern is shown in Fig. 2.8. In case of static speckle pattern the surface roughness scatters light in many different directions and creates a high contrast speckle pattern. While in dynamic speckle, which is time variant, the speckle pattern changes during the exposure time and the recorded speckle pattern results in a lower contrast. The time varying speckle patterns are more complex and these signal fluctuations can be studied by analyzing their temporal statistics [72]. Studying the temporal speckle fluctuation provides an extensive source of information over the sample, and this can be applied in different applications. For instance, to measure vibration and mechanical properties, viscoelastic and material stiffness [73] or dynamical behavior of the system such as velocity and displacement. In biological and living samples, the speckle dynamics can be rather complex. Different properties of the sample can have an influence, such as multiple scattering, interaction between different materials and combination of dynamic and static speckles. The time varying speckle patterns are mainly considered as translational and boiling speckles [74]. The translation speckle happens when an entire solid object moves, so that the whole speckle pattern translates or moves with the object. The boiling speckle are typically found in the case of living samples. In this case, the entire granular structure of speckles continuously changes as the speckle can deform or appear and disappear.

Static light scattering (SLS) is mainly used to study the structure of biological cells or tissue, by measuring the molecular weight using the relationship between the intensity of light scattered by a molecule and its molecular weight and size [75]. While dynamic light scattering (DLS) measures the dynamics of the system. This was mainly used for the measurement of particles suspended in a liquid. The first application of DLS was in photon correlation spectroscopy where it is capable of determining the size of particle and viscosity based on the temporal auto-correlation function [76]. The main relation which defines how a particle diffuses and changes its speed of motion is based on the translational diffusion coefficient which is derived using the well known Stokes-Einstein relation [76]. This time-dependent

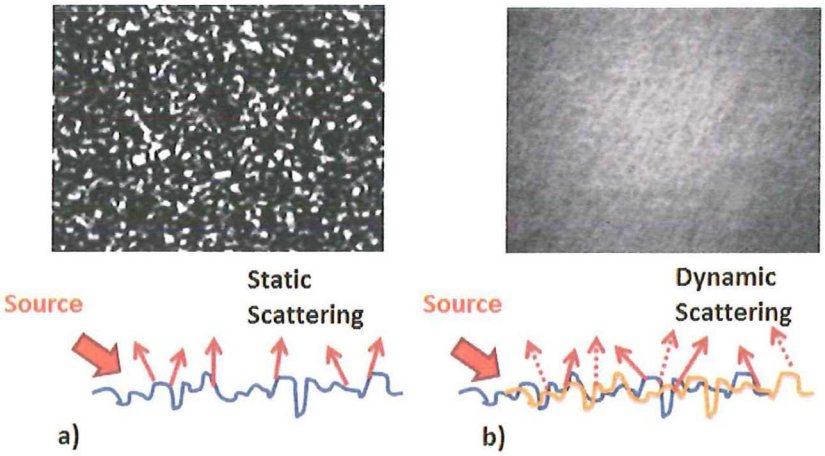

Figure 2.8: a) The speckle pattern created from a static object, b) The speckle pattern of a dynamics sample result in a slower contrast as the time variances are averaged over an exposure time.

diffusion coefficient will have a finite value in a solid system. However in a fluid this is not valid, as random collision between particles changes the mean square displacement in time. This continuous change in the distance between particles creates a Doppler shift between the frequency of the incident and the scattered light. This was first discovered by Robert Brown and later described mathematically by Einstein. This is the working principle of laser Doppler. Studying the frequency spectrum of the scattered light provides details of motion. The shape of spectrum indicates the type of motion (diffusive or ballistic) while changes in the diffusion coefficient changes the broadening of spectrum. [77]. Further applications of technique using DLS are diffusing wave spectroscopy (DWS) [78] and laser speckle contrast analysis (LASCA). The question if the fluctuations measured using laser speckle are the same as the frequency shift in laser Doppler, has been answered by Briers [79]. These two techniques have the same mathematical description relating the frequency of changes to the velocity of the scatterer. However, they are two different ways of looking at the same phenomena.

The displacements of the light scattering centers undergoing different fluctuations, such as Brownian motion, can be analyzed by studying their scattering patterns. In a dynamic sample with scattering particles, the measured light intensity will vary over time as particles diffuse in random directions. A quantitative measure of this fluctuation can be obtained by defining a statistical average of the temporal autocorrelation function of the scattered electric field, which expresses the displacement of moving particles integrated over time:

$$g_1(\tau) = \frac{\langle E(t)E^*(t+\tau)\rangle}{\langle E(t)E^*(t)\rangle} \tag{2.17}$$

here $g_1(\tau)$ is the normalized temporal autocorrelation function of the scattered electric field, τ is the autocorrelation delay time, T is the exposure time of the image, $E(t)$ is the time dependent electric field and $E^*(t)$ is the complex conjugate of $E(t)$. Instead of measuring the complex field, which is the result of the superposition of many other fields arriving at the detector, we record the speckle intensities in practical situations and quantify it using the normalized temporal intensity autocorrelation function:

$$g_2(\tau) = \frac{\langle I(t+\tau)I(t)\rangle}{\langle I(t)\rangle^2} \tag{2.18}$$

The measured temporal autocorrelation of intensity, $g_2(\tau)$, is related to field correlation, $g_1(\tau)$, through the Siegert relation [80]:

$$g_2(\tau) = 1 + \beta[g_1(\tau)]^2 \tag{2.19}$$

where β is dependent on the measurement setup and the laser stability. In an ideal situation, it can be assumed to be equal to one [81]. The direct measurements of temporal statistics has been traditionally used in DLS. In order to have a good signal to noise ratio, several averages of $g_2(t)$ over a certain image pixels (speckle) would be required, applying long acquisition time [82]. There is another statistical parameter used to measure the time fluctuation dynamics of speckle images, the speckle contrast. The speckle contrast (K) is defined as the ratio of standard deviation (σ) over the average intensity fluctuations ($\langle I\rangle$), of the intensity fluctuations,

$$K = \frac{\sigma}{\langle I\rangle} \tag{2.20}$$

The speckle contrast, K, a function of exposure time and the auto-covariance of the intensity temporal fluctuation $C_t(\tau)$ in a single speckle has been defined: [83]

$$K^2 = \frac{\sigma^2(T)}{\langle I\rangle^2} = \frac{1}{T^2\langle I\rangle^2}\int_0^T\int_0^T C_t(\tau-\tau')d\tau d\tau' = \frac{2}{T\langle I\rangle^2}\int_0^T(1-\frac{\tau}{T})C_t(\tau)d\tau \tag{2.21}$$

The auto-covariance is defined as:

$$C_t(\tau) = \langle I(t) - \langle I\rangle_t][I(t+\tau) - \langle I\rangle_t]\rangle_t \tag{2.22}$$

where $\langle\rangle_t$ is the time average of the quantity. The relation of the auto-covariance to the temporal autocorrelation is defined as :

$$g_2(\tau) = 1 + \frac{C_t(\tau)}{\langle I\rangle_t^2} \tag{2.23}$$

The use of $g_2(\tau)$ is convenient to define the relation between the velocity of the scattering particles and the influence of the scatterer velocity distributions. The scatterer velocity distribution can mainly be considered as Gaussian or Lorentzian. The Lorentzian distribution is appropriate only for Brownian motion, while the Gaussian distribution describes single particle dynamics. A comparison of the

contrast calculated based on the $g_1(\tau)$ measured from the two common velocity distribution can be seen in Fig. 2.9. The time averaged autocorrelation, $g_1(\tau)$, of the intensity fluctuations for the case of a highly scattering medium with a Lorentzian velocity distribution has the form of :

$$g_1(\tau) = \exp(-\frac{\tau}{\tau_c}) \tag{2.24}$$

The correlation time, (τ_c), is the actual decay time of the autocorrelation function which is inversely proportional to the velocity of scatterers.

A similar relation can be derived for the assumption of having a Gaussian velocity distribution [84]:

$$g_1(\tau) = \exp(-\frac{\tau^2}{\tau_c^2}) \tag{2.25}$$

We calculated the relation between the contrast and the correlation time at a given

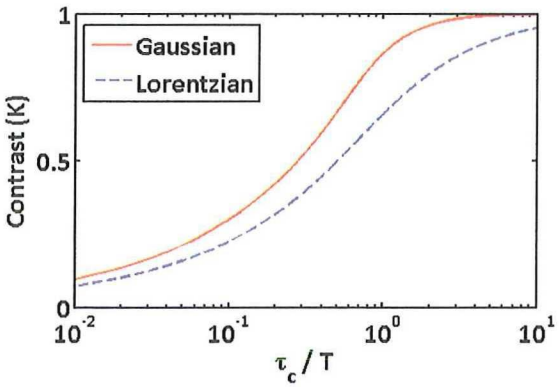

Figure 2.9: The plots of two velocity distribution, Gaussian and Lorentzian, show a noticeable difference between the measured contrast and the ratio (τ_c/T).

exposure time for these two different velocity distributions and the result is shown in the Fig. 2.9. The relation shows a characteristic curve with S-shape for both distributions, through the influence of the velocity distribution can be clearly seen. However, in order to describe real blood flow we need an intermediate model. In the case of blood flow, it has been suggested probably a Voigt profile, combination of Lorentzian and Gaussian profiles, would be a better approach, but in reality there are still more complex factors to considered [84]. To be able to convert the measured contrast of an image into more quantitative parameters we need to consider the important effect of perfusion. As the measured contrast does not only depend on velocity of the moving particles, but also on the concentration and number of particles. Several models relate perfusion to velocity measurements, but they are either not experimentally validated or suffer from several limitations [85]. In order to separate these two parameters, velocity and concentration, a more in depth study need to be done.

2.3.1 Theory of fractals

In a speckle image, a large number of wavelets contribute to form a dark or bright spot in the image plane. The contributing waves have encountered various path lengths on the surface or inside the medium. Since the irregular structure of scattered light patterns carry information of the underlined phenomena, fractal analysis can be adapted to describe the properties of dynamic speckle. Fractal analysis is usually applied to complex images as long as they cover certain features. The essential properties of fractals, self-similarity, scaling and non-integral dimension are often seen in speckle images [86,87]. The fragmentation of the image resembles a structure where smaller pieces can reproduce the statistical properties of the entire image. The fractal classification can vary depending upon the object of study. One major distinction can be between regular or exact fractals and random or statistical fractals. Exact fractals have features that replicate on different scales whereas an object is a statistical fractal when only the statistical properties of the object replicate on different scales. There are many physical systems to have the characteristics of being statistical fractals and scattering of coherent light from diffuse media formed into speckle patterns also fall in this category.

The study of certain properties that do not change as an object undergoes continuous deformation is described by topological dimension. This is represented by an example of Koch snowflake where the topological dimension stays the same even as the curve gains more complexity [88]. However, the fractality of the curve can reveal another dimension which mainly reflects the properties of the evolving curves and characterizes their texture. Fractal has been first introduced by Mandelbrot to describe common shape profile in nature. The study of fractals in nature can vary from studying coastlines, heartbeats, snowflakes to the capillary network in lungs. The word 'Fractal' comes from the Latin word fractus meaning irregular segments. To quantify irregularity as a term of roughness of an object, scale is of a major importance as it can be seen in the Fig. 2.10. Although the same image of a hand is shown, the scale variation can have an impact on the image and change the perception of roughness [89].

To address this issue and to quantify scaling, fractal mathematics has been established. Fractal dimension is a scale invariant parameter that has been used to quantify the roughness of objects. This dimension describes how densely the object occupies the space it lies in. Euclidean geometry is a common tool to describe object properties. In this case, the dimension of a finite point is zero, a line is one and plane or surface is two. The nature is full of such complex systems that can not be studied in terms of simple primitive structures and these usual dimensions can not be used in case of objects with fractal properties. To define the fractal dimension, imagine a line with length of ϵ can be segmented into N similar pieces of length $1/\epsilon$, so we need a magnification of ϵ to get the length of the original line. So the number of segments is $N = \epsilon$. A similar concept can be applied to a square with a side length of one, where a grid of small squares with side length of $1/\epsilon$, is required to fill the whole square. Then $N = \epsilon^2$ squares are required to fill the unit square. To generalize this concept [90, 91], for the object

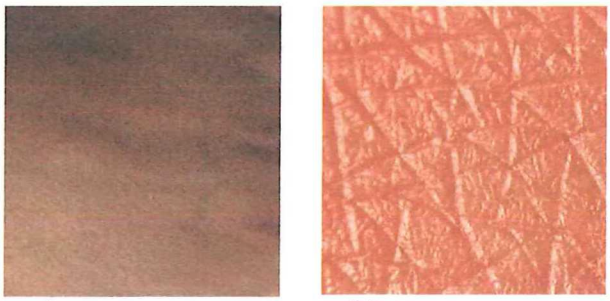

Figure 2.10: Scale variation and its influence on the object appearance. The image of skin taken at different scales a) and b) shows the importance of scale.

with a measure of D we need the $N \sim \epsilon^D$ units to occupy it, where the object dimension is calculated as:

$$D = \log N / \log \epsilon$$

This fractal dimension is usually referred as *Similarity* dimension but it can not be generally applied. As not all the fractals are strictly self similar or topologically flexible. A deformed square should still have a dimension of two which this definition can not fulfill.

There exist many practical methods to estimate the fractal dimension. One of these is the Divider method [92]. As it can be seen from the name, this is based on the implementation of a walk along the line and recording the number of steps required to cover the line. This approach is then systematically repeated for different step sizes. Then a relation can be found between the step size and the total length. So the line with a length of L can be defined with N number of steps with dependent size r. If the data follows a fractal model, then the calculation of fractal dimension is given by:

$$L(r) = Fr^{1-D} \tag{2.26}$$

where D is the fractal dimension and defines how the roughness changes with the scale of observation and F is a constant which shows the steepness of the profile. Plotting $L(r)$ versus $log(r)$ in log scale, the plotted line has a slope equal to $1 - D$. This approach suffers from theoretical and practical limitations. The main problem is that usually non-integer number of steps is required to cover the whole length which has been commonly solved by adding a fractional step length. Furthermore, the initial and final step must be carefully chosen.

The dimension estimation using box-counting is the most frequently used method as it can be applied to multidimensional data. This method computes the fractal dimension by subdividing the image with multiple boxes of a specific size and

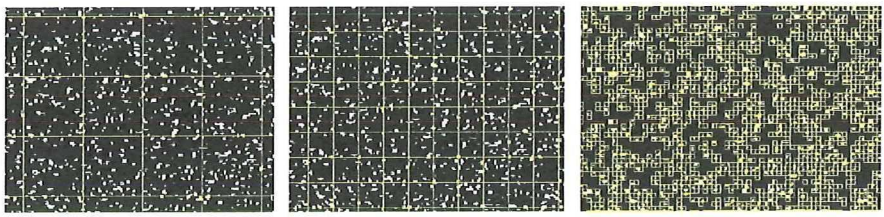

Figure 2.11: The technique of box counting is illustrated with arbitrary unit of sampling size.

estimating how many of them are required to cover the entire object [93]. This process is repeated for a range of sizes. An example of how this is done with a speckle image is shown in Fig. 2.11. If $N(s)$, number of boxes, is estimated across a range of s, then there should be linear relationship between $log(N(s))$ and $log(1/s)$, where the measure slope is an indication of the fractal dimension. The fractal dimension can be written as:

$$FD = \lim_{s \to 0} \frac{logN_s}{log(\frac{1}{s})} \tag{2.27}$$

2.4 Data analysis

In this section we provide a summary of the methods for analyzing the speckle patterns that will be used in the rest of the thesis. In this work, we are mainly studying the time calculation of speckle patterns to study the dynamics of pulsatile flow.

2.4.1 Laser speckle contrast analysis

One of the methodologies for analyzing time fluctuation dynamics of speckle images, is based on laser speckle contrast, Eq.(2.20), which was first introduced by Briers and Webster [94]. In this method, speckle images have been recorded using a camera with an exposure time (typically 1 to 20 ms). In each acquisition, the time integrated speckle images are recorded with blurred speckle patterns. This is due to the integration time being longer in comparison to the speckle decorrelation time, induced by the motion of scatterers [95]. This blurring of the speckle data is quantified by the contrast term, to study the dynamic evolution of the motion. The contrast would have lower value in case of a sample which has moving scatterers due to the fact that the standard deviation of the intensity would decrease while the average intensity remains constant. The main schemes of analyzing the speckle images from raw data are temporal, spatial or a combination of these two.

In the temporal case, a pixel based calculation is made on a sequentially collected speckle images. For the spatial case, the speckle is computed using a single speckle image by sliding a window over the image. In this case, a super pixel of $N \times N$ pixels, where N is an odd number, is chosen such that the contrast value is determined by the central pixel. A typical value of 5 or 7 pixels is usually chosen. A more detailed description can be found in reference [66, 95].

2.4.2 Correlation based analysis

To quantify the rate of speckle fluctuations we measure the correlation coefficients between the successive speckle frames over time. The statistical properties of speckle are studied as space-time cross correlation in the imaging (observation) plane. Based on the correlation models, the degree of variation can be converted to a correlation coefficient. To do so, we measure correlation coefficient for each frame [96]:

$$cc = \frac{\sum_{m=1}^{N}\sum_{n=1}^{N}(f_{mn} - \bar{f})(g_{mn} - \bar{g})}{\sqrt{\sum_{m=1}^{N}\sum_{n=1}^{N}(f_{mn} - \bar{f})^2}\sqrt{\sum_{m=1}^{N}\sum_{n=1}^{N}(g_{mn} - \bar{g})^2}} \tag{2.28}$$

where $f_{mn}(m, n = 1..N)$ is the raw image intensity for a given pixel in a frame which is correlated with the raw image intensity for a given pixel in a subsequent frame g_{mn}. Here N indicates the number of pixels in a frame row or column, which was equal in the present work. This is calculated for the entire time sequence. The average value for each matrix is denoted by $\bar{f}$ and $\bar{g}$ respectively. The two dimensional correlation coefficients have been calculated for all the pixels in the speckle image data and result in a value ranging from 0 (uncorrelated) to 1 (fully correlated). As the particles scatter more, the signal fluctuation increases and the average correlation value decreases. Applying correlation analysis for speckle measurements can be limited as it depends on the resolution of the system and the amplitude of the motion. In case the speckle motion between successive frames falls into only a fraction of a pixel, a better sampling rate and higher resolution would be required to use this technique.

2.4.3 Fractal based analysis

The original idea of box counting has been extended to differential box counting (DBC) by considering an image as a surface where its height is proportional to its image gray value or intensity. In comparison with other methods, DBC has its advantage due to its simplicity [97, 98]. This is a good measure of how structure or coarseness is distributed on a surface area and can be clearly related to the spatial distribution measured in a speckle pattern. The time evolution of the fractal

dimension is then applied in studying dynamical systems. In our analysis, the differential box counting has been carried out on the speckle images to extract the fractal dimension. An example of the speckle image recorded with pulsatile flow is shown in Fig. 2.12, along with the image transformed into the corresponding fractal image.

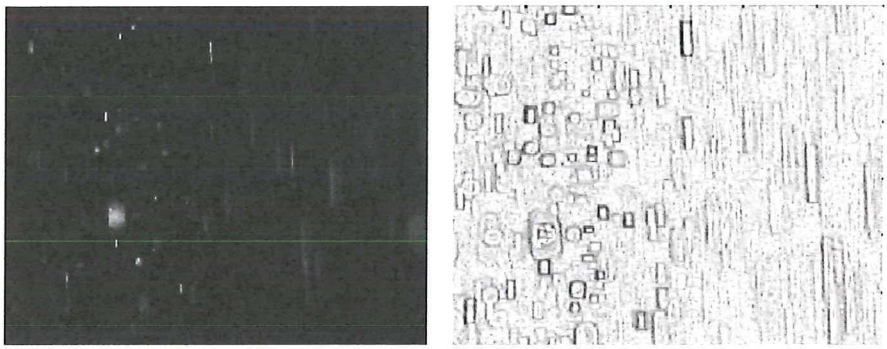

a) b)

Figure 2.12: a) Raw speckle image of pulsatile flow. b) The speckle image converted to corresponding fractal image.

This method was first proposed in [99]. In the present work, a speckle image is considered as a $3D$ spatial surface where two coordinates are the spatial coordinates of the pixel and the third one is the gray level. The original speckle images are transformed to the fractal images. For differential box counting for a image of size M divided in $3D$ space into blocks $(s \times s \times s')$ where, s, is the size of the square and, s', is gray level of the block. If the total gray level of the image is G then we can write $\frac{G}{s'} = \frac{M}{s}$. To determine the required thickness of the blanket needed to cover the image surface we need to know that the minimum gray level falls in the box number k and the maximum gray level falls into box number l. Then the thickness of the blanket coverage on the grid (i, j) is:

$$n_s(i,j) = l - k + 1 \tag{2.29}$$

The total number of boxes is calculated for different values of s as:

$$N_s = \sum_{\substack{1 \le i \le M/s \\ 1 \le j \le M/s}} n_s(i,j) \tag{2.30}$$

The fractal dimension was calculated for each image from the slope of the linear regression line fit to the log plot of total number of boxes N_s versus the dimension scale or the box size s. This approach is mainly used in medical setting for feature extraction [100]. To study dynamics, a time series of fractal dimension has been used to determine the corresponding frequency spectrum.

2.5 Summary

In this section, we introduced laser speckle imaging which is an attractive tool to map blood flow using simple setup. The recorded speckle bears an imprint of the flow properties, however measuring absolute flow velocity is fundamentally difficult using LSI. To estimate the velocity of flow using speckle images, DLS theory is applied. In this approach, the fluctuations of moving scatterers is described by auto-covariance of scattered light, which statistically describes the correlation between light intensities with a time delay. This can be further related to the measured speckle contrast but its dependency to flow distribution model was explained. Finally, the methods that will be used in this thesis for analyzing the recorded speckle images were introduced. In the next chapter, we will describe the experimental setup with different phantoms and scattering mediums that were used in our measurements. We will address the influence of several parameters on the measured contrast for steady and pulsatile flow under different experimental settings.

CHAPTER

3 Experimental setup for fluid parameter analysis

It doesn't matter how beautiful your theory is, it doesn't matter how smart you are. If it doesn't agree with experiment, it's wrong.

Richard P. Feynman

Flow measurement is a complex problem and many different aspects of it can be addressed. The particular behavior of flow can be due to complexity in the geometry or fluid dependent properties. To monitor flow using an optical technique as laser speckle, a careful systematic study need to be done. It was seen from previous chapter that speckle patterns are generated by interference of scattered wavefronts and these pattern can change due to movement of scattering particles. However, there are several hidden factors that can influence quantitative studies using measurements of these speckle patterns. This chapter presents several experimental methods to isolate each one of the presented parameters. The parameters that have been studied here are changes in flow rate of fluid, difference in optical properties of medium and presence of static scatterers, concentration and density of scattering particles, and additional changes in the flow which are created by changes in flow volume rather than velocity of the particles. We describe the experimental setup used for laser speckle measurements to address the influence of some of these factors in our measurements using speckle patterns. These experiments were mostly done for the steady flow. Furthermore, we show the possibility of measuring a pulsatile flow in a scattering medium. In this chapter, we also provide a description over different experimental setups that will be used in the remainder of the thesis.

3.1 Experimental setup

In this section, an overview of different parts of experimental setup will be given. The main components of the system are illumination source, flow phantoms and optical acquisition. In order to set the experiment based on biomedical flow characteristics, certain conditions of flow need to be addressed first. Two different scattering liquids have been used which is explained in details in the section 3.2.

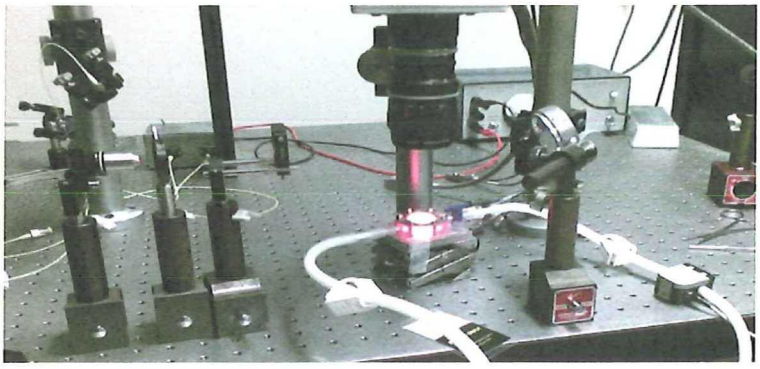

Figure 3.1: The laser speckle experimental setup for flow measurement: The flow cell containing milk flow is illuminated using the laser light and the speckle patterns are recorded from top through the imaging system.

The experimental setup for laser speckle measurements is shown in Fig. 3.1. For illumination, we used 30 mW Helium-Neon laser (MellesGriot) at wavelength of 633 nm. The output beam is collimated and passed through a lens, creating a circular and uniformly distributed beam shape. The beam is directed to the sample using the beam steering mirror. The speckle patterns are recorded with the high speed camera (Photron $SA3$, model $120K-M2$) located vertically at the 20 cm distance from the flow system. The captured images are saved, digitized (RAW format, 12 bit) in to the PC and further processed with Matlab.

3.1.1 Flow generation

Two sets of flow systems have been used to study flow, one enables a simple pulsatile and steady flow while the other flow system simulates the human cardiovascular flow. In each system, measurements are done for both steady and pulsatile flow. For the steady flow, the flow cell is accompanied by a velocity pump and works based on the Bernoulli's principle. It consists of two containers which can be set at different heights and thus creates a flow rate. The pump is capable of generating flow at the range of $0-110$ ml/min. This is monitored by measuring the flow rate in tube with an ultrasound sensor based on the Doppler shift theorem. To generate a pulsatile flow with a controlled frequency in our flow cell, we used a roller pump (Minipuls®3) using five rollers. In the second flow system, we

created a more realistic pulsatile flow, where we use a Medos Ventricular Assist Device (VAD) including the driving unit and ventricular pump, connected to a flow setup which is compatible for different working fluids. This system creates a realistic flow profile of human heart beat pulse waveform. A complete schematic of the flow loop of this system is shown in Fig. 3.2. This system has the option of enabling a pulsatile or steady flow. To study a wide range of flow regimes, a bypass valve and mechanical control valves were installed. The system also has an air ventilation so that it can be easily filled and maintained in an air bubble free state. The electromagnetic flow meters (MAG-VIEW, model MVM-005-Q) were coupled to the system and used for real time monitoring of flow rate. In the VAD settings, we used a systolic pressure (Psys) of 270 $mmHG$ and diastolic pressure (Pdias) of -30 $mmHG$ with a systolic time interval of 35 (%) with a ventricular pump of 60 $ccm\,(ml)$ volume. The frequency of the cardiac pulsation is set for 40 beats per minute corresponding to 0.67 Hz.

3.1.2 Flow properties

There are two important parameters in pulsatile flow studies, which are the Reynolds number (Re) and Womersley number (α). The Reynolds number describes the ratio of inertial forces to viscous forces in a flowing fluid and is defined as:

$$Re = \frac{v_s L}{\nu} \tag{3.1}$$

where v_s is the time averaged velocity, L is the characteristic length (in present case this is the diameter of the cylinder or diameter at the inlet of the carotid artery), and ν is the kinematic viscosity of the fluid. Reynolds number is directly proportional to velocity and inversely proportional to viscosity. The measured values in different parts of the human circulatory system shows that blood flow in majority of vessels follows a laminar behavior [101]. In general, laminar flow has a regime of $Re < 2000$ where the pulsatile flow results in a lower Reynolds number compared to the steady flow [102]. The mean Reynolds number of 512 was estimated for our glycerol solution at fluid temp of 25^oC.

The Womersley number is a dimensionless number which relates the pulsation frequency to viscosity. It is often used in biofluid mechanics, and in general where there is a non-constant pressure gradient flow in the system, like in case of heart pump flow. This value in healthy humans can vary between 1 and 12.5 which is influenced by the physiological condition of human body [103]. The Womersley number is dependent on the pulsation frequency and physical properties of the vessel, and is defined as:

$$\alpha = R\sqrt{\frac{\omega}{\nu}} \tag{3.2}$$

where ω is the angular frequency given by the frequency of pulsation (f) as $\omega = 2\pi f$ and R is the pipe radius. In this measurement, the flow with a Womersley number

of 4.5 has been studied. In these set of measurements, we have been trying to keep both the Reynolds and Womersley numbers in typical range that is found in the human carotid artery.

The outflow division between the Internal Carotid Artery (ICA) and the External Carotid Artery (ECA) has been defined as:

$$\gamma = \frac{Q_{ICA}}{Q_{ECA}} \tag{3.3}$$

The division of flow between the internal and external branches varies during the cardiac cycle. The flow has been regulated with two additional valves, where the outflow division ratio of 50/50 between internal carotid artery and external carotid artery.

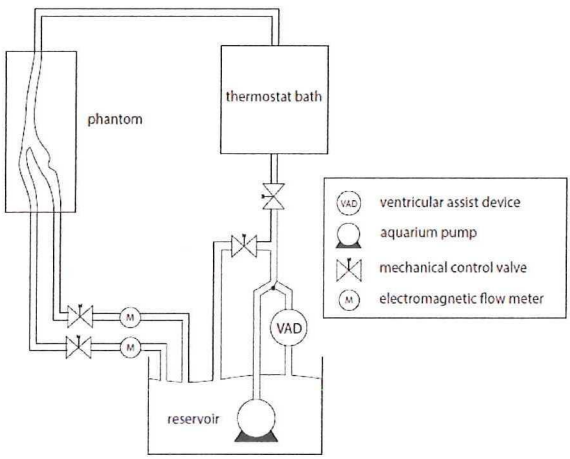

Figure 3.2: The schematic of the experimental flow loop including the phantom, pump (VAD), few mechanical valves and electromagnetic flow meters.

3.2 Fluid properties

The two flow systems used different scattering fluids since we were interested in separate physical effects. These fluids are described blow.

3.2.1 Glycerol Solution

The glycerol solution is commonly used to mimic blood flow, as it is easy to use, non-toxic and dissolves easily in water. The liquid we used is a mixture of water and glycerol, so there is a refractive index match between the working liquid and

the Polydimethylsiloxane (PDMS) phantom. To visualize the flow in an optically transparent platform, we needed to use tracer particles. Choosing the right seeding particles is the most important parameters as the particles have to fit different requirements to be suitably detected using all the techniques while keeping the desired flow characteristics. In case of using water as fluid, the commonly used tracers particles are either the hollow glass or polystyrene spheres with a diameter size of 2 to 20 μm.

3.2.2 Milk

The other scattering fluid we used was milk. Milk was used as it is cheap and easy to work with it. It also mimics the blood flow as the fat particles in milk scatter light similar to RBCs in blood [104, 105]

3.3 Experimental phantoms for flow study

The flow cell is primarily a phantom to study the flow. The flow conditions can differ depending upon the geometry of the phantom. In this section, a description of three phantoms with their particular geometries is given. The three phantoms were a rectangular channel, a straight cylindrical tube and a carotid artery like phantom. The rectangular phantom has been used in many experiments, as the phantom components were made in several copies and it has the flexibility of measuring different parameters when the measurement conditions were similar.

3.3.1 Rectangular based phantom

The rectangular flow cell, including its components is shown in Fig. 3.3. It consists of a base plate, rectangular shaped insert and a top membrane. As can be seen in the Fig. 3.3(b), the flow cell has a semi-rectangular channel with a length of 20 mm and a depth of 1 mm to represent a homogeneous, thin layer of flow. To characterize and mimic the skin optical properties, a diffuse scattering Delrin window ® (polyoxymethylene, POM) is used as the top membrane of the cell [106]. However, to create a reference platform, a glass window is used which lowers the chance of measuring the static scatterers. The insert is made of polycarbonate which models a flow channel with different thickness of 0.5, 1 and 2 mm. The insert is mounted on the stainless steel basis, and the bottom material of this channel is defining the amount of light which can be absorbed or reflected. The flow cell can have two configurations depending upon the requirements of the experiment. The channel can be made flexible, allowing for volume changes with pulsation mimicking blood vessels or made rigid, having only velocity changes. This is done by replacing the bottom layer with a flexible silicon membrane or a rigid material.

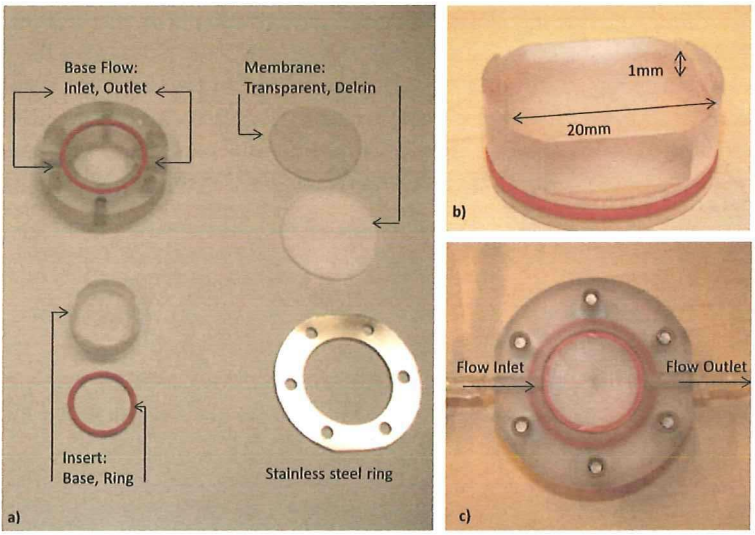

Figure 3.3: Flow phantom: a) Components of the flow sample: the base flow cell with the inlet and outlet, the rigid insert that is placed in the base flow cell defining the channel depth, the flow cell membrane which can be either transparent or Delrin and the stainless steel ring which is used in bottom and top to fix the flow cell. b) The insert with the flow channel. c) An assembled version of the flow cell.

3.3.2 Straight cylindrical based phantom

To create a straight cylindrical tube, made of cured PDMS, a wax candle with outer diameter of 20 mm was used as a mould to case the PDMS. This can be seen in Fig. 3.4. We use an aqueous glycerol solution with the same refractive index as our phantom housing ($n = 1.413$). This was done for refractive index matching which can be seen in the Fig. 3.4(b). This technique is commonly used in PIV and is also beneficial in laser speckle images to avoid extra scattering due to sample structure irregularities at the boundaries.

3.3.3 Carotid artery based phantom

To create the carotid artery phantom, a $3D$ wax print of the artery of a patient was made. The geometry of the patient specific carotid artery was obtained using a Computed Tomography (CT) scanner images of a patient suffering from atherosclerosis. This has then been used as a mould for casting the PDMS liquid. The wax was removed without applying any heat to avoid any diffused wall effect and results in a clear phantom. To have the phantom compatible for PIV measurements, we use an aqueous glycerol solution with the same refractive index as our phantom housing ($n = 1.413$). The effect of refractive index matching can be clearly seen in the Fig. 3.5(b).

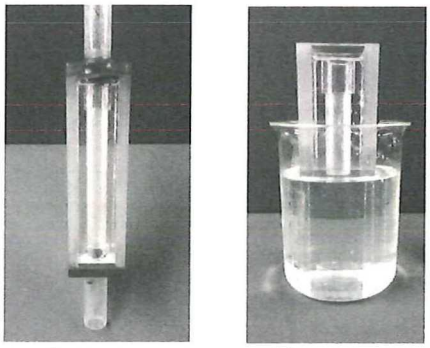

Figure 3.4: Straight cylindrical flow phantom: a) in water and b) with refractive index matched solution. The extra scattering due to irregularities in the boundaries are removed due to index matching.

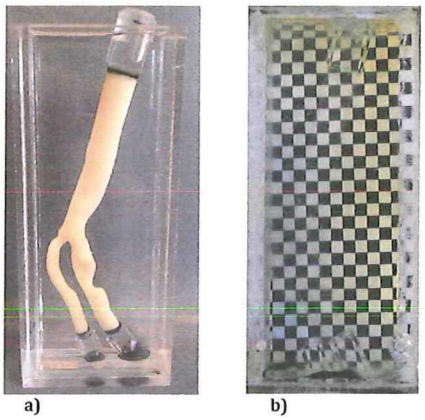

Figure 3.5: Flow phantom of patient based carotid artery: a) in water and b) with refractive index matched solution. The extra scattering due to irregularities in the boundaries are removed due to index matching.

3.4 Flow analysis and contrast dependent flow variables

We initially conducted experiments to study the steady flow and how that relates to the speckle measured contrast. We analyzed the data using the spatial speckle contrast approach mentioned in section 2.4.1. The recorded raw speckle images were converted to speckle contrast using a spatial window of 7×7. In most of the measurements, a combination of boiling and translation is observed in the recorded speckle data. Pure boiling only happens at the focus of the imag-

ing plane [107]. In case the object has motion with a uniform velocity boiling of speckle is more dominant. The use of spatial analysis for an event evolving in time is based on ergodic assumption that statistics of the spatial and temporal variations are the same. However, this would mean the absence of dynamic changes and that the contribution of the static scatters is negligible during the multiple exposure measurements. However in medical setting, due to good time resolution of the capture of the images of rapidly changing flow dynamics, spatial contrast is commonly used as a quantitative parameter. For a full field technique such as laser speckle imaging, speckle contrast is measured over a region of interest. To be able to evaluate the relative measured speckle contrast for different experiments, a good understanding over the medium and its dynamics is required. It has been mentioned in chapter 2, there exists a large literature on the study of speckle and widely applied models to relate the measured contrast to the speckle decorrelation. Each of these models is based on several assumptions of single or multiple scattering. The lack of a realistic model of a dynamic system as human body with all the complex cardiovascular structure in the tissues, forces further research into this field for future medical devices. The overall measured contrast reflects many other measured parameters while reflecting the dynamics of moving scatters inside a micro vascular network. This chapter includes several experiments which have been done for a systematic set of parameters: flow rate, concentration of scattering particles, volume of scattering fluid and influence of static scatterers by measuring the speckle contrast with respect to each parameters. We then continued with the experiments and simulated the pulsatile flow. Along with the speckle contrast we also used the correlation analysis. These measurements were done to study two important factors of having different top membrane, which is then a static scattering layer and also including volume changes in the measurements.

3.4.1 Steady flow analysis

We first describe the result of experimental study on the steady flow which has no pulsation properties.

Influence of Flow rate

This set of measurements have been done for different flow rates and we use glass as the top membrane. In the Fig. 3.6, the speckle contrast has been measured at each exposure for a stack of images. The plot shows the result of the contrast measured for the flow rates of 10, 20, 30 and 40 ml/min which has been measured with exposure time ranging from 0.3 to 2 ms. The exposure time is one of the primary factors which determined the flow dependent parameter in the calculated contrast images. For long exposure times, speckle contrast approaches zero, while the blurring of the image freezes at very short exposure times and the value of contrast would be closer to one. This result shows a good agreement with theory, where you expect to have the maximum measured contrast for the no (directional) flow case and as soon as you have flow in the system the contrast starts to drop.

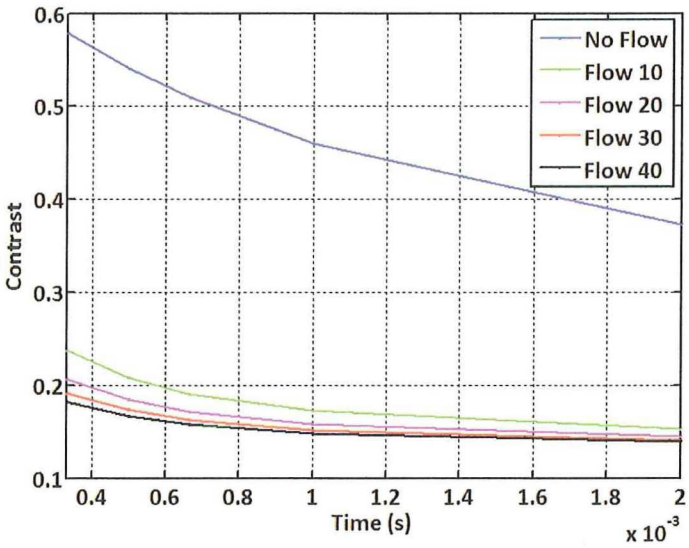

Figure 3.6: Changes in speckle contrast are measured for a range of exposure times and shown for different flow rates (ml/min). These measurements were done using glass as the top membrane. For the case of no (directional) flow, the highest speckle contrast is measured and the contrast level decreases as the flow rate increases.

Influence of static scatterers

One of the problems of linking scattering dynamics to fluctuations in a system is the influence of different parameters which can not be easily separated. Due to structural complexity of the tissue, there is a contribution of the static components which in reality can be due to different layers of the skin or bone for instance [81,108]. To study the influence of scattering layers, two sets of measurements have been done using two different top membranes of Delrin and glass. The comparison was done for two cases, one having flow and the second no flow, only Brownian motion. The result of these measurements is shown in Fig. 3.7.

By comparing these measurements, we can observe the influence of the static scattering layer but also the differences in the shape of the plots in case of Brownian motion or directional flow. In both cases of having flow and no flow, the measurements with a Delrin membrane are measured with a higher spatial contrast as it contains a layer of static scatterers. In case of no (directional) flow, where only Brownian motion is present, a higher contrast is measured for both Delrin and glass membrane compared with the case of directional flow. This is also caused due to monitoring a larger number of static scatterers, which raise to a higher contrast level. The multi scattering effect due to motion causes the speckle

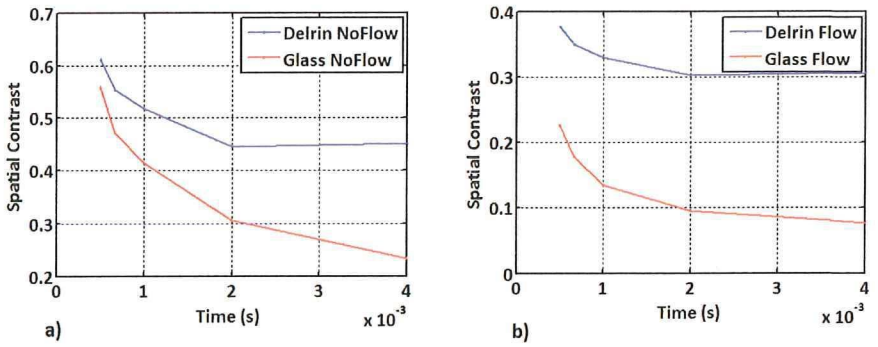

Figure 3.7: Changes in speckle contrast are measured for a range of exposure times and show the influence of static scattering layer: Glass and Delrin were used as the top membranes. These measurements are compared for case of a) no (directional) flow and b) flow with a given flow rate.

to blur effect, so the contrast level decreases. For a higher exposure time (T), the influence of averaging speckle contrast over a longer time interval, is measured with a lower level of speckle contrast.

Influence of scattering particle concentration

Another parameter which plays a role in these measurements, is the concentration of scattering medium. In order to check the effect of scatterer concentration on the speckle contrast, we did two sets of experiments in which we directly changed the concentration of the particles by diluting the milk. Another approach is to have same concentration level but more particles was due to change in channel depth, leading to more fluid volume. The first experiment is shown here. To study the effect of scatterer concentration on the speckle contrast, a multi-exposure measurement was done with full milk (100%) and for the diluted milk with full milk percentage of (80, 60, 40 and 20%). Each measurement was repeated under the conditions that only one variable, in this case the concentration level changes. The measurement was done with a glass membrane on top which does not include any static scatterers.

The result of the experiment can be seen in Fig. 3.8(a) for the case of no flow. The same set of measurements with the same concentration levels of milk was repeated for the case of flow and this can be seen in Fig. 3.8(b). It can be observed that not only the plot shape changes, but also it becomes more difficult to distinguish on different concentration levels, specially in the case of no (directional) flow. Same series of measurements have been done for the case of flow by replacing the top membrane with Delrin. All these measurements were done with a milk flow rate of 30 ml/min.

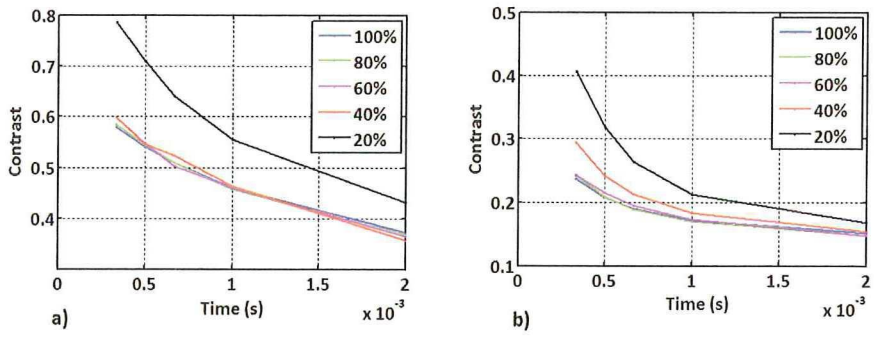

Figure 3.8: Changes in speckle contrast are measured for a range of exposure times and show the influence of concentration (fat particles in milk). These measurement were done in the phantom with a glass membrane and is compared for the case of a) no (directional) flow and b) flow with a given flow rate.

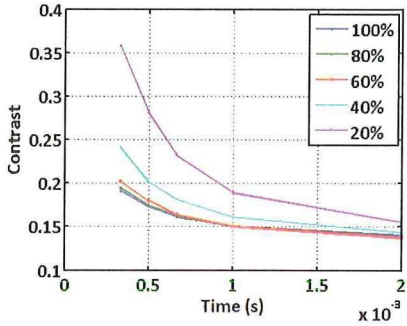

Figure 3.9: Changes in speckle contrast are measured for a range of exposure times and show the influence of concentration (fat particles in milk). These measurement were done in the phantom with Delrin as membrane, for a flow with given flow rate.

It can be seen in Fig. 3.9 that changes in the measured speckle contrast has a similar behavior as the previous measurements which were done with glass membrane, meaning that the measured contrast decreases with increasing the concentration levels. However, these are the results of having the flow in the system as it is rather difficult to distinguish any difference in the concentration level in case of no (directional) flow and using Delrin as the top membrane.

Influence of volume

In order to evaluate the influence of volume changes in the steady flow, we use different insert levels in the flow cell. These inserts were made with same material

and only different thicknesses so that the changes in fluid depth can be monitored.

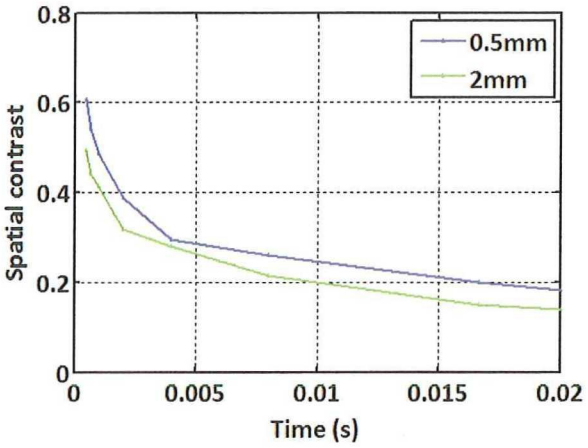

Figure 3.10: Changes in speckle contrast are measured for a range of exposure times and show the influence of channel depth (insert thickness in flow cell). These measurements were done with no (directional) flow.

In the Fig. 3.10, we observe the result of measured contrast for insert thickness of 0.5 and 2 *mm*. In the case of 2 *mm* depth, there is a thicker milk volume in the flow cell, such that a lower contrast is measured. One of the hypotheses for this observation is due to multiple scattering. Although in both cases same level of concentration for fluid has been used, the thickness of fluid plays a similar behavior in measured contrast and shows the sensitivity of speckle contrast to volume of scattering medium.

3.4.2 Pulsatile flow analysis

For the case of pulsatile flow, a series of measurements were carried out in the same phantom using Delrin and glass as the top membrane. We also report the result of measurements which have been done in a flexible phantom to see the influence of volume changes in addition to the velocity of the moving scatterers.

Influence of volume changes

In order to simulate the *in-vitro* heart rate, we generate pulses at the rate of 1 Hz in milk using the roller pump. To study the behavior of the simulated signal, the measurements were done on the flow sample using both the rigid and flexible channel. In the case of the rigid channel, we only monitor laser speckle contrast variation with respect to velocity changes caused by the roller pump. In comparison, in the flexible setting we add one more variable which is the variation

of fluid volume. The results of the measurements are shown in Fig. 3.11. On the top panel of the figure, the fluctuation of speckle contrast for pulsatile flow in a rigid channel is shown, both in temporal and spectral domain. It can be seen that there are harmonics of the main frequency of pulsation (1 Hz). This is caused by the squared pulse shape generated with the roller pump.

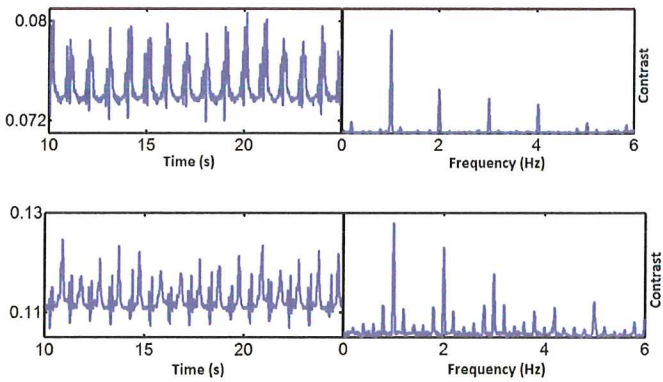

Figure 3.11: Speckle contrast variation in time and spectral domain are shown for a milk pulsation of 1 Hz for a rigid (upper plot) and flexible membrane (lower plot).

The lower plot in Fig. 3.11 shows the fluctuation of speckle contrast of the pulsatile flow in a flexible channel both in time and spectral domain. By comparing the result of both measurements, in case of phantom with flexible membrane, the volume changes can be seen as an additional modulation in the signal. This is clearly visible in the lower plot. These measurements were done using a Delrin membrane with a thickness of 1 mm.

Influence of static scatterers

In order to show the influence of scattering medium on the measured signal, another series of measurements were done with glass membrane, which contains no static scatterers. In this measurement, correlation analysis as mentioned in section 2.4.2, where used as a comparison to the speckle contrast. The Fig. 3.12 shows the effect of having different materials in top membrane, using speckle contrast (left panel) and correlation based analysis (right panel). Both of these analysis show a more clear signal using glass as the top membrane (upper plot) while the signal appears to be more distorted when we use Delrin as the top membrane (lower plot).

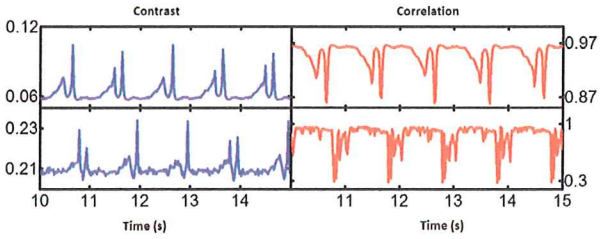

Figure 3.12: The effect of medium is shown for milk pulsation of 1 Hz using glass (upper plot) and Delrin (lower plot) based on a) speckle contrast and b) correlation analysis.

3.5 Summary

In this chapter, we presented some features of our flow setups and how they can be monitored using laser speckle technique. We analyzed the influence of different parameters on the flow, such as changes in flow rate, concentration, static particles and pulsatile flow. In each measurement, the time integrated speckle images have been recorded with a specific exposure time. The motion in flow, makes speckles appear blurry due to longer integration times compared to the speckle decorrelation time. This effect has been recorded along with changes of certain parameters in the setup. To proceed with the analysis of flow dynamics for pulsatile flow, we have used the known method of particle image velocimetry as a comparison. It is a non-intrusive full-field technique which can accurately measure velocity maps of the fluid. PIV can measure the properties of the fluid seeded with micron-sized tracer particles. PIV provides detailed quantitative information over flow structure and velocity profiles and LASCA gives an analysis of the flow pulse evolution. Combining LASCA and PIV efficiently can provide a better use of current technologies to make a more efficient tool to study complex flow geometries having pulsatile flow like human circulatory network. This is studied in the following chapter.

Chapter

4

Experimental comparison of two full field optical techniques

there is light enough for what I have got to do.

Charles Dickens (Bill Sikes)

Particle image velocimetry is able to measure fluid by tracking single particles. This technique provides a complete velocity map of flow thorough complex flow geometries which is very useful in studying human circulatory network and diseases which arise there. In this chapter, we study the flow dynamics in a patient specific carotid artery phantom. The common carotid artery, which splits after bifurcation into the internal and external carotid artery, is the major artery connecting heart and head, whose role is to supply the brain with oxygenated blood. It is recognized in medical literature [109, 110] that the majority of the cardiovascular diseases occur in the coronary and carotid artery bifurcations. For example, one of the most common cause of stroke is a blockage (narrowing or stenosis) in the carotid arteries. This behavior is a characteristic of ailments like atherosclerosis [111] which is a common cause of death. Research has shown that the influence of stenosis on hemodynamic parameters bears a direct correlation with this disease. A through and detailed study of hemodynamics can play a major role in diagnosis and early detection of atherosclerosis [112]. This has been a major motivation in conducting a through study with complementary optical diagnostic methods. In this chapter, we are mapping flow dynamics using two optical techniques particle image velocimetry (PIV) and dynamic speckle. The common feature of these two methods is the ability to capture entire optical field for the flow measurement. Furthermore, both approaches are non-intrusive and can be made with no contact with the sample. The LASCA measurements have a high temporal resolution and can study the frequency spectrum of the flow pulse accurately, without any direct imaging. However, PIV provides instantaneous velocity measurements with high

accuracy. Using the technique of PIV in a different geometry, a complete $3D$ velocity map can be constructed. In order to increase the understanding of flow variations at each cardiac pulse, different moments in the cardiac pulse cycle was analyzed for various regions in the carotid artery phantom.

4.1 Materials and experimental setup

In this section, an overview of different parts of the setup will be given. The main components of the system are the illumination source, the flow phantoms, the optical acquisition and analyzing systems for both techniques.

4.1.1 Optical experimental setups

A general setup is shown in Fig. 4.1. This is the main setup which has been used for the PIV experiment. The measurements were done with a double pulse Nd:YAG laser. The Nd:YAG laser output with a 1064 nm wavelength has been filtered for safety and only the laser light at the visible range of 532 nm is used for the experiment. To create a two-dimensional light sheet for illumination of the flow field, a cylindrical and spherical lens were applied to converge the laser beam into an actual sheet with a thickness of 1 mm.

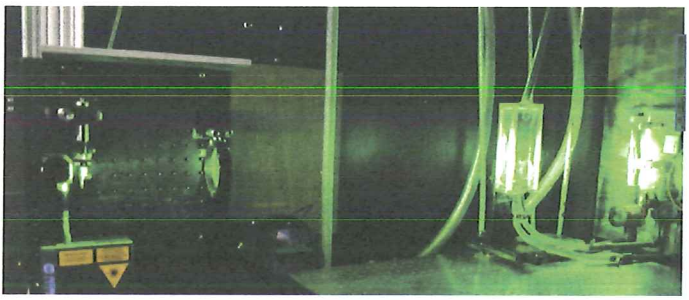

Figure 4.1: The experimental setup illuminated during PIV measurements.

For image acquisition and analysis, a standard PIV-package from LaVision including PIV-camera, frame-grabber and programmable-timing-unit (PTU) was used. The digital camera of LaVision has been used as a high resolution and sensitive camera is crucial for the PIV applications. In order to have an accurate measurement of velocity profile, a good synchronization between the event and the recording of it, is needed, so the pulsed laser is used in combination with a timing unit coupled to the camera. To prevent optical deformation of the laser sheet and thus the images the laser and the camera are perpendicular to each other with respect to the phantom. For timing control, the capturing process and

the analysis of the images, the software package DaVis provided by LaVision was used.

For the laser speckle based measurements, same arrangement was used except for the illumination source and camera. The laser in this case is at 532 nm with 600 mW power and directly illuminates the sample. For our detection system, we used a variable frame rate high speed camera (Photron Fastcam SA3) with the pixel size of 17×17 μm and changeable aperture. Using the F-number of 32 and a magnification factor of 0.5 for the optical system we ensure a good average speckle size of 3-4 pixels.

4.1.2 Fluid

In order to choose a fluid in our experiment, we need to consider its compatibility for both the measurement techniques PIV and dynamic speckle. Besides this the fluid also has to mimic some of the blood flow properties. For the PIV imaging, the main requirements are that solution should be transparent and have the same refractive index as the material used for phantom. The present measurements were done by adding tracer particles, hollow glass balls with an average diameter of 10 μm into the liquid as mentioned in section 3.2.1. In case of PIV, these are the tracer particles. For speckle, the hollow glass particles are main source of scattering of the incoming laser light and creating the speckle patterns. We calibrated the system and the density of the particles using the water as the main fluid. If the flow is seeded sufficiently, a speckle pattern will be formed by the collective scattered light field from the seeding particles.

4.1.3 Phantoms

In order to understand the flow properties, before doing the measurement directly on the main phantom, a set of measurements were done on a simple setup using a straight cylindrical phantom mentioned in section 3.3.2. Then the same parameters were used to study the flow in a carotid artery phantom, which has been described in section 3.3.3.

4.2 Full field optical studies

4.2.1 Particle imaging velocimetry

At present, particle imaging velocimetry is a developed method and is considered as a standard technique for non-intrusive measurements of velocity fields. It is an optical technique which is used for imaging the flow seeded with tracer particles. In comparison to laser Doppler velocimetry, PIV is considered to be less time consuming, being a whole field method and measuring instantaneous flow

field. To monitor flow properties of the fluid, it is important that particles are chosen such that, they do not influence the flow dynamics itself but rather follow it [113]. The technique is based on three possible strategies: a) two images can be captured after a short time, and by knowing the exact timing and applying a cross correlation on the successive images a vector field can be obtained, or b) using two bursts of light, the possible displacement of tracers can be observed in single image and the other approach, c) is again based on one image being taken with short enough exposure time such that the movement of the particles can be visualized. In this work, we are using the first approach so that the cross correlation analysis of two consecutive images can be made. That results in a vector field where two velocity components can be measured using one camera. In this particular work, a sequence of images was recorded by the camera with a fixed time interval. This time interval is dependent on the flow conditions and can be set by the user accordingly. The method used to estimate the average particle displacement and eventually the velocity is based on statistical cross correlation in each corresponding region between the first and the second frames [114]. The recorded images will be divided into interrogation regions. The size of the regions is chosen such that there is almost a uniform motion and displacement of particles. Small fraction volume of particles is used as they should be homogeneously distributed and instead of influencing the flow, they should only follow the flow. In case of high particle density, it would be more difficult to follow individual tracers and might lead to wrong combination of the particles in two images, which lead to noise rather than displacement. The sample has been illuminated with a laser sheet with a thickness of around 1 mm for a beam width of 7 ns. A set of images has been recorded as can be seen in Fig. 4.2 with the time interval of 750 ns between them. The pulse duration is short enough to avoid significant blurring due to motion in the images.

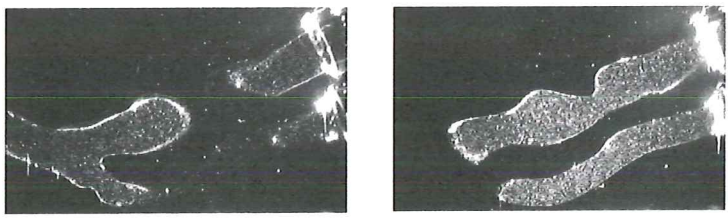

Figure 4.2: Two typical PIV images used for data analysis. The two characteristic cross-sections can be seen with tracer particles arise from two arms of the carotid artery phantom.

To achieve high contrast between the background and scattering particles, also to reduce the noise from background, certain measures are taken and data is processed for noise as explained below. In order to compute the flow vectors, the recorded images were further processed using the software package Davis 6.2. To improve the distinction between light reflected by the tracer particles and the background light, which results in wrong vectors, the average over all sets

of two images was subtracted from each set of two images. After that a mask is applied to the images. The mask removes all the areas where the laser sheet does not cross the artery and results in the much cleaner image of the illuminated tracer particles. A series of these images has been further analyzed using the PIV algorithm. The main principle is based on a standard cross correlation via Fast Fourier Transformation between two images [115]. This program has the option of making multiple iterations with different interrogation sizes to result in an accurate measurement. The different interrogation areas from each image are cross correlated and gives a final signal where the peaks indicate the displacement of each particle. For accurate PIV data analysis, the data should be captured such that an average particle displacements of about eight pixels that travel no further than the interrogation window. With a sufficient number of particle pairs and using a smaller pixel size for the chosen kernel, a more accurate displacement and ultimately a more realistic flow field can be extracted. To ensure, no loss of information we need to make sure that the velocity for each particle is smaller than the side length of the interrogation area, so following the relation:

$$\frac{\frac{s'}{s} V \Delta t}{d_{IA}} < 0.25 \tag{4.1}$$

where $\frac{s'}{s}$ is the image magnification, V is the absolute velocity, Δt is the time interval between the two recorded images and d_{IA} is the side length of the interrogation area. The interrogation window was chosen to be eight by eight pixels with a 50% overlap resulting in a four by four pixel resolution. The camera scales used were 1 pixel per $7.559 \cdot 10^{-5} m$ resulting in a final resolution of 0.3 mm by 0.3 mm. To find the direction and amplitude of the velocity, the displacement of all the tracer particles is determined.

4.2.2 Laser speckle contrast analysis

Laser speckle contrast imaging is based on analysis of laser speckle images as described in section 2.4.1. These images are created as a result of illuminating a diffuse sample with a coherent light source. The light scattered as many different wavelets, with variable optical path length, are interfere to create a grainy pattern called speckle. In the case of a static sample, this pattern remains stationary but as soon as the scatterers in the sample start to move, these patterns would have dynamic properties. The fluctuations in the speckle images corresponds to the displacement of the particles.

Studies of these images can reveal properties of the sample under investigation. For the case of a strong diffuser a different speckle pattern is observed compared to a weak diffuser. We have done the laser speckle measurements with the same experimental setup as the PIV, that is in an optically transparent sample with only a certain density of moving scattering particles. These measurements have been done for both phantoms. A raw speckle image along the carotid artery is shown in Fig. 4.3.

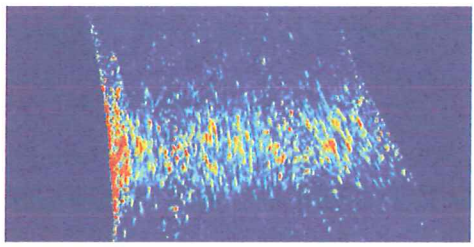

Figure 4.3: A typical laser speckle raw image along the carotid artery phantom.

4.3 Results and Discussion

4.3.1 PIV measurements

In the case of PIV measurements, the cross correlation for each interrogation window from the captured images, was repeated to yield a velocity vector map over the whole area. In this way, all the measured cross correlations of the individual image pairs for the chosen interrogation window were summed. Using this method, 80 instantaneous velocity vector fields were extracted and ensemble averaged to obtain the final velocity vector map at each time point. The result, Fig. 4.4, shows a better signal to noise ratio than if the velocity vector map was extracted using the instantaneous cross-correlations.

In the case of the cylindrical phantom, due to its symmetrical geometry, measurements were done only in the middle plane. However, the geometry of the carotid artery phantom is more complex so the measurements were done in two orthogonal planes. To view the flow field from two orthogonal perspectives, two sets of configurations were measured. To cover the whole sample volume, initially the velocities in the XY plane were measured (V_x and V_y) and then by rotating the phantom over 90^o, the velocities in XZ plane (V_x and V_z) were measured. For each data set, the velocity has been plotted as $V = \sqrt{V_x^2 + V_y^2}$ and $V = \sqrt{V_x^2 + V_z^2}$ respectively. The velocity profile through the entire phantom, is shown using 20 contour slices in Fig. 4.5. The left set of slices was made by using the XZ-planes while the right set of slices was made using the XY-planes.

4.3.2 Laser Speckle Contrast Analysis

For the case of the measurements done with the laser speckle contrast analysis, we have captured a timed sequence of images keeping the flow parameters the same as for the PIV measurements. For each measurement 2700 images were recorded with an exposure time of 20 ms. The speckle contrast for each image from the time sequence was then calculated using a spatial window size of 7×7 camera

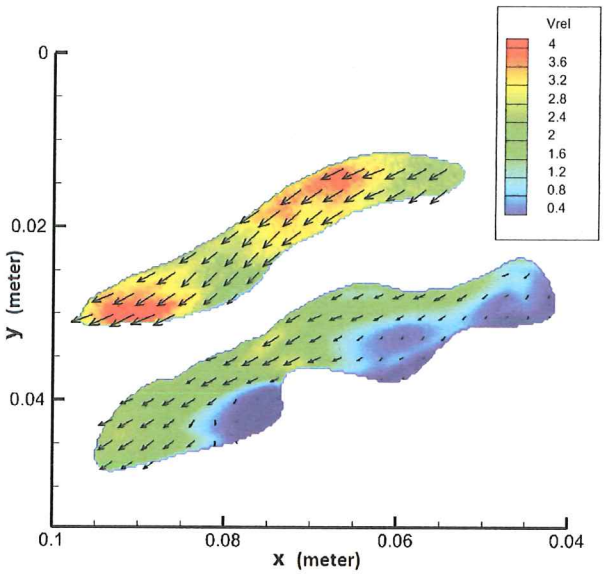

Figure 4.4: Final velocity map of the carotid artery phantom. Color indicates the velocity vectors amplitude. Vrel is the dimensionless velocity defined as ratio of velocity and mean inflow velocity.

pixels. The resulting contrast time series was then Fourier transformed to obtain the frequency spectrum of the speckle contrast which arises due to fluctuations arising due to different processes, for the entire duration of each measurement. This gives an insight into all the frequencies that contribute to the flow pulse along with the modulation which is imposed on the flow due to the complexity of the structure into which the fluid is flowing.

4.3.3 Spectral analysis of pulse from PIV and LASCA

Spectral analysis was done for both PIV and LASCA data. In Fig. 4.6 we show for PIV, the evaluation of velocities from the pulsatile flow in the cylindrical phantom. As explained before in chapter 3, section 3.1.1, the flow has been generated by pulses from VAD. In order to plot the pulse, the laser and camera were triggered at the highest flow rate during the pulse. The flow rate profile was measured using the electromagnetic flow meters and the highest flow rate during the pulse was used as the triggering signal. In this way, 10 points in the cardiac cycle for the cylindrical phantom was measured. The average flow rate is measured as 2.85 liter/min with the max flow rate of 4 liter/min.

By establishing the feasibility of this technique in the simplified phantom, we conducted a similar study on the more complex carotid artery phantom. The same procedure has been implemented for the carotid artery phantom. Due to its

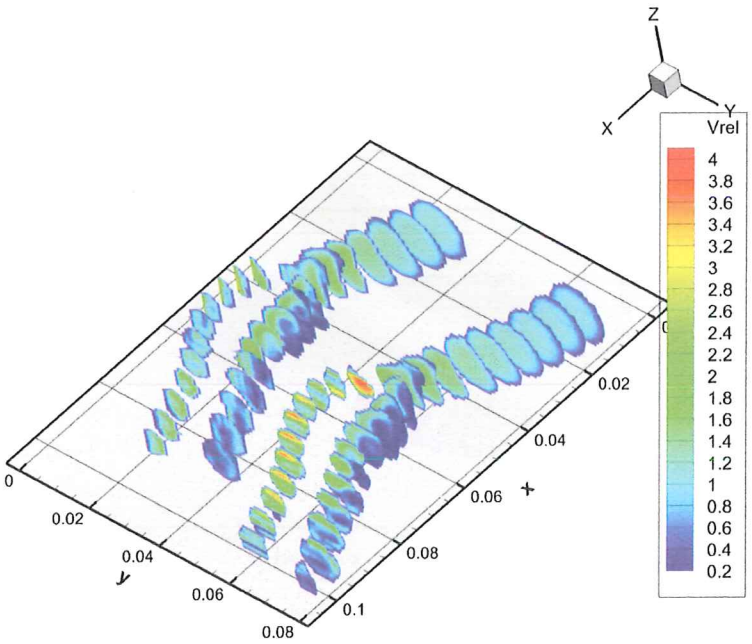

Figure 4.5: Contour profile through the carotid artery phantom. The length scale is in meter for both axes. The left set of slices was made by using the XZ-planes while the right set of slices was made using the XY-planes. Again Vrel is the dimensionless velocity.

complex geometry, the phantom of the carotid artery has been analyzed at five different locations of: bifurcation in common carotid artery (zone 1 and zone 2), internal carotid artery (zone 3), stenosis (zone 4) and external carotid artery (zone 5). The zones are shown in Fig. 4.7 with the squares. The time series for the measurements with PIV for zone 2 can be seen in Fig. 4.7(a) and for the LASCA measurements can be seen in Fig. 4.7(b), where we can see the difference between the two. For the LASCA measurements, regions of interest at these five locations were analyzed using the time sequence of speckle images as explained before. In all five zones we can see the complexity of the VAD pulses including the regions of back flow.

The time sequence was then Fourier analyzed to get the frequency spectrum from both measurement techniques. We observe that in case of PIV the frequency spectrum from the indicated five zones are almost the same. This spectrum can be seen in Fig. 4.8(f). The LASCA measurements contain more detail in the frequency spectrum and each zone gives rise to a different spectrum. These spectra are shown in Fig. 4.8(a-e). The main difference is in the density of data being used to generate the frequency spectra. In case of PIV, the data is sparse along the pulse whereas in case of LASCA, the large number of captured images provides more detail in the time properties of the flow pulses. However, we observe that

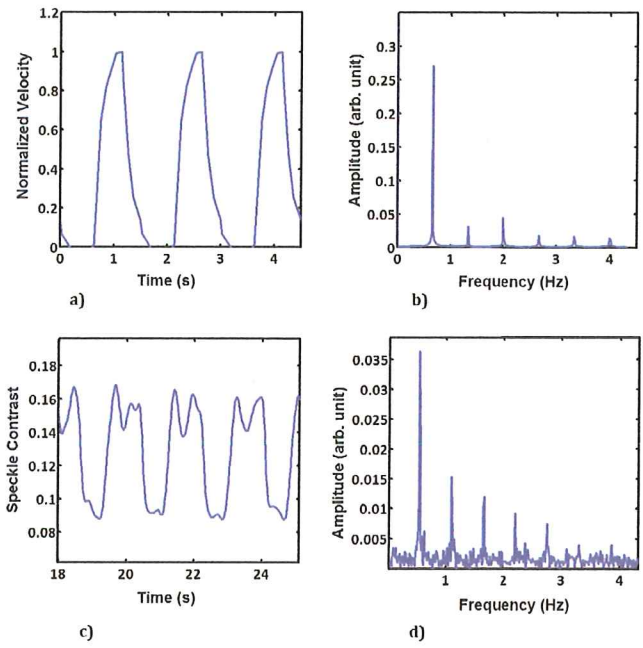

Figure 4.6: Time sequence of (a) PIV and (c) LASCA generated from images recorded during pulsatile flow in the cylindrical phantom. Frequency spectrum extracted from the time sequence for (b) PIV and (d) LASCA measurements.

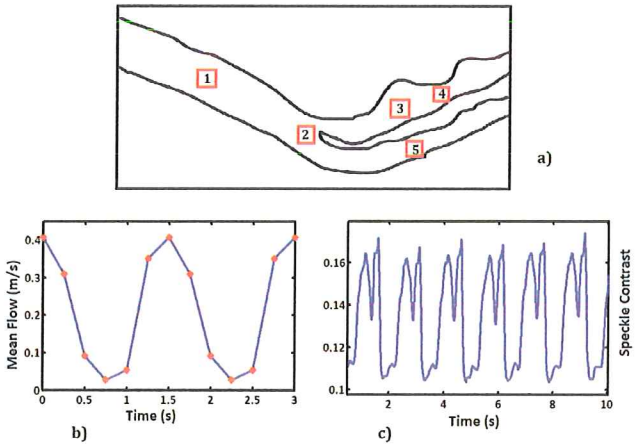

Figure 4.7: a) The selected zones for analysis from carotid artery phantom. b) Time sequence for PIV , c) Time sequence for LASCA, in zone 2.

both techniques measure the main frequency of the pulsation of the flow, 0.67 Hz, quite clearly.

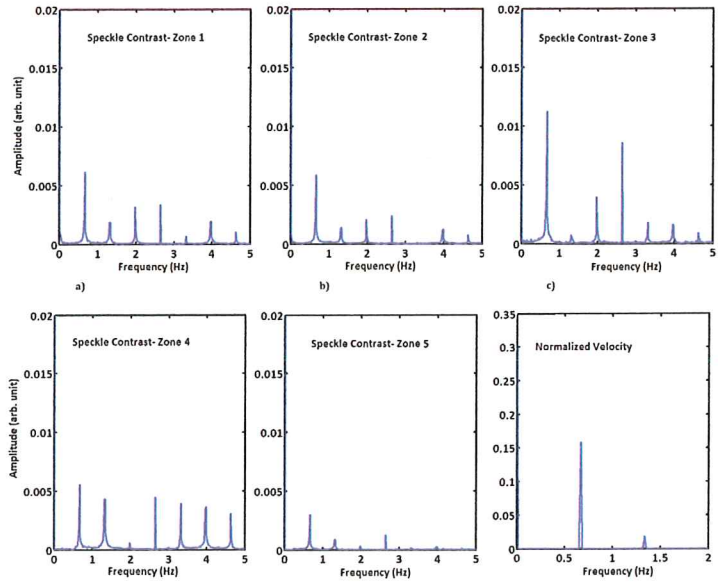

Figure 4.8: a) - e) Spectral analysis of the speckle contrast is shown for the five selected zone along the carotid artery phantom. f) Due to sparse data, the spectral analysis for the PIV data in five different zones along the carotid artery phantom are the same.

4.4 Summary

In this chapter, we report an initial comparative study of pulsatile flow in a carotid artery phantom using the full field techniques of PIV and LASCA. The measurements using two techniques were used to extract complementary properties of the pulses from the VAD device. In spite of the significant progress made in studying flow using both methods, each technique has its own limitations. PIV is expensive and time consuming even though stereoscopic PIV is becoming increasingly popular. This technique provides a complete velocity map of flow thorough complex flow geometries which is very useful in studying the human circulatory network and diseases which arise there. The imaging needed for this technique, makes it quite difficult to capture with high resolution the temporal properties of the flow. That is not very efficient in case of studying dynamics in pulsatile flow. In comparison, technique of LASCA is quite economical considering the complexity of equipment needed since no direct imaging is done. This is also a disadvantage for LASCA since no imaging information can be extracted from the LASCA data. The high resolution in the temporal data however makes LASCA quite efficient in

studying the time evolution of the fluid pulses in various locations of a flow network. So the frequency spectrum measured using LASCA is quite rich and gives complete details of the pulse. This makes the combination of techniques particularly attractive, since using both the disadvantage of the individual techniques can be overcome and a complete analysis of the dynamics of pulsatile flow can be done. The following chapter introduces a novel approach to address the data analysis of the captured data, by exploring the fractal nature of speckle data.

CHAPTER

5 Fractal analysis in speckle images

If we knew what it was we were doing, it would not be called research, would it?

Albert Einstein

In the previous chapters an experimental setup for the flow analysis has been presented together with several classic data analysis tools. In this chapter, a different approach has been used to process the speckle images from pulsatile flow. We study the fractal dimension changes in speckle images caused by pulsatile flow and compare it with speckle contrast analysis. Monitoring dynamic speckle to study pulsatile flow can be used to yield essential information about the underlying process. We report the results of experiments to study pulsatile flow with speckle images, under different optical and complex flow configurations. We also incorporate a layer of static scatterers between the imaging system and flow, where the fluid itself is a bulk scatterer. The fractal dimension is a more sensitive measure than speckle contrast since it can measure the texture of image. It is also extremely responsive to rapid changes in the texture and this can be exploited to study the time evolution in more complex media just by observing the dynamic fractal dimension of the scattering from it. Measurements were also carried out *in-vivo* situations to test the feasibility of devices based on this technique.

5.1 Introduction

Fractal statistics is very relevant in studying biological systems. In a living sample, a level of complexity of the system is considered normal and other behavior can indicate disease [116]. In most physiological processes, the measured values usually

fluctuate in time and this can also be studied for fractal behavior. This has been investigated in studies like that of cardiac inter-beats for healthy volunteers and patients [117]. Fractal statistics is being used to study speckle images [86,118,119] in many recent studies. Analyzing speckle data with fractal statistics provides a measure of the fluctuations of an evolving process at different temporal resolutions. This reveals the self similarity and order which underlies the apparent chaotic changes in the signal. This behavior where statistical properties of smaller parts are proportional to statistical properties of the whole can be addressed using power law scaling in fractal statistics. A brief introduction of fractal is given in section 2.3.1. The fractal dimension of an image mainly corresponds to the perception of roughness, where it is mathematically described. In this chapter, we study flow pulsation using systems where we vary the pumping mechanism which generates the fluid pulsation, keeping the frequencies close to the human heart. Using the differential box counting approach described in section 2.4.3, we have measured the changes of fractal dimensional over time for speckle images. The speckle images were measured from different phantoms and with underlying pulsating flow with different scattering fluid. This data was also analyzed using the standard speckle contrast analysis. A time series of fractal dimension has been used to determine the corresponding frequency spectrum. These experimental data were also analyzed using the standard speckle contrast analysis. The speckle contrast is then calculated for the entire image in total or using a sliding spatial window, as mentioned in chapter 2, section 2.4.1. The resulting contrast time series are then Fourier transformed to obtain the frequency spectrum. The characteristics of frequency spectrum arising from these two techniques are then compared to study their sensitivity to a particular phenomena. This frequency spectrum has information about all the fluctuations arising in the flowing media for the entire duration of each measurement. This is also a function of camera exposure time and acquisition rate.

5.2 Pulsatile flow measurements

In this chapter, the measurements were carried out in three different settings. In the first case, the pulsatile flow was generated using a simple roller pump and milk as an opaque scattering fluid. In these measurements, we also studied the effect of having a layer of static scatterers on top of the fluid. The second case was done with a Medos Ventricular Assist Device (VAD), a pump with pulsatile flow which resembles the heart, together with a transparent fluid with seeding particles which scatter. The third case was *in-vivo* measurements. For each measurement, the same experimental format has been used which is composed of illumination, detection and the sample itself. In all three cases, detection was done with a high speed camera (Photron Fastcam SA3) with the pixel size of 17×17 μm. The camera is placed perpendicular to the plane formed by the direction of the fluid motion and incoming laser light. The camera exposure time is 20 ms and frame rate is 50 Hz.

5.2.1 Influence of static scatterers

These experiments were carried out on a semi-rectangular channel phantom described in chapter 3, section 3.3.1. In this experiment, the pulsatile flow was generated using the roller pump (Minipuls® 3) with a controlled frequency and milk has been used as a scattering fluid. The measurements aimed to observe the influence of a top membrane and consider the effect of additional static scatterers besides the scattering along the flow on the dynamic speckle images. The three configurations considered included a top membrane of glass, Delrin with 1 mm thickness and 2 mm thickness. The dynamic speckle images were then analyzed and the results of the time series can be seen in Fig. 5.1. The analysis using standard speckle contrast can be seen in Fig. 5.1(a, b, c) and using the fractal dimension of the images can be seen in Fig. 5.1(d, e, f).

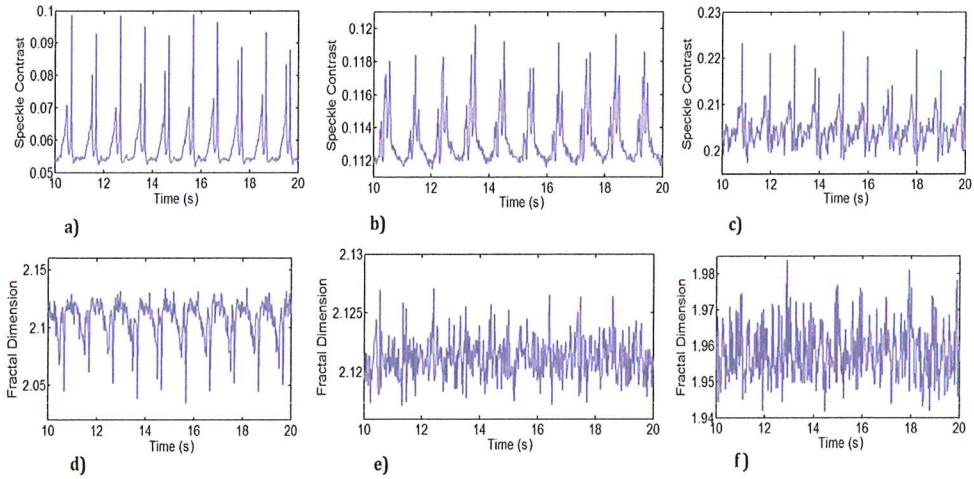

Figure 5.1: The time series signal measured for pulsatile flow in the rectangular flow channel with different top membrane. a) Glass membrane, images analyzed, with speckle contrast. b) 1 mm thick Delrin membrane, images analyzed, with speckle contrast. c) 2 mm thick Delrin, images analyzed, with speckle contrast. d) Glass membrane, images analyzed, fractal dimension. e) 1 mm thick Delrin membrane, images analyzed, fractal dimension. f) 2 mm thick Delrin membrane, images analyzed, fractal dimension.

The effects of changes in velocity of the scatterers and the changes in particle density in the pulsatile fluid signal leaves a different imprint on the contrast and fractal dimension of the images. This can be seen clearly in Fig. 5.1. The frequency spectrum of the time series of data shown in Fig. 5.1, is presented in the Fig. 5.2. In the absence of static scatterers in the Fig. 5.1(a, d), we can see that the time series data is similar for both analysis techniques. The bulk scattering in the milk does make the time series of the fractal dimension of the images more noisy than those analyzed with speckle contrast. The frequency spectra seen in the Fig.

5.2(a, d) are very similar. The addition of the extra static scattering layer adds to complexity but the time series data with laser contrast analysis can still monitor the pulsating flow, in comparison the fractal dimension of the images changes more rapidly with the thickness of the layer of static scatterers, to be able to monitor the pulsating flow. This is also reflected in the frequency spectra of the respective time series, though both techniques could determine the primary frequency of pulsation of the pump which was at 1.25 Hz.

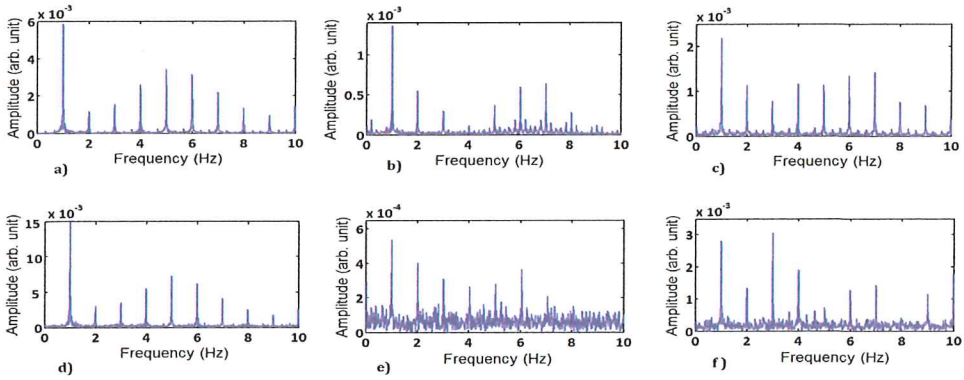

Figure 5.2: The spectral analysis of the time series measured for pulsatile flow in the rectangular flow channel with different top membranes. a) Glass membrane, images analyzed, with speckle contrast. b) 1 mm thick Delrin membrane, images analyzed, with speckle contrast. c) 2 mm thick Delrin, images analyzed, with speckle contrast. d) Glass membrane, images analyzed, fractal dimension. e) 1 mm thick Delrin membrane, images analyzed, fractal dimension. f) 2 mm thick Delrin membrane, images analyzed, fractal dimension.

5.2.2 Complex pulsatile flow

For the second case, we studied the pulsatile flow generated using the the Medos Ventricular Assist Device (VAD), which bears a strong resemblance to a pulsating heart. For the details about VAD settings, please see chapter 3, section 3.1.1. With this pump we used two transparent phantoms of different geometry, a cylindrical tube described in chapter 3, section 3.3.2 and the other a carotid artery phantom described in section 3.3.3.

Cylindrical Phantom

The cylindrical tube phantom which can be seen in Fig. 3.3, was used with the VAD as the pump. The fluid in this case was an aqueous glycerol solution with the same refractive index, n = 1.413, as the phantom housing.

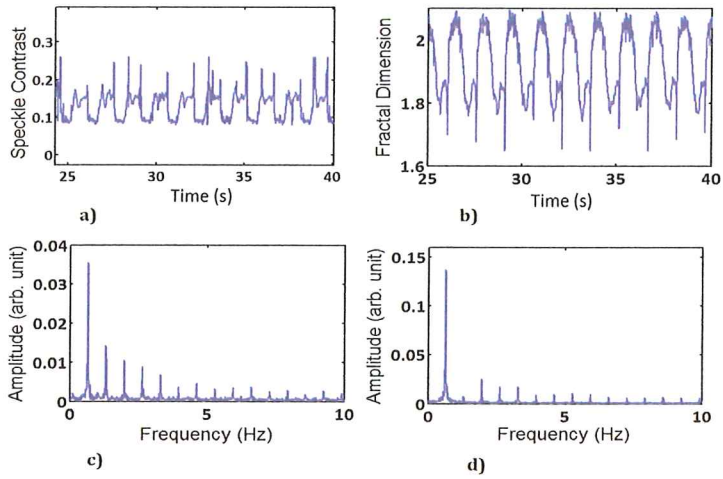

Figure 5.3: The time series signal of speckle images from pulsatile flow in the cylindrical phantom. a) Images analyzed with speckle contrast. b) Images analyzed with fractal dimension. Spectral decomposition of images analyzed with c) speckle contrast and d) fractal dimension respectively.

In Fig. 5.3(a), the time series generated using the speckle contrast analysis on the measured images with cylindrical phantom can be seen and in Fig. 5.3(b) the time series generated using the fractal dimension analysis using the cylindrical phantom can be seen. The rate of pulsation was set to be 0.6 Hz. As compared to the case of the bulk scattering fluid we observe that in the case of the transparent phantom and low seeding the contrast values are low in comparison to the changes in the fractal dimension, which is stronger. In both cases again the frequency analysis of the time series reveals the primary frequency of pulsation of the pump of 0.6 Hz.

Carotid artery phantom

The carotid artery phantom, is described in section 3.3.3. In this case, we also use a aqueous glycerol solution with the same refractive index (n = 1.413) as the phantom. Due to its complex geometry, the measurements from the phantom of the carotid artery have been analyzed at different locations which are indicated in Fig. 5.4.

These locations are the bifurcation in common carotid artery (*zone* 1), stenosis (*zone* 2) and external carotid artery (*zone* 3). These are the most common locations for the plaque formation along the carotid artery. Therefore, it is advantageous to study the full system with multiple zones for data analysis, to provide an insight into the flow dynamics. We observe that the flow dynamics is very complicated in this scenario as seen in Fig. 5.4. The speckle contrast time series

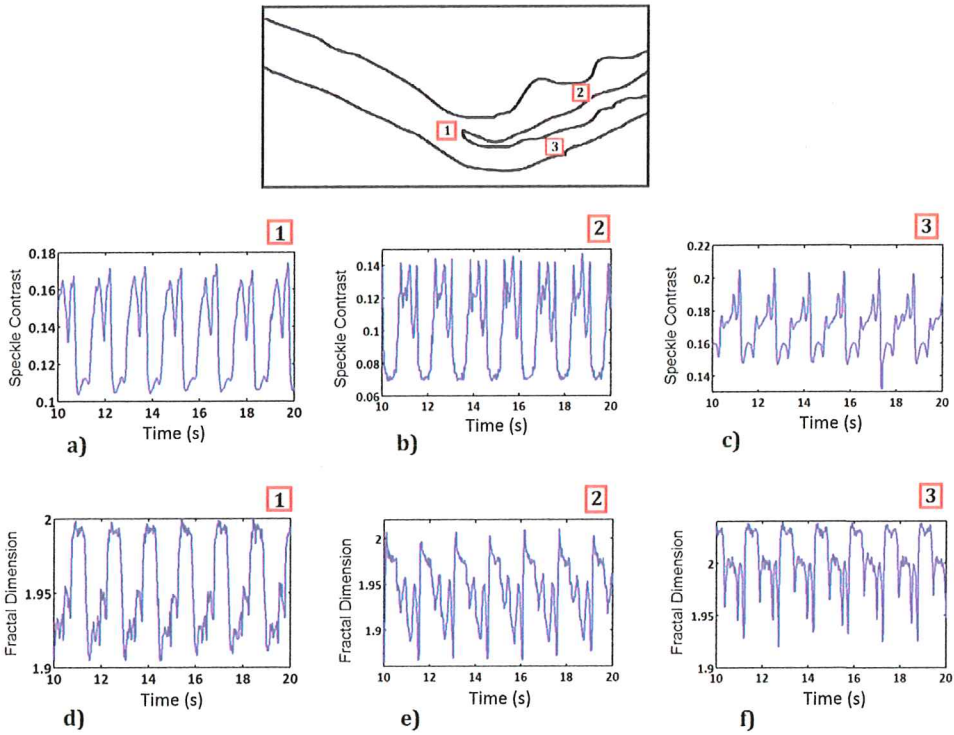

Figure 5.4: The time series of speckle images from the three (1, 2 and 3) locations along the carotid artery phantom as shown above. Images analyzed using speckle contrast a), b) and c) for zones 1, 2 and 3 as seen above. Images analyzed using fractal dimension d), e) and f) for the for zones 1, 2 and 3 as seen above.

as seen in Fig. 5.4(a, b, c) and the fractal dimension time series as seen in Fig. 5.4(d, e, f), reflect different aspects of this complexity. The frequency spectrum of the time series seen in Fig. 5.4 is shown in Fig. 5.5. The frequencies contributing to the pulse are reflected with different amplitudes in the speckle contrast time series and the fractal dimension time series. It is noted that the spectra using both techniques largely reflect the major contributing frequencies.

5.2.3 *In-vivo* measurements

The flow pumps in the above two cases maintain a steady pulsation rate, in contrast a heart changes its pulsation rate. To investigate the feasibility of these techniques for *in-vivo* situations we investigated the speckle dynamics for blood flow in a volunteer for two different situations. First we captured the speckle images, in reflection geometry from a volunteer with laser light illuminating the finger. The flow in a finger is different to that from one fluid bearing channel since it arises

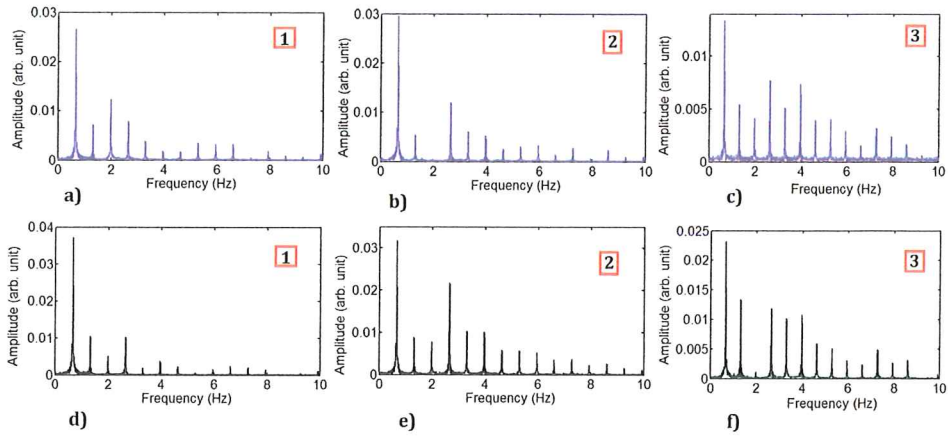

Figure 5.5: The spectral analysis of the time series of speckle images from the three (1, 2 and 3) locations along the carotid artery phantom as shown in Fig. 5.4. Spectra of images analyzed using speckle contrast a), b) and c) for zones 1, 2 and 3 in the phantom. Spectra of images analyzed using fractal dimension d), e) and f) for the for zones 1, 2 and 3 in the phantom.

from a large network of capillaries. The time series of dynamic speckle from finger, using speckle contrast and fractal dimension analysis can be be seen in Fig. 7.4(a) and Fig. 7.4(b) receptively. There is a layer of static scattering skin which also contributes to the speckle images. The capillary network also has no unique direction of flow. Thus we see that though the speckle contrast time series does seem to reflect the pulsating behavior of the underlying blood, in the fractal dimension time series this is not very clear. The frequency analysis Fig. 7.4(c, d) on the other hand shows that both techniques capture the principle frequency, which is the heart rate.

The second situation was to record speckle images of the right carotid artery of a volunteer, again in reflection geometry with laser illumination. In this case again there is a layer of static scattering skin, but the flow direction is unique. The time series for both the speckle contrast and fractal dimension clearly reflect the periodic pulsation in the flow. The frequency analysis of using both time series is also quite similar and captures the principle frequency in both cases. In both the *in-vivo* cases the heart beat of the volunteer was monitored with a wrist heart rate monitor and correspond to our measurements, which are recorded as 61 and 82 beats per minute for finger and carotid artery measurements, respectively. Further work is necessary to investigate the possible conditions for devices to work on this principle.

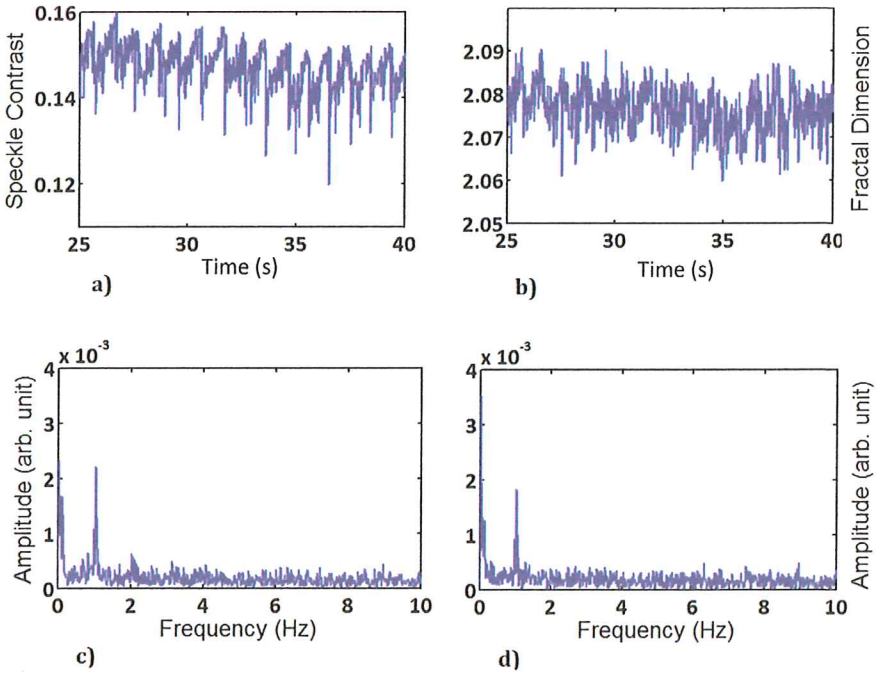

Figure 5.6: The time series of speckle images measured from the finger of a volunteer analyzed with a) speckle contrast and b) fractal dimension. Spectral analysis of the times series from c) speckle contrast and d) fractal dimension.

5.3 Summary

The multiscale analysis of time series of light scattered from a sample can be a useful tool for better understanding the complex underlying mechanisms of the medium. In this paper, we studied the fractal dimension change of speckle images of pulsatile flow and compare it to speckle contrast analysis. We address the result of measured fractal dimension in the case of a pulsatile flow in case of different phantom top membrane. We observe that in case of a 2 mm thick layer of Delrin as the top membrane, (high number of static scatterers), the fractal dimension does not reflect the pulsation and changes in flow. Whereas the laser speckle analysis can still capture the changes in the pulsatile flow. We also studied the speckle images generated by pulsatile flow from a Ventricular Assist Device in a transparent fluid where the scattering was only generated through seeding particles. Here we observe that the two techniques capture different aspects of the complexity of the flow, though in a transparent settings the fractal dimension is more sensitive than laser contrast. Measurements were also performed on a realistic phantom where the flow becomes complex due to the geometry of the

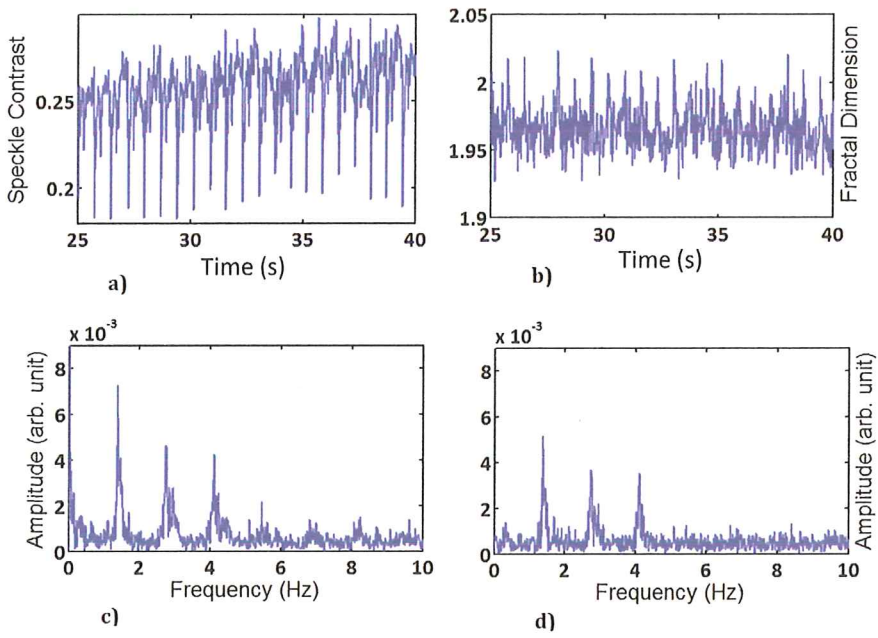

Figure 5.7: The time series of speckle images measured from the carotid artery of a volunteer analyzed with a) speckle contrast and b) fractal dimension. Spectral analysis of the times series from c) speckle contrast and d) fractal dimension.

channel. In this case we observed that even though the rapid changes in the flow leave different imprints on the fractal dimension change and the contrast, the essential frequencies were captured by both techniques. We also attempted to test the method for *in-vivo* case and observe that the changes in the fractal dimension and in the contrast of the speckle images manage to capture the heart rate. The fractal dimension is a more sensitive measure than speckle contrast since it can measure the texture of image. It is also extremely responsive to rapid changes in the texture and this can be exploited to study the time evolution in more complex media just by observing the scattering from it.

CHAPTER

6 Multi layer flow analysis using speckled speckle

Subjects that often appear to be well understood and perhaps even a little old-fashioned have frequently some surprises in store for us.

Emil Wolf

In the previous chapters, we presented experimental and data analysis tools to study pulsatile flow (heart beat). However, as indicated before, its analysis in real-world scenarios presents several challenges, such as presence of motion artifacts or anatomical properties which differ from a simulated phantom and across individual from different origins. This leads to the presence of variations in the data and thus a lack of standardization in the resulting signal as it results from a mixture of acquisitions from several layers whose properties can differ. The measurement complexity arises from having dynamic scatterers in presence of several layers of static scatterers with different composition, leading to different scattering properties. In this chapter, the flow measurement in presence of several layers is presented. The motivation behind this study is the observation that speckle patterns measured in such scenarios (multiple layers) present different properties from the speckle pattern generated from a single diffuser.

6.1 Introduction

The sensitivity of optical methods to motion is an asset which can be explored in the context of blood flow measurements. However additional motion artifacts in the site of measurements interfere with the measured signal, leading to potentially erroneous measurements. In our application, the most common sources of motion

artifacts are caused by both the relative body and sensor position variations and the absolute body motion. The latter can cause displacement of blood in the vessels, leading to variation in localized blood flow. This is called sloshing effect, where the blood displacement can cause a disturbance on the arterial blood flow signal which is generated by cardiac pulse. When a body part moves, the blood in its tissue tends to resist the change and causes a variation in blood flow dynamics [120]. Such a signal disturbance can be created by any mechanism modifying the systemic circulation of blood in arteries or veins like coughing, tremor or changes in local circulation [121, 122]. The influence of relative motion between the different consistent layers and sloshing was the research question to be explored in this chapter.

For this purpose, the experimental setup in chapter 3, Fig. 3.1, was modified to simulate sloshing, such that there is a non-linear interaction between the top surface and the underlying fluid, the blood flow. This can be done in two ways. The first approach is having the pulsatile flow in the flow cell which has been placed on the top of a moving surface itself. This surface is subject to periodic motion, with different ranges of amplitudes, in the horizontal direction. Then, for the static part (skin), another membrane made of Delrin is kept above a distance from the flow cell to ensure a separation from the fluid. The second simpler approach is to keep the flow cell static and use an in-motion diffuser with a layer of static diffuser on top. Although this does not alter the dynamics of the flow itself, it monitors the pulsatile flow through a layer of dynamic and static diffusers.

However, any of the above experimental setups, modifies the speckle behavior, as an additional separation layer is created. This leads to deviations from the expected measurements, making them perhaps unusable to study the pulsating blood flow in presence of the sloshing behavior, using speckle patterns. As a first step in this direction, we discuss a different scattering configuration. In this approach, the recorded speckle pattern is generated in presence of an additional diffuser. We elaborate on this below.

The speckle patterns arising from the additional diffuser are the so called *speckled speckle* and they were first studied by Fried who was mainly investigated the eye safety with laser related devices [123]. Furthermore, the statistical properties of the double diffuser setup was derived by Donnel [124]. Traditional speckle statistics are dependent on coherence length of light and amount of scattering they face in the medium. In a single speckle pattern, based on the central limit theorem, it is assumed that the number of scattering events are large and the amplitude and phase of the field is described by zero mean Gaussian random variables [125]. However, the statistical behavior of speckled speckle are reported to be different and has been shown to have non-Gaussian intensity distribution [124, 126]. It has been further shown that scattered speckles will not obey Gaussian statistics when both diffusers are either in motion or motionless [127, 128]. However, this kind of configurations have been mainly used for speckle suppression [129].

In the case of double diffusers experiments, it has been shown that generated speckle decorrelation effects are influenced by relative diffuser displacement or

variations in the illuminating wave field [130]. In our setup, the diffuser is kept constant and the scattered flow dynamics is changing.

In this chapter, we explore the presence of an additional diffuser which provides illumination for the pulsating fluid. The resulting fluctuating speckle patterns from the flow is then transmitted to the camera through the same diffuser. In this case, the recorded speckled pattern will not only be influenced by the intensity distribution of the illuminating spot but also by structures of the illuminating speckles. The result of these measurements are analyzed with laser speckle contrast and the fractal analysis approach presented in the previous chapter.

6.2 Experimental Setup

The schematic of the experimental setup is shown in Fig. 6.1. For illumination, a HeNe laser with an emission wavelength of 630 nm and optical output power of 30 mW was used. The measurements were performed on the phantom, as explained in chapter 3, section 3.3.1. The pulsatile flow in milk was generated using the roller pump with a controlled frequency. This is very similar to the previous setup. However to simulate the dynamics of speckle patterns created by illumination of another speckle pattern at a certain distance, we use a static 1 mm thick membrane, either glass or Delrin. This membrane is placed on the top of flow cell, with a separation distance which can be varied from 2 to 5 cm.

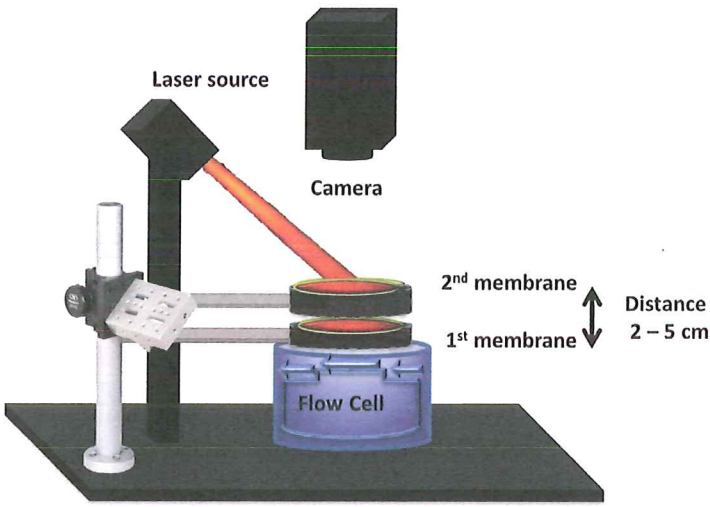

Figure 6.1: Schematic of the experimental setup to study pulsatile flow under multi layer arrangement. The properties of the membranes can be changed by using Delrin or glass.

The speckle patterns are recorded over time with 50 frames per second sampling rate and exposure time of 8 ms. The changes in flow corresponded to the changes in speckle pattern as a result of motion of scatterers in the fluid. In order to study the dynamic fluctuation of speckle images, we measure the speckle contrast, mentioned in chapter 2, section 2.4.1. We calculated the speckle contrast for each image with a spatial window size of 7×7 camera pixels. The calculated contrast for the series of images was then Fourier transformed to obtain the frequency spectrum of the speckle contrast fluctuations for the entire time of each measurement. Speckle data were also analyzed using the fractal dimension, mentioned in chapter 2, section 2.4.3. The original speckle images has been transformed to the fractal images, and a time series of these fractal dimension is measured. The speckle contrast and fractal dimension has been calculated for each measurement over a set of 2700 images. The result of the spectral analysis is compared using fractal dimension and speckle contrast, has been compared.

6.3 Results and Discussion

We performed several experiments where a combination of different settings has been applied through the modification of the membrane properties. A schematic representation shown in the Fig. 6.2 shows the four different cases which arise. The results of these measurements are described below.

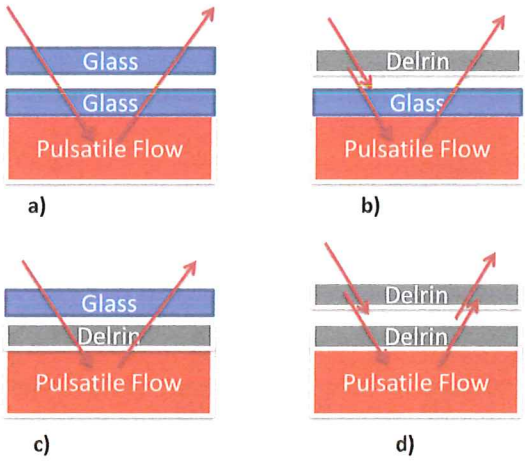

Figure 6.2: A schematic representation of different setting (a-d) in order to monitor the pulsation of flow while different membranes are placed on the top of the flow cell.

The experiment was initiated with Fig. 6.2(a), for the case of having the flow cell covered with a glass membrane while another glass membrane is placed on the

top of the flow cell. The result of the measurement is shown in Fig. 6.3. As it can be observed, the result of fractal and contrast analysis are similar. By monitoring the pulsatile flow through a glass membrane we are avoiding the influence of any additional static scattering. This is similar to the case as we were directly monitoring the changes through one single glass membrane, as it has been shown in the previous chapter in Fig. 5.2(a).

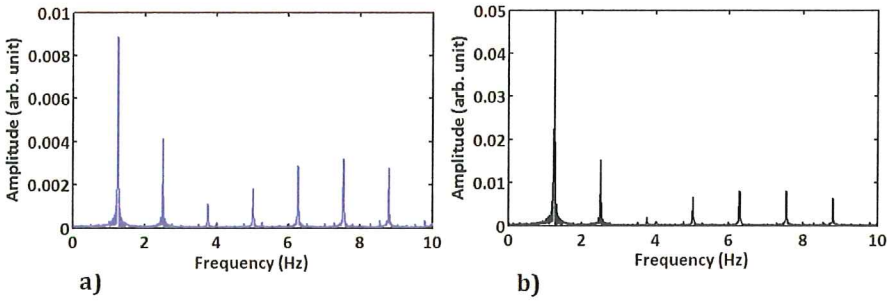

Figure 6.3: The spectral analysis for a) Speckle contrast, b) Fractal dimension. This measurement was done for the flow cell covered with glass membrane, while holding another glass membrane on top. The main frequency of pulsation is at 1.25Hz.

The second experiment was performed, as shown in Fig. 6.2(b), where the second glass membrane is replaced by the Delrin membrane. The result is shown in Fig. 6.4. We observe that in this case the measured spectrum are different from each other. The spectral analysis of the laser speckle contrast only measures the double frequency instead of main frequency of pulsation, while we still have the main frequency of pulsation recorded at 1.25 Hz using fractal analysis.

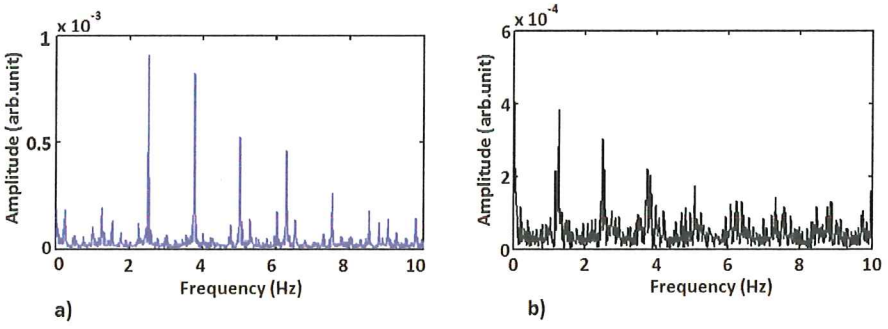

Figure 6.4: The spectral analysis for a) Speckle contrast, b) Fractal Dimension. This measurement was done for the flow cell covered with glass membrane, while holding another Delrin membrane on top. The main frequency of pulsation is 1.25Hz.

For the third set of measurement, as shown in Fig. 6.2(c), the flow cell is directly covered with a Delrin membrane while the second glass membrane, is placed on

top. The result of these measurements are shown in the Fig. 6.5. The main difference is that we have a static layer directly on top of pulsatile flow and we measure the changes by choosing either a glass or Delrin for the second membrane.

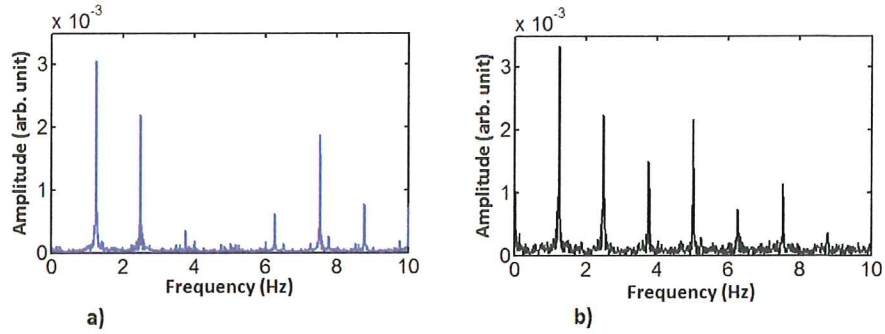

Figure 6.5: The spectral analysis for a) Speckle contrast, b) Fractal Dimension. This measurement was done for the flow cell covered with Delrin membrane, while holding another glass membrane on top. The main frequency of pulsation is 1.25Hz

These results show that both methods measure the main frequency of pulsation. However, we can notice different sensitivity in these two analysis, as we still measure the other harmonics using fractal analysis. In comparison to the previous case, where there is a reverse order between Delrin and glass membrane. This shows that having a direct contact of static scatterers with the flow leads to different results than having the flow illuminated through a layer of static scatterers.

For the last experiment, as shown in the Fig. 6.2(d), the glass membrane is replaced with Delrin, such that both membranes are Delrin. The result is shown in Fig. 6.6. In this arrangement, the fractal analysis monitors the main frequency of pulsation while laser speckle can only measure the double frequency. These plots indicate clearly the difference in having only one static diffuser as it was in the previous configurations. It is also shows the importance of where the static diffuser is placed, as seen in the second experiment.

A similar behavior has been observed when these measurements were repeated for different image plane (out of focus). The result of these measurements is referred through literature as the speckled speckle. These speckle patterns are created when the reflected light from dynamic scatterers is not directly collected through camera but first through another layer of stationary scatterers. In our experiment, this behavior was mainly observed when there was a separation distance between the two diffusers in the reflection mode.

Measurements were also performed in the transmission mode where the fluid cell was illuminated from below using a laser directly. In this case the fluid was not illuminated by a speckle pattern and only the fluctuating speckle pattern was transmitted through a diffuser to camera. In the transmission mode, we measure the direct behavior of the flow pulsation, which is the main frequency of fluid

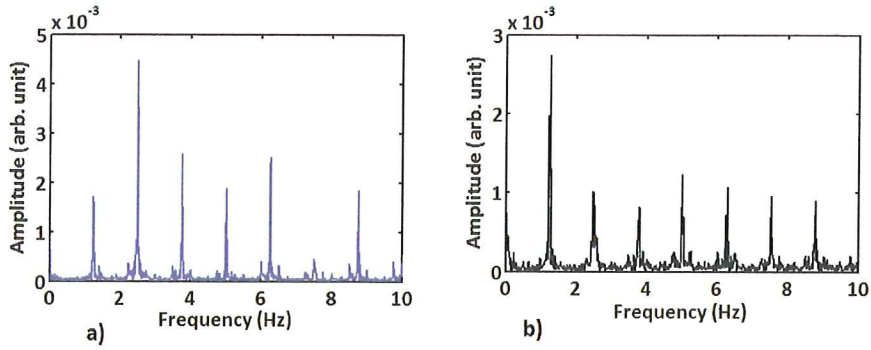

Figure 6.6: The spectral analysis for a) Speckle contrast, b) Fractal Dimension. This measurement was done for the flow cell covered with Delrin membrane, while holding another Delrin membrane on top. The main frequency of pulsation is 1.25Hz.

pulsation. This was observed for both contrast and fractal analysis. The result is shown in the Fig. 6.7.

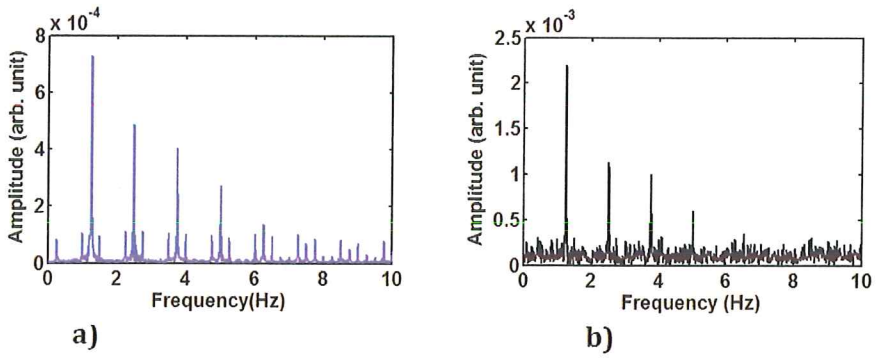

Figure 6.7: The spectral analysis for a) Speckle contrast, b) Fractal Dimension. This measurement was done for the flow cell covered with Delrin membrane, while holding another Delrin membrane on top, in the transmission configuration. The main frequency of pulsation is 1.25Hz.

The result of interference of a coherent source due to a layer of static scatterers creates Gaussian speckles whereas the case of having cascade of diffusers, causes speckled speckle to be created that give rise to non-Gaussian distributions. The main difference is that these non-Gaussian distributions predict larger amplitude and intensity fluctuation. Therefore, the hypotheses is the difference in the spatial properties of these patterns. It has been also shown by Donnell [124], that the speckled speckle are not spatially ergodic and that can possibly explain why using spatial contrast we are not able to retrieve the main frequency of pulsation. However, we believe that more studies need to be done and a better theory would

be needed to explain the complexity of the problem.

6.4 Summary

In order to simulate sloshing as an induced motion artifacts, we had to separate the static layers from the fluid itself. While doing the measurement, we studied the behavior of speckle through a layered structure. The result of having a pulsatile flow under a cascade of diffuser has been presented here. This analysis brings the measurement of flow in *in-vivo* subjects closer to reality and can be important in imaging applications where double propagation of light through a random medium is of interest. In this set of measurements, the laser illuminating the flow cell creates a speckle pattern which is incident upon the second diffuser. The resulted speckle is then imaged by the imaging system. We have demonstrated the possibility of using fractal analysis to measure the pulsatile flow in presence of several static layers. Although using the laser speckle contrast, we can detect the expected pulsatile frequency in some configurations, fractal theory showed to be more sensitive to these fluctuations.

CHAPTER

7

Flow analysis in presence of motion induced artifacts

We cannot solve our problems with the same thinking we used when we created them.

Albert Einstein

In this chapter, we address a totally different problem based on the speckle technique. As mentioned in the beginning of this thesis, one portable non-invasive optical monitoring device widely used to monitor cardio-vascular complications is the pulse oximeter, which works based on the photoplethysmogram (PPG) principle. However, these devices are prone to motion induced artifacts. We propose laser speckle for monitoring pulsatile flow in presence of motion induced artifact. The main difference between speckle based measurement and PPG is the fact that instead of measuring volume changes we measure time dependent velocity changes of the scattering particles such as red blood cells (RBC). The possibility of measuring hemodynamic parameters in presence of relative motion between the optical components and sample using speckles, is still an open question [131]. We will address the possibility of measuring a pulsatile flow in a noisy environment using speckle dynamics. Specifically, we measure pulsation or the heart rate in presence of motion between the illumination and the *in-vitro* or *in-vivo* sample.

7.1 Experimental measurements

7.1.1 Experimental setup

We initially did an *in vitro* study to investigate the influence of the motion artifacts on the signal in a controlled lab environment. The schematic of the setup for the

in-vitro and *in-vivo* is shown in the Fig. 7.1(a) and Fig. 7.1(b) respectively. For illumination, we used a vertical-cavity surface-emitting laser diode (VCSEL) with an emission wavelength of 850 nm and spectral bandwidth of 0.3 nm. The laser diode has a coherence length of 2.4 mm and an optical output power of 0.5 mW. We used a roller pump (Minipuls®3) to generate a pulsatile flow with a controlled frequency in our flow cell using five rollers. For our detection system we used a high speed camera (Photron Fastcam SA3) with pixel size of $17 \times 17\mu$m. For magnification we could couple the camera to a stereomicroscope with overall magnification of 6.4 where needed.

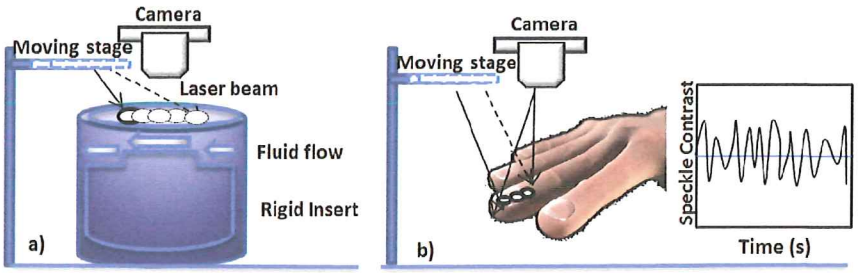

Figure 7.1: The experimental setup a) *in-vitro* and b) *in-vivo*. The motion artifacts are generated by the motion of the laser beam which creates a different penetration depth, illumination spot and distance to the detector. The speckle contrast has been calculated over the whole illuminated area.

In the experiments we simulated a scenario of measuring the pulse rate in a phantom in case of artifacts generated by systematic and random motion. We have used these two main categories as we can compare the systematic motion or a rhythmic hand motion, which occurs for instance during sport and random motion which resembles complex hand motion of patients in the medical setting. To generate the motion we used a mini-shaker which has been driven through an amplifier using a program based on Labview. The laser diode is attached to the shaker, which moves with the defined linear or random motion. The movement of the beam spot will affect the position on the sample being illuminated and the separation distance between the laser beam and the detector. This continuous movement will create the main motion induced artifact due to changing the optical path through the sample and changing the depth at which the sample would be monitored. By positioning the light source and detector at different distances, we influence the light propagation. This principle has been mainly applied in time domain measurements to calculate the optical properties along the tissue. The time domain photon migration describes the temporal dispersion dependence of the light pulse to tissue optical properties [36, 132].

To simulate the *in-vitro* heart rate, we generated a pulsation rate of 1 Hz and 1.25 Hz, with an amplitude per stroke of 6.7 ml and 7.8 ml respectively. The base flow rate for 1 Hz and 1.25 Hz, was measured to be 40 ml/min and 47 ml/min

respectively. The motion induced artifacts have been generated using the shaker to move the illuminating laser at three different frequencies (0.7 Hz, 1.4 Hz and 2.8 Hz) with two different amplitudes (0.5 mm and 2 mm). Each measurement has been recorded for 45 sec with 50 frames per second (fps). The exposure time for each frame was 20 ms. The images have been recorded with the full camera frame of 1024 by 1024 pixels.

7.1.2 Speckle contrast analysis for *in-vitro* experiments

For each individual measurement, we captured a time sequence of images and calculated the speckle contrast for each image with a spatial window size of 7×7 camera pixels. The resulting contrast time series was then Fourier transformed to obtain the frequency spectrum of the speckle contrast due to fluctuations arising due to different processes, for the entire duration of each measurement. The experimentally measured contrast for milk pulsation at 1 Hz and 1.25 Hz is shown in Fig. 7.2. The left panel displays the contrast calculated for the recorded images in time for two different pulsation frequencies of the milk flowing in the sample cell. The panel on the right is the spectral composition of the speckle contrast variation arising due to the pulsation of the fluid in the sample and the motion artifacts generated by the moving illuminating source, which has been extracted from the images measured by the camera. The result of measured signal is shown for the best and worst signal visibility which is the case for 0.5 mm and 2 mm displacement amplitude of the laser by the shaker, respectively. For each measurement the signal has been low-pass filtered at 6 Hz and plotted for the same range of frequencies.

As can be seen in the figure, the visibility of pulsation signal compared to the motion signal on the laser has decreased. The main reason for bigger drop in case of 1.25 Hz pulsation is due to the speed of flow. In the current setup, a higher pulsation rate also causes a higher speed of flow. The measured signal quality drops due to the speckle patterns being more blurry, which results in a lower contrast value. The main aim of these measurements is to be able to distinguish and reliably detect the pulsatile signal in face of the noise elements around it. We must state that in the current experimental setup with speckle imaging we cannot distinguish between two opposite directions of motion of the laser. This leads to the double frequency signal of the laser motion (1.4 Hz, 2.8 Hz and 5.6 Hz) being more prominent in our spectral decomposition graphs. In the *in-vitro* case we have the specific advantage of knowing the frequency of the signal we would like to detect since it is the frequency of our pump. So in this case we can separate it from the other frequencies in our setup for instance the modulation frequency of the shaker which moves the laser. We have observed that neglecting the spectral signal arising from the known frequency of the shaker and calculating the signal to noise ratio for the signal arising from the pump, the average signal to noise ratio of 14 dB makes the measurement of the pulsation signal still feasible. A surprising point was that the signal was still distinguishable for the case of pulsation at 1.25 Hz and laser oscillation frequency of 0.7 Hz which has a bigger amplitude at the double frequency of 1.4 Hz. In case the frequencies of the signals is even closer

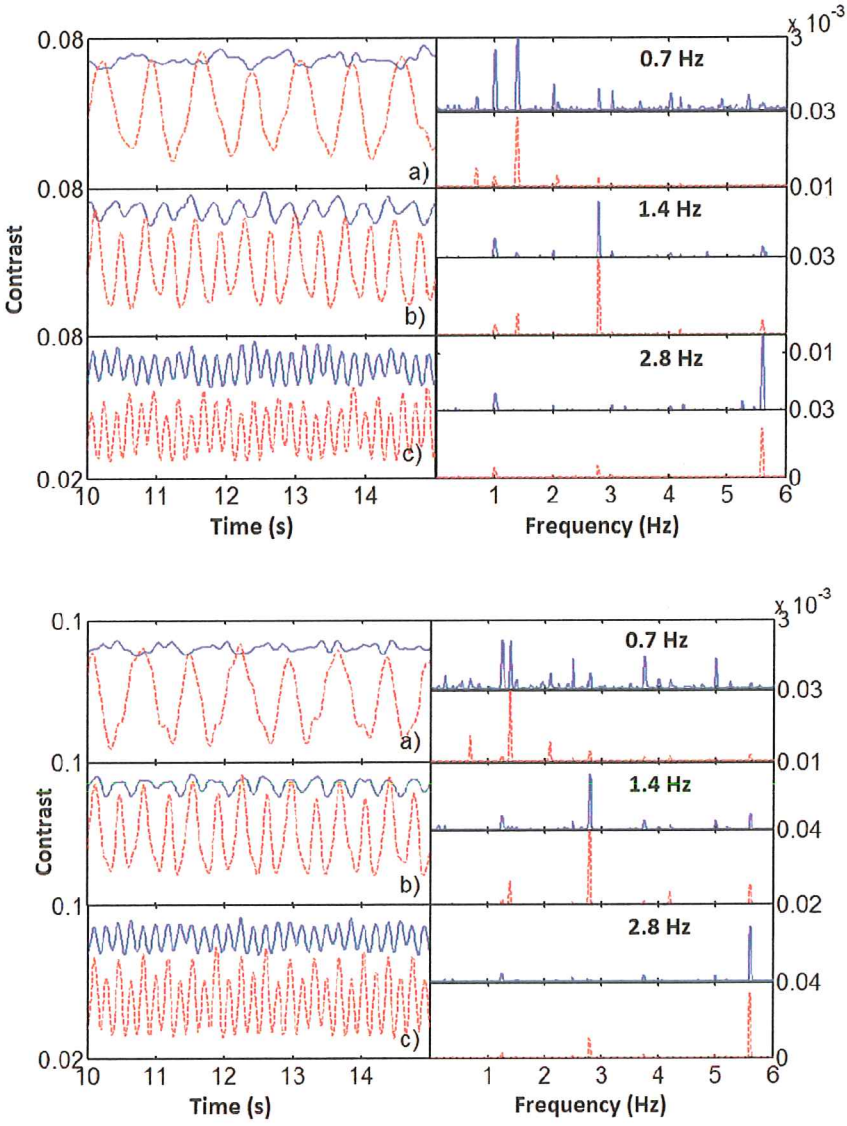

Figure 7.2: Speckle contrast variation in time on the left and spectral analysis of the contrast curve on the right. Milk pulsation in the flow cell with frequencies 1Hz (upper plot) and 1.25Hz (lower plot) for two displacements of the illuminating laser: 0.5mm (upper continuous line) and 2mm (lower dashed line) at the frequencies of a) 0.7Hz, b) 1.4Hz and c) 2.8Hz.

or overlap it is probably not possible to detect the pulsation frequency clearly. From the figure we observe that even for the case of maximum displacement of 2 mm and a shaker frequency of 2.8 Hz we are still able to see the signal, but we would like to emphasize that the detection possibility of the signal deteriorates with increasing amplitude and/or the oscillation frequency of the shaker which moves the laser because of speckle contrast modulation decreases. To be able to quantify this we show in table 7.1 the ratio between the amplitude of the pulsation signal from the spectral decomposition to the amplitude of the double frequency signal of the laser motion seen in the same spectral decomposition.

Table 7.1: Ratio of amplitude of pulsation signal to double frequency of laser motion signal in the spectral decomposition.

Flow pulse \ Frequency motion	1.4Hz	2.8Hz	5.6Hz	Amplitude
1Hz	0.82	0.34	0.19	0.5mm
1Hz	0.13	0.14	0.17	2mm
1.25Hz	1.03	0.27	0.11	0.5mm
1.25Hz	0.074	0.06	0.06	2mm

To be able to extend our study to a more general case we decided to move the shaker and hence the laser randomly using a band limited white noise signal with frequencies in the range of 0.1 to 10 Hz. The choice of this frequency range was made based on literature which states that the PPG pulsatile cardiac signal is in the range of 0.5 to 4 Hz with the low frequency range of respiration signal of 0.2 to 0.4 Hz. [133, 134]. The results of this study are shown in the Fig. 7.3, where we see that the pulsation signal is visible clearly for the case of lower amplitude of motion of the laser which is 0.5 mm.

For the white noise measurements the signal was observable only up to the laser motion amplitude of 1 mm above this amplitude it is difficult to detect anything as can be seen in Fig. 7.3 for the case of laser motion amplitude of 2 mm. Therefore amplitude of the motion with respect to the illuminating source is the deciding factor for the detectability of the signal in the case of random motion.

7.1.3 Speckle contrast analysis for *in-vivo* experiments

We then implemented the measurement *in-vivo* by placing a finger of a volunteer in the place of the flow cell. The volunteer also wore a commercial pulse oximeter on the thumb so that our measurements could be verified. The analog signal from the pulse oximeter was synchronized with the camera frames recorded for the measurement. To keep the heart rate values similar, the measurements for the two amplitudes of the shaker which moves the illuminating laser, at 0.5 mm and 0.8 mm, were performed sequentially in time. The results of the measurements can be seen in Fig. 7.4 for the three different motion frequencies, of 1 Hz, 1.4 Hz

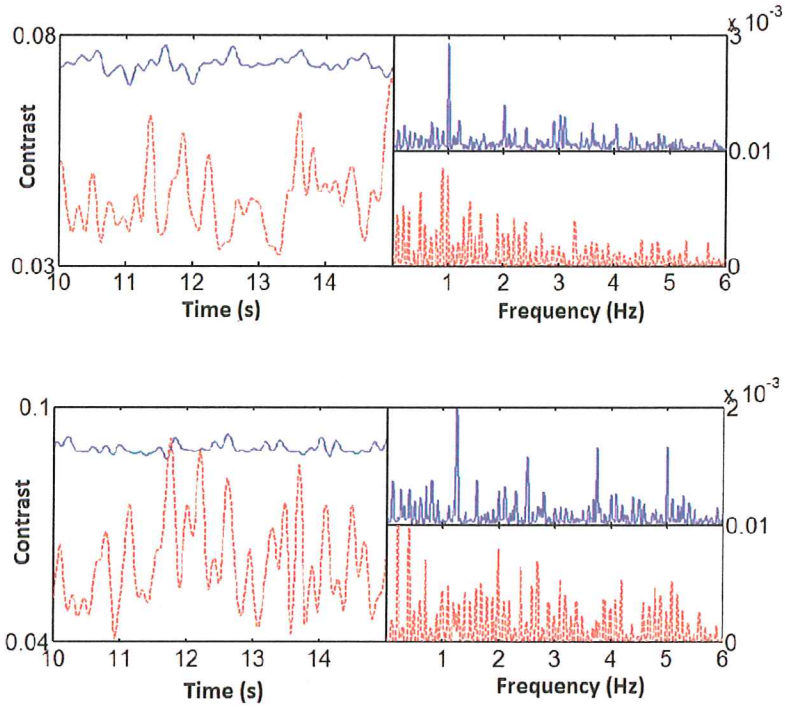

Figure 7.3: Speckle contrast variation in time on the left and spectral analysis of the contrast curve on the right. Milk pulsation in the flow cell with frequencies 1Hz (upper plot) and 1.25Hz (lower plot) for random displacement of the illuminating laser at the amplitudes: 0.5mm (upper continuous line) and 2mm (lower dashed line).

and 2.8 Hz of the illuminating laser, at the two different amplitudes. The results confirm our expectations from the *in-vitro* measurements that the detectability of the signal drops for higher motion amplitudes and frequencies. We see this even more in the case of random motion of the shaker moving the illuminating laser in Fig. 7.5. The heart rates indicated in Fig. 7.4 and Fig. 7.5 were those measured independently by the commercial pulse oximeter.

7.2 Characterization of *in-vitro* experiments on motion induced artifacts

To study further the effect of additional perturbation on the optical signal from the scatterers due to relative motion between light source and flow sample, several experimental configurations were studied. The flow pulsation frequency was kept at 1.25 Hz. The flow cell was kept in the rigid configuration to avoid the extra

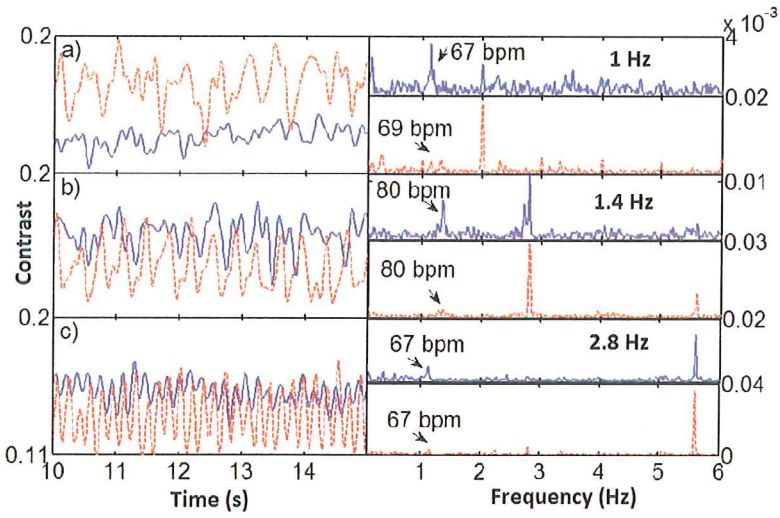

Figure 7.4: Speckle contrast variation in time on the left and spectral analysis of the contrast curve on the right. Measurement with human finger for the illuminating laser displacement of: 0.5mm (upper continuous line) and 0.8mm (lower dashed line) at the frequencies of a) 1Hz, b) 1.4Hz and c) 2.8Hz.

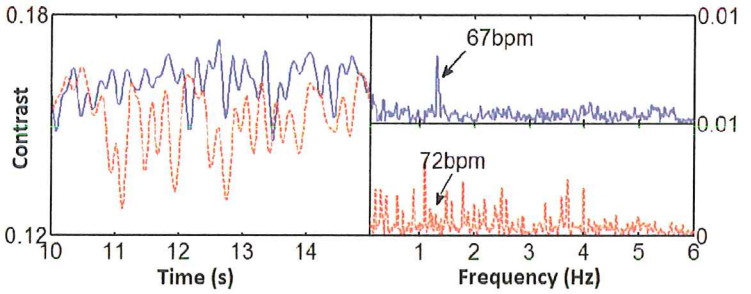

Figure 7.5: Speckle contrast variation in time on the left and spectral analysis of the contrast curve on the right. Measurement with human finger for two random displacements of the illuminating laser at the amplitudes: 0.2mm (upper continuous line) and 0.8mm (lower dashed line).

oscillations seen in the case where the volume is allowed to change. The generated motion artifact has been extended to move the laser at different frequencies (0.7 Hz, 1.4 Hz, 2.8 Hz, 3.2 Hz, 3.6 Hz, $4Hz$ and 4.5 Hz) with different amplitudes (0.5 mm, 1 mm, 2 mm and 3 mm) and two different angle of illuminations. Each measurement has been recorded with different exposure times of 20 ms, 16 ms, 8 ms and 4 ms. These measurements were then analyzed using the contrast, as mentioned in chapter 2, section 2.4.1 and correlation formalisms, as mentioned in

chapter 2, section 2.4.2. The modified setup is shown in Fig. 7.6

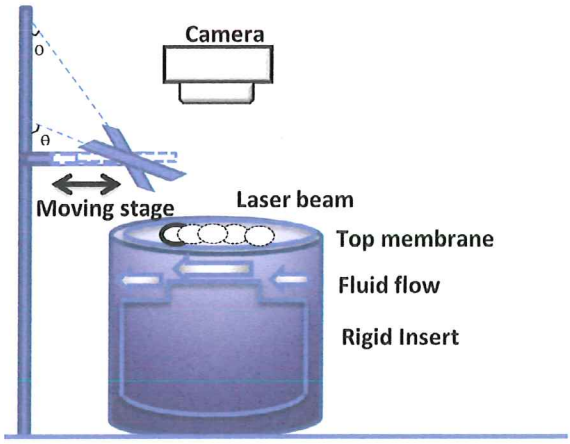

Figure 7.6: The experimental setup. The motion artifacts are generated by the motion of the laser beam which creates a different penetration depth, illumination spot and distance to the detector.

Out of these measurements, we show only the extreme cases, *i.e.*, at the frequency of $0.7Hz$ with 0.5 mm and 3 mm amplitude and at the frequency 4.5 Hz with 0.5 mm and 3 mm in Fig. 7.7 and Fig. 7.8. The rest of the measurements show the same trend as seen for the extreme cases. The measurements were also performed at two different angles, 70° and 20° of the illumination laser with the camera, which is placed directly above the sample. The results of measurements at 70° are shown in Fig. 7.7 and 20° in Fig. 7.8. To study the impact of the camera exposure time on the measurements, we measured for exposure times of 20 ms, 16 ms, 8 ms and 4 ms, as shown in Fig. 7.7 and Fig. 7.8, in the panels a), b), c) and d), respectively. These correspond to camera frame rates of 50 fps, 60 fps, 125 fps and 250 fps, respectively.

7.2.1 Speckle contrast analysis compared with correlation for experiment with motion induced artifacts

The plots in Fig. 7.7 and Fig. 7.8 show the results of the measurements using both analysis techniques after being smoothed and low pass filtered at 10 Hz. It can be observed that we are able to differentiate the fluid pulsation rate from the induced motion effects. However, the spectral composition of the signal extracted from the temporal analysis of the contrast and correlation measurement exhibit some major differences. The spectrum obtained from this speckle contrast technique appears cleaner due to the extensive spatial averaging. The spectrum from the correlation analysis is more sensitive to fluctuations and more detailed. The contrast analysis mainly measures the double frequency of the induced motion as contrast analysis

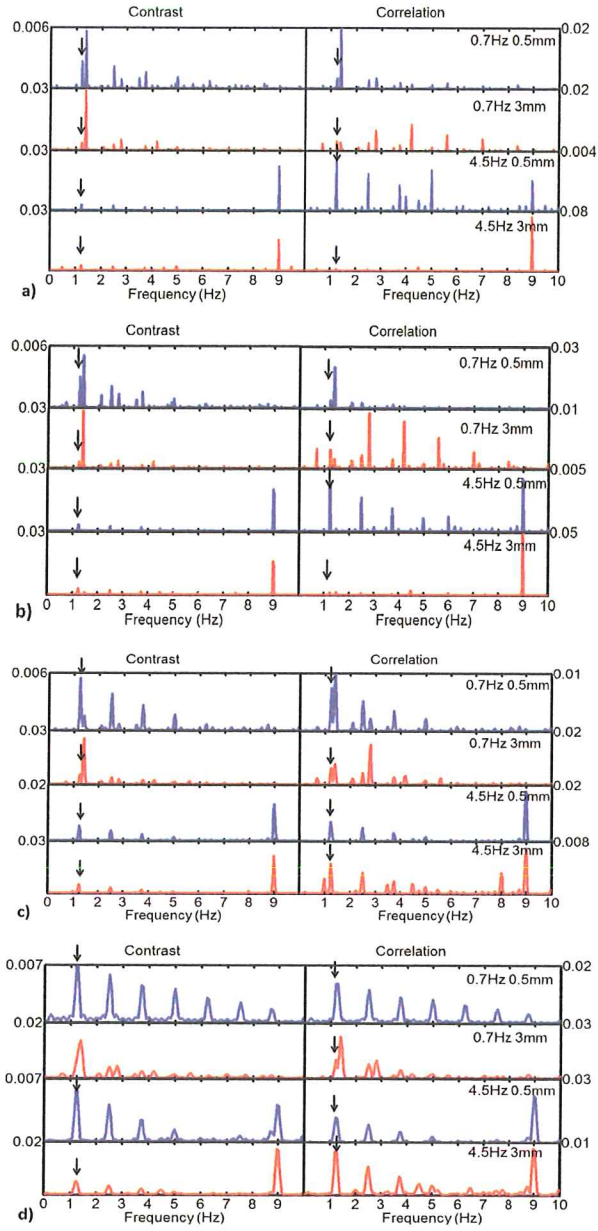

Figure 7.7: Spectral analysis is shown for two displacements of the illuminating laser with an angle of 70° with the camera: 0.5mm (blue line) and 3mm (red line) displacement amplitudes and at the frequencies of 0.7Hz and 4.5Hz measured with exposure times of a) 20ms, b) 16ms c) 8ms and d) 4ms. The plot shows the result of measurements using the correlation analysis (right panel) and speckle contrast (left panel) for milk pulsation at 1.25Hz. The y-axis shows the amplitudes of the correlation analysis and speckle contrast on the right and left side of each panel, respectively.

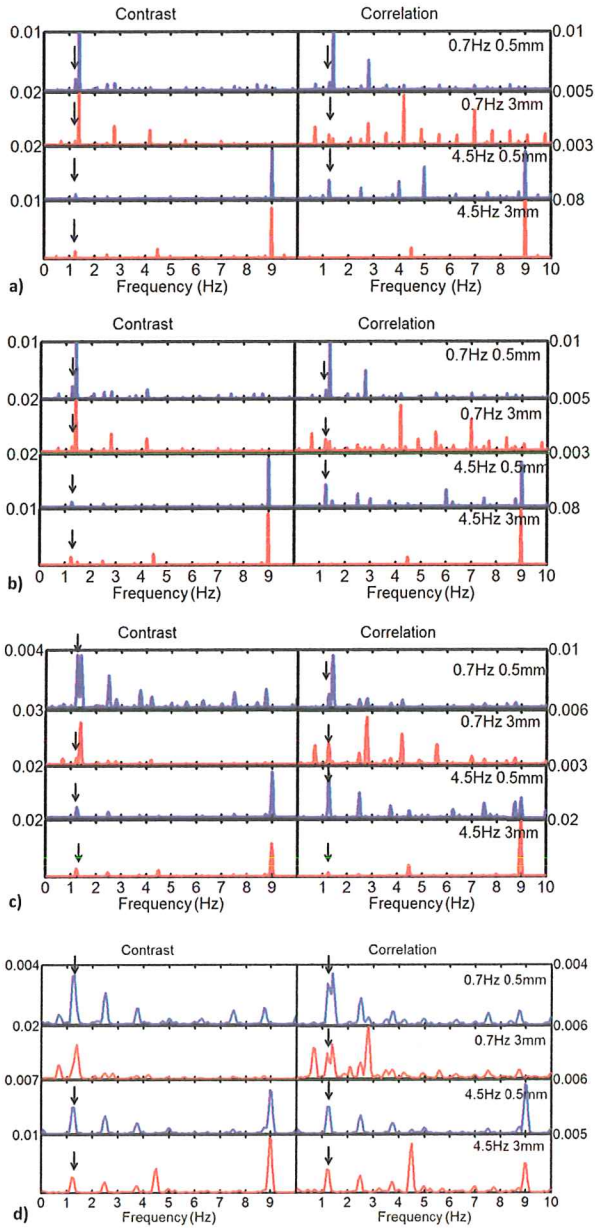

Figure 7.8: Spectral analysis is shown for two displacements of the illuminating laser with an angle of 20° with camera: 0.5mm (blue line) and 3mm (red line) at the frequencies of 0.7Hz and 4.5Hz measured with exposure times of a) 20ms, b) 16ms c) 8m and c) 4ms. The plot shows the result of measurements using the correlation analysis (right panel) and speckle contrast (left panel) for milk pulsation at 1.25Hz. The y-axis shows the amplitudes of the correlation analysis and speckle contrast on the right and left side of each panel, respectively.

cannot distinguish the difference of the direction of laser motion. Speckle contrast analysis provides good visibility specially for low amplitude and frequency of laser motion. Increasing the amplitude and frequency of laser motion decreases the signal visibility for the contrast analysis for longer exposure times. Longer exposure times lead to more averaging and thus averages out the weaker optical signal from the flow pulse and emphasizes the laser motion. However, the performance using contrast analysis for higher frequencies is better for shorter exposure times of 8ms and 4ms. This result cannot be improved further without decreasing the spectral resolution of the data set unless the recording time is increased or a smaller area of the camera chip is used. In comparison, correlation provides a richer spectrum which has more features. The signal visibility in the case of higher amplitude and frequency is better for correlation based analysis of the measurements. This is more obvious for shorter exposure times. It can also be seen that for large amplitude, low frequency measurements, the correlation technique fails to pick up the correct spectrum of the induced motion. Mainly because the harmonics have a higher amplitude. This is again better for the shorter exposure times.

The measurements done with a 70° angle of the illumination laser with the camera show better signal than the 20° measurements. The 70° configuration has a larger elongated illumination spot leading to a bigger area contributing to the speckle pattern on the detection plane. Also, there is more uniformity of illumination over the spot being studied. This can explain the reason for the observed difference. In the measurements mentioned above, the direction of motion of the laser is the same as the direction of flow, since this is the worst case scenario. The case where the flow direction was perpendicular to the laser motion was also measured and analyzed for all the configurations shown above. These results are omitted since no discernible differences are seen in comparison to the case shown above, where the flow and motion directions are parallel. For applicability to compact devices, we also studied the statistical correlation between the intensity fluctuations at two pixel locations for the time sequence of images from a measurement which is discussed next.

7.3 Pixel based analysis for feasibility of use in compact devices

For some device applications, the need for compactness and lower cost is imperative, therefore a trade-off between speckle image size and measurement sensitivity comes into play. For these applications, we decided to analyze our measurements using two groups of 2×2 pixels, positioned at locations opposing each other, across the beam diameter. The distance between the super-pixels thus varied according to the beam size, in the two cases of the 70° and 20° configurations of measurement and was typically, 150 and 100 pixels, respectively. These super pixels mimic independent local detectors and were chosen in direction parallel to and perpendicular to the axis of motion of the laser. The result of this analysis has been shown in

Fig. 7.9. In this figure, the analysis result for both parallel and perpendicular directions of motion for 0.7 Hz and 4.5 Hz with the minimum and maximum displacement amplitude of 0.5 mm and 3 mm, is shown. The exposure time for each frame shown in Fig. 7.9 was 8 ms.

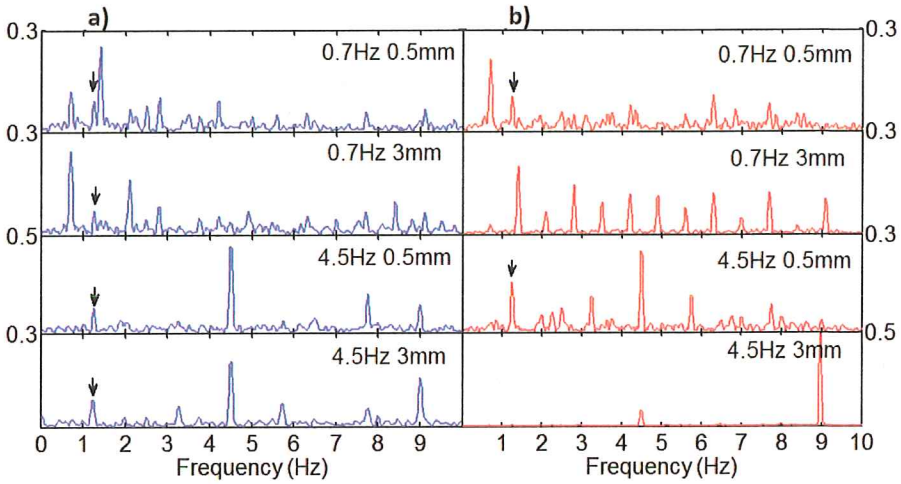

Figure 7.9: Spectral analysis for pixel correlation is shown for frequencies of 0.7Hz and 4.5Hz with displacement amplitudes of 0.5mm and 3mm after being analyzed in a) perpendicular and b) parallel directions to the induced motion artifact. In each plot, the arrow points at the fluid pulse rate. The y-axis shows the amplitudes of the parallel configuration and perpendicular configuration on the right and left side of each panel, respectively.

In Fig. 7.9, we see that for low amplitude of displacement of the laser, two super-pixels are sufficient to measure the motion and the fluid pulsation using the correlation coefficients of speckle intensity. However, for higher amplitudes of laser motion the position of the super-pixels or in a device the detectors, with respect to the motion between the sensor and the subject, can play a significant role in the measurement results. In case of a parallel configuration of the super-pixels with respect to the laser motion, only the induced motion is detected when the laser motion is large.

7.4 Summary

We study a system based on dynamic light scattering and techniques to extract physical parameters of the scatterers. This was done specially for pulsatile flow in face of motion induced artifacts. Measurements for a full parameter set, including different amplitudes and frequencies for motion of the illumination, alignment configurations of illumination and detection, and camera exposure time were carried out. This measurement data was then analyzed with different analysis techniques

based on speckle contrast and correlation. In general, we observed that, correlation based analysis is more robust against high amplitude laser motion, particularly when combined with short exposure times. Also, a larger angle between illumination and detection yields a better signal. Measurements were also performed on the finger of a volunteer and analyzed using the two techniques. The *in-vivo* measurement results agreed with the results of the *in-vitro* case. The measurements were analyzed again using only a few pixels from the entire camera image to mimic independent local detectors. It was observed that a few pixels from the image were sufficient to extract the necessary parameters, which is useful in case of compact devices. Therefore, we conclude that several speckle based techniques, can be used to understand the effect of motion induced artifacts. These studies can be incorporated in future devices to make them more robust.

CHAPTER

8 Discussion and conclusions

Look deep into nature, and then you will understand everything better.

Albert Einstein

In this thesis, we demonstrated the possibility of using laser speckle imaging for monitoring pulsatile flow, specifically in presence of induced motion artifacts. This is especially important in the context of continuous health monitoring devices, as these pose additional challenges when compared to static monitoring devices: since they are worn while the user is performing regular routine activities, these typically involve motion, which has been a known challenge in several monitoring applications. Although optical based techniques have been around for many years, the extraction of the signal in the presence of motion artifacts has been an exploratory research. In this project, we investigated a hardware based solution to address this problem where we applied laser speckle technique. It has been a question in the literature whether speckle based techniques could be made robust against motion artifacts [131]. The research provided in this thesis, brings the answer to this question closer, which we believe can spark more research and development efforts towards integrating the presented techniques into products.

The project was initiated by building a setup to monitor flow using laser speckle technique. The main challenge was the lack of understanding over detailed surface structure and light behavior in the tissue using laser speckle. To confront with such an issue in experimental cases, we developed a platform to conduct a systematic study on flow dynamics, with an attempt to understand the influence of different parameters on the flow measurement. In this work, we were able to study the influence of each variable individually. We have shown that statistical approach is a valuable tools to study the speckle patterns. The outcome of this study

demonstrate a deeper understanding into the properties of the dynamic speckle arising from pulsatile flow.

The properties of the flow and the scatterers which can be retrieved from the speckle pattern yield more information about the system being studied. We advanced this further by combining the laser speckle flow measurements with another full-field optical technique as particle image velocimetry (PIV). We showed that we can measure complementary parameters using the secondary analysis of PIV, where it can accurately compute the flow velocity using tracer particles. We use the high spatial resolution of PIV to generate a full velocity map of the flow field and the high temporal resolution of LASCA to extract the detailed frequency spectrum of the fluid pulses. This work showed that for a bifurcating system the frequency spectrum of pulsatile flow is location dependent. Using this combination of techniques a complete study of complex pulsatile flow in an intricate flow network can be studied. These experiments have been reported for the study of pulsatile flow using ventricular assist device in a patient-specific carotid artery phantom.

In the second part of this thesis, a different technique has been explored for monitoring pulsatile flow. We applied fractal analysis for processing of the speckle pattern. The random spatial distribution of bright and dark spots in a speckle image displays the self similarity, scaling, and statistics which we are familiar with in fractals. To demonstrate using fractal dimension changes due to pulsatile, these measurements have been done in comparison with laser speckle analysis and for different experimental configurations. Multiscale analysis of time series of scattered data can be a useful tool for better understanding the underlying complex dynamics in the medium. Further, the fractal analysis has been applied to a different scattering configuration where the scattered wavefront illuminates the pulsatile flow and is recorded after propagation through another scattering medium. It has been shown that under these conditions, the laser speckle contrast analysis can not detect the main frequency of pulsation, where analysis of fractal dimension promises great potential for monitoring changes through a multi-layered system with different scattering properties.

We have to emphasize the advantage of using laser speckle to convey important information in scenarios where motion artifacts are present and perhaps this can be an option to be implemented in future products. The artifact generated due to relative motion between the source, detector and sample can also be studied so that they can be handled when studying the system, thus making the parameter retrieval more robust. We demonstrated the results for *in-vitro* and *in-vivo* cases. The results have been compared using laser speckle contrast analysis and correlation. Changing the parameters of the measurement showed that different analysis techniques were successful for different cases. In general, the *in-vivo* and the *in-vitro* measurements showed similar results for similar analysis techniques. In this set of experiments, we also perform analysis on a selected set of pixels from the collected data to show the feasibility of having a more compact devices for the future products. This data analysis was done using only few image pixels, which

was seen to be sufficient to extract the heart rate. Thus further work needs to be done to further characterize these techniques.

8.1 Suggestions for future work

In this thesis, we have provided experimental studies for monitoring pulsatile flow based on laser speckle techniques. Although we have shown for the first time the application of laser speckle with induced motion artifacts, we only focused on one way of realizing it. We mainly address one of the predominant errors where the existing devices (not based on speckle) have, which is the sensor movement with respect to the skin. However, more experiments are required to address all different source of artifact for different scenarios. Further clinical studies with large population diversity need to be taken into consideration, to iron out the differences arising due to different skin type and physiological variations. For our present studies this may eventually lead to better medical devices which are low cost and robust. Further work may include applying the technique to analyze the complex hemodynamics. This can include the difference in the metabolic transients between arterial and venous blood flow. This can be applied by using dual wavelength concept to study the metabolic changes induced by the level of oxy- and deoxy-hemoglobin. These are some of the possible features, however the application of present study can be extended to any kind of flowing samples, where possibilities for further theoretical and experimental exploration are vast.

Bibliography

[1] A. Pantelopoulos and N. Bourbakis, "A survey on wearable sensor-based systems for health monitoring and prognosis," *IEEE Transactions on Systems, Man, and Cybernetics, Part C: Applications and Reviews*, vol. 40, no. 1, pp. 1–12, Jan 2010. [Online]. Available: http://ieeexplore.ieee.org/stamp/stamp.jsp?tp=&arnumber=5306098&isnumber=5314168

[2] M. Wintermark, J. P. Thiran, P. Maeder, P. Schnyder, and R. Meuli, "Simultaneous measurement of regional cerebral blood flow by perfusion ct and stable xenon ct: a validation study," *American Journal of Neuroradiology*, vol. 22, no. 5, pp. 905–14, May 2001. [Online]. Available: http://www.ncbi.nlm.nih.gov/pubmed/11337336

[3] C. C. Bishop, S. Powell, D. Rutt, and N. L. Browse, "Transcranial doppler measurement of middle cerebral artery blood flow velocity: a validation study," *Stroke*, vol. 17, no. 5, pp. 913–915, Sep. 1986. [Online]. Available: http://stroke.ahajournals.org/cgi/doi/10.1161/01.STR.17.5.913

[4] J. S. Raynaud, S. Duteil, J. T. Vaughan, F. Hennel, C. Wary, a. Leroy-Willig, and P. G. Carlier, "Determination of skeletal muscle perfusion using arterial spin labeling nmri: validation by comparison with venous occlusion plethysmography," *Magnetic Resonance in Medicine*, vol. 46, no. 2, pp. 305–11, Aug. 2001. [Online]. Available: http://www.ncbi.nlm.nih.gov/pubmed/11477634

[5] Z. Chen, T. E. Milner, D. Dave, and J. S. Nelson, "Optical doppler tomographic imaging of fluid flow velocity in highly scattering media," *Optics Letters*, vol. 22, no. 1, pp. 64–6, Jan. 1997. [Online]. Available: http://www.ncbi.nlm.nih.gov/pubmed/18183104

[6] C. E. Elwell and C. E. Cooper, "Making light work: illuminating the future of biomedical optics," *Philosophical Transactions. Series A, Mathematical, Physical, and Engineering Sciences*, vol. 369, no. 1955, pp. 4358–79, Nov. 2011. [Online]. Available: http://www.ncbi.nlm.nih.gov/pubmed/22006895

[7] A. Gibson and H. Dehghani, "Diffuse optical imaging," *Philosophical Transactions. Series A, Mathematical, Physical, and Engineering Sciences*,

vol. 367, no. 1900, pp. 3055–72, Aug. 2009. [Online]. Available: http://www.ncbi.nlm.nih.gov/pubmed/19581255

[8] V. Roberts, "Photoplethysmography- fundamental aspects of the optical properties of blood in motion," *Transactions of the Institute of Measurement and Control*, vol. 4, no. 2, pp. 101–106, Apr. 1982. [Online]. Available: http://tim.sagepub.com/cgi/doi/10.1177/014233128200400205

[9] A. Sola, L. Chow, and M. Rogido, "Pulse oximetry in neonatal care in 2005. a comprehensive state of the art review," *Anales de pediatr (Barc)*, vol. 62, no. 3, pp. 266–81, Mar. 2005. [Online]. Available: http://www.ncbi.nlm.nih.gov/pubmed/15737290

[10] P. S. Addison, J. N. Watson, M. L. Mestek, and R. S. Mecca, "Developing an algorithm for pulse oximetry derived respiratory rate (rr(oxi)): a healthy volunteer study," *Journal of Clinical Monitoring and Computing*, vol. 26, no. 1, pp. 45–51, Feb. 2012. [Online]. Available: http://www.pubmedcentral.nih.gov/articlerender.fcgi?artid=3268017&tool=pmcentrez&rendertype=abstract

[11] K. Forrester, C. Stewart, J. Tulip, C. Leonard, and R. Bray, "Comparison of laser speckle and laser doppler perfusion imaging: Measurement in human skin and rabbit articular tissue," *Medical and Biological Engineering and Computing*, vol. 40, no. 6, pp. 687–697, 2002. [Online]. Available: http://dx.doi.org/10.1007/BF02345307

[12] D. A. Boas and A. K. Dunn, "Laser speckle contrast imaging in biomedical optics," *Journal of Biomedical Optics*, vol. 15, no. 1, p. 011109, 2010. [Online]. Available: http://www.pubmedcentral.nih.gov/articlerender.fcgi?artid=2816990&tool=pmcentrez&rendertype=abstract

[13] J. D. Briers and A. F. Fercher, "Retinal blood-flow visualization by means of laser speckle photography," *Investigative Ophthalmology and Visual Science*, vol. 22, no. 2, pp. 255–259, Feb. 1982. [Online]. Available: http://www.iovs.org/content/22/2/255.abstract

[14] K. R. Forrester, J. Tulip, C. Leonard, C. Stewart, and R. C. Bray, "A laser speckle imaging technique for measuring tissue perfusion," *IEEE Transactions on Biomedical Engineering*, vol. 51, no. 11, pp. 2074–2084, Nov. 2004. [Online]. Available: http://europepmc.org/abstract/MED/15536909

[15] A. K. Dunn, H. Bolay, M. A. Moskowitz, and D. A. Boas, "Dynamic imaging of cerebral blood flow using laser speckle," *Journal of Cerebral Blood Flow and Metabolism*, vol. 21, no. 3, pp. 195–201, Mar. 2001. [Online]. Available: http://www.ncbi.nlm.nih.gov/pubmed/11295873

[16] C. Stoianovici, P. Wilder-Smith, and B. Choi, "Assessment of pulpal vitality using laser speckle imaging," *Lasers in Surgery and Medicine*, vol. 43, no. 8, pp. 833–837, Sep. 2011. [Online]. Available: http://dx.doi.org/10.1002/lsm.21090

[17] V. V. Tuchin, E. I. Galanzha, and V. P. Zharov, "In vivo image flow cytometry," in *Advanced Optical Flow Cytometry*. Wiley-VCH Verlag GmbH Co KGaA, 2011, pp. 387–431. [Online]. Available: http://dx.doi.org/10.1002/9783527634286.ch14

[18] L. B. Wood and H. Asada, "Low variance adaptive filter for cancelling motion artifact in wearable photoplethysmogram sensor signals," *IEEE Conference Engineering in Medicine and Biology Society*, vol. 2007, pp. 652–5, Jan. 2007. [Online]. Available: http://www.ncbi.nlm.nih.gov/pubmed/18002040

[19] A. Volmer and R. Orglmeister, "Wireless body sensor network for low-power motion-tolerant synchronized vital sign measurement," *Annual International Conference of the IEEE Engineering in Medicine and Biology Society*, vol. 2008, pp. 3422–5, Jan. 2008. [Online]. Available: http://www.ncbi.nlm.nih.gov/pubmed/19163444

[20] A. C. M. Dassel, R. Graaff, A. Meijer, W. G. Zijlstra, and J. G. Aarnoudse, "Reflectance pulse oximetry at the forehead of newborns: the influence of varying pressure on the probe," *Journal of Clinical Monitoring*, pp. 421–428, 1996. [Online]. Available: http://link.springer.com/article/10.1007/BF02199702

[21] C. C. Y. Poon, Q. Liu, H. Gao, W. Lin, and Y. Zhang, "Wearable intelligent systems for e-health," *Journal of Computing Science and Engineering*, vol. 5, no. 3, pp. 246–256, Sep. 2011. [Online]. Available: http://koreascience.or.kr/journal/view.jsp?kj=E1EIKI&py=2011&vnc=v5n3&sp=246

[22] M. Raghuram, K. V. Madhav, E. H. Krishna, N. R. Komalla, K. Sivani, and K. A. Reddy, "Dual-tree complex wavelet transform for motion artifact reduction of ppg signals," *2012 IEEE International Symposium on Medical Measurements and Applications Proceedings*, pp. 1–4, May 2012. [Online]. Available: http://ieeexplore.ieee.org/lpdocs/epic03/wrapper.htm?arnumber=6226643

[23] R. Yousefi, M. Nourani, and I. Panahi, "Adaptive cancellation of motion artifact in wearable biosensors," *Annual International Conference of the IEEE Engineering in Medicine and Biology Society*, vol. 2012, pp. 2004–8, Jan. 2012. [Online]. Available: http://www.ncbi.nlm.nih.gov/pubmed/23366311

[24] M. R. Ram, K. V. Madhav, E. H. Krishna, N. R. Komalla, and K. A. Reddy, "A novel approach for motion artifact reduction in ppg signals based on as-lms adaptive filter," *IEEE Transactions on Instrumentation and Measurement*, vol. 61, no. 5, pp. 1445–1457, 2012. [Online]. Available: http://ieeexplore.ieee.org/stamp/stamp.jsp?tp=&arnumber=6111474&isnumber=6178360

[25] Y. S. Yan, C. C. Poon, and Y. T. Zhang, "Reduction of motion artifact in pulse oximetry by smoothed pseudo wigner-ville distribution," *Journal*

of Neuroengineering and Rehabilitation, vol. 2, no. 1, p. 3, Mar. 2005. [Online]. Available: http://www.pubmedcentral.nih.gov/articlerender.fcgi?artid=553999&tool=pmcentrez&rendertype=abstract

[26] G. E. Nilsson, T. Tenland, and P. Oberg, "Evaluation of a laser doppler flowmeter for measurement of tissue blood flow," *EEE Transactions on Biomedical Engineering*, vol. BME-27, no. 10, pp. 597–604, Oct 1980. [Online]. Available: http://www.ncbi.nlm.nih.gov/pubmed/6449469

[27] D. J. Pine, D. A. Weitz, P. M. Chaikin, and E. Herbolzheimer, "Diffusing wave spectroscopy," *Physical Review Letters*, vol. 60, pp. 1134–1137, Mar 1988. [Online]. Available: http://link.aps.org/doi/10.1103/PhysRevLett.60.1134

[28] S. L. Jacques, "Optical properties of biological tissues: a review," *Physics in Medicine and Biology*, vol. 58, no. 11, p. R37, 2013. [Online]. Available: http://stacks.iop.org/0031-9155/58/i=11/a=R37

[29] S. Mallidi, G. P. Luke, and S. Emelianov, "Photoacoustic imaging in cancer detection, diagnosis, and treatment guidance," *Trends in Biotechnology*, vol. 29, no. 5, pp. 213 – 221, 2011. [Online]. Available: http://www.sciencedirect.com/science/article/pii/S0167779911000175

[30] S. Svanberg, *Atomic and Molecular Spectroscopy: Basic Aspects and Practical Applications*, ser. Springer Series on Atomic, Optical, and Plasma Physics. Springer Berlin Heidelberg, 2012. [Online]. Available: https://books.google.nl/books?id=GnXtCAAAQBAJ

[31] C. Raulin and S. Karsai, *Laser and IPL Technology in Dermatology and Aesthetic Medicine*. Springer Berlin Heidelberg, 2011. [Online]. Available: https://books.google.nl/books?id=yY7fz5J4g4sC

[32] B. C. Wilson and M. S. Patterson, "The physics, biophysics and technology of photodynamic therapy," *Physics in Medicine and Biology*, vol. 53, no. 9, p. R61, 2008. [Online]. Available: http://stacks.iop.org/0031-9155/53/i=9/a=R01

[33] L. Wang and S. L. Jacques, "Error estimation of measuring total interaction coefficients of turbid media using collimated light transmission," *Physics in Medicine and Biology*, vol. 39, no. 12, p. 2349, 1994. [Online]. Available: http://stacks.iop.org/0031-9155/39/i=12/a=015

[34] J. Swartling, J. S. Dam, and S. Andersson-Engels, "Comparison of spatially and temporally resolved diffuse-reflectance measurement systems for determination of biomedical optical properties," *Applied Optics*, vol. 42, no. 22, pp. 4612–4620, Aug 2003. [Online]. Available: http://ao.osa.org/abstract.cfm?URI=ao-42-22-4612

[35] D. J. Cuccia, F. Bevilacqua, A. J. Durkin, F. R. Ayers, and B. J. Tromberg, "Quantitation and mapping of tissue optical properties using modulated

imaging," *Journal of Biomedical Optics*, vol. 14, no. 2, pp. 024 012–024 012–13, 2009. [Online]. Available: http://dx.doi.org/10.1117/1.3088140

[36] M. S. Patterson, B. Chance, and B. C. Wilson, "Time resolved reflectance and transmittance for the noninvasive measurement of tissue optical properties," *Applied Optics*, vol. 28, no. 12, pp. 2331–2336, Jun 1989. [Online]. Available: http://ao.osa.org/abstract.cfm?URI=ao-28-12-2331

[37] L. Wang and H. Wu, *Biomedical Optics: Principles and Imaging*. Wiley, 2012. [Online]. Available: https://books.google.nl/books?id=EJeQ0hAB76gC

[38] A. Yaroshevsky, Z. Glasser, E. Granot, and S. Sternklar, "Transition from the ballistic to the diffusive regime in a turbid medium," *Optics Letters*, vol. 36, no. 8, pp. 1395–1397, Apr 2011. [Online]. Available: http://ol.osa.org/abstract.cfm?URI=ol-36-8-1395. DOI:10.1364/OL.36.001395

[39] K. van As, "Interferometric scattering of light by an ensemble of flowing spherical particles: A numerical study," Delft University of Technology, Tech. Rep., 2015. [Online]. Available: http://www.kevinvanas.nl/TUDelft/MSc/Report.pdf

[40] K. Anders and H. Jiangping, "Numerical simulations of light scattering by red blood cells," *IEEE Transactions on Biomedical Engineering*, vol. 52, no. 1, pp. 13–18, 2005. [Online]. Available: http://ieeexplore.ieee.org/xpls/abs_all.jsp?arnumber=1369584

[41] A. M. Nilsson, P. Alsholm, A. Karlsson, and S. Andersson-engels, "T-matrix computations of light scattering by red blood cells," *Applied Optics*, vol. 37, no. 13, pp. 10–16, 1998. [Online]. Available: http://www.ncbi.nlm.nih.gov/pubmed/18273219

[42] A. J. Welch, G. Yoon, and M. J. C. Van Gemert, "Practical models for light distribution in laser-irradiated tissue," *Lasers in Surgery and Medicine*, vol. 6, no. 6, pp. 488–493, 1987. [Online]. Available: http://dx.doi.org/10.1002/lsm.1900060603

[43] M. S. Patterson, B. C. Wilson, and D. R. Wyman, "The propagation of optical radiation in tissue i. models of radiation transport and their application," *Lasers in Medical Science*, vol. 6, no. 2, pp. 155–168, 1991. [Online]. Available: http://dx.doi.org/10.1007/BF02032543

[44] A. Ishimaru, *Wave Propagation and Scattering in Random Media*. Academic Press, 1978. [Online]. Available: http://www.sciencedirect.com/science/article/pii/B9780123747013500016

[45] K. Mitra, M. Lai, and S. Kumar, "Transient radiation transport in participating media within a rectangular enclosure," *Journal of Thermophysics and Heat Transfer*, vol. 11, no. 3, 1997. [Online]. Available: http://arc.aiaa.org/doi/pdf/10.2514/2.6255

[46] A. J. Welch and M. J. C. van Gemert, *Optical-Thermal Response of Laser-Irradiated Tissue*. Springer Netherlands, 2011. [Online]. Available: https://books.google.nl/books?id=rdo-z-06_4AC

[47] G. Thomas and K. Stamnes, *Radiative Transfer in the Atmosphere and Ocean*, ser. Atmospheric and space science. Cambridge University Press, 2002. [Online]. Available: https://books.google.nl/books?id=DxR2nEp0CUIC

[48] S. A. Prahl, M. J. C. van Gemert, and A. J. Welch, "Determining the optical properties of turbid media by using the adding doubling method," *Applied Optics*, vol. 32, no. 4, pp. 559–568, Feb 1993. [Online]. Available: http://ao.osa.org/abstract.cfm?URI=ao-32-4-559

[49] D. L. Andrews, *Photonics, Biomedical Photonics, Spectroscopy, and Microscopy*, ser. A Wiley-Science Wise Co-Publication. Wiley, 2015. [Online]. Available: https://books.google.nl/books?id=QJzTBgAAQBAJ

[50] X. Wang, L. V. Wang, C. W. Sun, and C. C. Yang, "Polarized light propagation through scattering media: time-resolved monte carlo simulations and experiments," *Journal of Biomedical Optics*, vol. 8, no. 4, pp. 608–617, 2003. [Online]. Available: http://dx.doi.org/10.1117/1.1606462

[51] E. Alerstam, T. Svensson, and S. Andersson-Engels, "Parallel computing with graphics processing units for high-speed monte carlo simulation of photon migration," *Journal of Biomedical Optics*, vol. 13, no. 6, pp. 060 504–060 504–3, 2008. [Online]. Available: http://dx.doi.org/10.1117/1.3041496

[52] J. Beuthan and O. Minet, "The spatial variation of the refractive index in biological cells," *Physics in Medicine and Biology*, vol. 369, 1996. [Online]. Available: http://iopscience.iop.org/0031-9155/41/3/002

[53] S. Chandrasekhar, *Radiative Transfer*, ser. Dover books on advanced mathematics. Dover Publications, 1960. [Online]. Available: https://books.google.nl/books?id=zPVQAAAAMAAJ

[54] T. Khan, "On derivation of the radiative transfer equation and its diffusion approximation for scattering media with spatially varying refractive indices," *Clemson University Mathematical Sciences Technical*, 2003. [Online]. Available: http://www.clemson.edu/ces/math/technical_reports/TR2003_07_TK.pdf

[55] S. R. Arridge, "Optical tomography in medical imaging," *Inverse Problems*, vol. 15, no. 2, p. R41, 1999. [Online]. Available: http://stacks.iop.org/0266-5611/15/i=2/a=022

[56] S. L. Jacques and B. W. Pogue, "Tutorial on diffuse light transport," *Journal of Biomedical Optics*, vol. 13, no. 4, p. 041302, 2015. [Online]. Available: http://www.ncbi.nlm.nih.gov/pubmed/19021310

[57] W. Star, "Diffusion theory of light transport," in *Optical-Thermal Response of Laser-Irradiated Tissue*, A. J. Welch and M. J. van Gemert, Eds. Springer Netherlands, 2011, pp. 145–201. [Online]. Available: http://dx.doi.org/10.1007/978-90-481-8831-4_6

[58] J. D. Briers, "Time-varying laser speckle for measuring motion and flow," *SPIE Proceedings, Saratov Fall Meeting 2000*, vol. 4242, pp. 25–39, 2001. [Online]. Available: http://proceedings.spiedigitallibrary.org/proceeding.aspx?articleid=898877

[59] Y. Gan and W. Steinchen (deceased), "Speckle methods," in *Springer Handbook of Experimental Solid Mechanics*, J. Sharpe, William N., Ed. Springer US, 2008, pp. 655–674. [Online]. Available: http://dx.doi.org/10.1007/978-0-387-30877-7_23

[60] S. Donati, *Electro-Optical Instrumentation: Sensing and Measuring with Lasers*. Upper Saddle River, NJ, USA: Prentice Hall PTR, 2004.

[61] J. W. Goodman, *Statistical properties of laser speckle patterns*, ser. Topics in Applied Physics. Springer Berlin Heidelberg, 1975, vol. 9. [Online]. Available: http://dx.doi.org/10.1007/BFb0111436

[62] J. C. Dainty, "The statistics of speckle patterns," *Progress in Optics*, 1977. [Online]. Available: http://optics.nuigalway.ie/people/chris/chrispapers/Chapt%20Bk002.pdf

[63] J. Goodman, *Speckle Phenomena in Optics: Theory and Applications*. Roberts & Company, 2007. [Online]. Available: https://books.google.nl/books?id=TynXEcS0DncC

[64] J. Dainty, "An introduction to gaussian speckle," *Proceedings of the Society of Photo-Optical Instrumentation Engineers*, 1980. [Online]. Available: http://www.nuigalway.ie/research/applied_optics/people/chris/chrispapers/Conf017.pdf

[65] Sirohi, *Speckle Metrology*, ser. Optical Science and Engineering, T. . Francis, Ed., 1993. [Online]. Available: https://books.google.nl/books?id=UlUchvvgLfEC

[66] Q. Jianjun, L. Pengcheng, L. Weihua, W. Jia, Z. Hongyan, and L. Qingming, "Spatiotemporal laser speckle contrast analysis for blood flow imaging with maximized speckle contrast," *Journal of Biomedical Optics*, vol. 15, no. 1, p. 016003, 2010. [Online]. Available: http://www.ncbi.nlm.nih.gov/pubmed/20210450

[67] E. P. MacKerrow and M. J. Schmitt, "Measurement of integrated speckle statistics for co 2 lidar returns from a moving, nonuniform, hard target," *Applied Optics*, vol. 36, no. 27, pp. 6921–6937, 1997. [Online]. Available: http://www.opticsinfobase.org/abstract.cfm?uri=ao-36-27-6921

[68] C. Glazowski and M. Rajadhyaksha, "Optimal detection pinhole for lowering speckle noise while maintaining adequate optical sectioning in confocal reflectance microscopes," *Journal of Biomedical Optics*, vol. 17, no. 8, p. 085001, Aug. 2012. [Online]. Available: http://www.pubmedcentral.nih.gov/articlerender.fcgi?artid=3412991&tool=pmcentrez&rendertype=abstract

[69] W. Welford, "First order statistics of speckle produced by weak scattering media," *Optical and Quantum Electronics*, vol. 7, pp. 413–416, 1975. [Online]. Available: http://link.springer.com/article/10.1007/BF00619839

[70] S. S. Ulyanov, "Speckled speckle statistics with a small number of scatterers: Implication for blood flow measurement," *Journal of Biomedical Optics*, vol. 3, no. 3, pp. 237–245, 1998. [Online]. Available: http://dx.doi.org/10.1117/1.429879. DOI:10.1117/1.429879

[71] H. J. Tiziani and J. Klenk, "Vibration analysis by speckle techniques in real time," *Applied Optics*, vol. 20, no. 8, pp. 1467–1470, Apr 1981. [Online]. Available: http://ao.osa.org/abstract.cfm?URI=ao-20-8-1467. DOI:10.1364/AO.20.001467

[72] R. R. Cardoso, A. G. Costa, C. M. B. Nobre, and R. A. Braga, "Frequency signature of water activity by biospeckle laser," *Optics Communications*, vol. 284, no. 8, pp. 2131–2136, Apr. 2011. [Online]. Available: http://linkinghub.elsevier.com/retrieve/pii/S0030401811000216

[73] Z. Hajjarian and S. K. Nadkarni, "Evaluation and correction for optical scattering variations in laser speckle rheology of biological fluids," *PloS one*, vol. 8, no. 5, p. e65014, Jan. 2013. [Online]. Available: http://www.pubmedcentral.nih.gov/articlerender.fcgi?artid=3660338&tool=pmcentrez&rendertype=abstract

[74] H. Rabal and R. Braga, *Dynamic Laser Speckle and Applications*, ser. Optical Science and Engineering. CRC Press, 2008. [Online]. Available: https://books.google.nl/books?id=T4MA_XtWAwMC

[75] R. Gurjar, V. Backman, and L. Perelman, "Imaging human epithelial properties with polarized light-scattering spectroscopy," *Nature medicine*, pp. 1245–1248, 2001. [Online]. Available: http://www.nature.com/nm/journal/v7/n11/abs/nm1101-1245.html

[76] W. Tscharnuter, "Photon correlation spectroscopy in particle sizing," *Encyclopedia of Analytical Chemistry*, no. 2, 2000. [Online]. Available: http://onlinelibrary.wiley.com/doi/10.1002/9780470027318.a1512/full

[77] D. B. Sattelle, "Quasielastic laser light scattering and laser doppler electrophoresis as probes of synaptic and secretory terminal function," *Journal of Experimental Biology*, vol. 252, pp. 233–252, 1988. [Online]. Available: http://jeb.biologists.org/content/139/1/233.short

[78] D. Pine, D. Weitz, P. Chaikin, and E. Herbolzheimer, "Diffusing wave spectroscopy," *Physical Review Letters*, vol. 60, no. 12, 1988. [Online]. Available: http://journals.aps.org/prl/abstract/10.1103/PhysRevLett.60.1134

[79] J. D. Briers, "Laser doppler and time-varying speckle: a reconciliation," *Journal of the Optical Society of America A*, vol. 13, no. 2, pp. 345–350, Feb 1996. [Online]. Available: http://josaa.osa.org/abstract.cfm?URI=josaa-13-2-345

[80] B. J. Berne and R. Pecora, *Dynamic light scattering : with applications to chemistry, biology, and physics*, unabridged ed. Dover Publications, Aug. 2000. [Online]. Available: http://www.amazon.com/exec/obidos/redirect?tag=citeulike07-20&path=ASIN/0486411559

[81] D. A. Boas and A. G. Yodh, "Spatially varying dynamical properties of turbid media probed with diffusing temporal light correlation," *Journal of the Optical Society of America A*, vol. 14, no. 1, p. 192, Jan. 1997. [Online]. Available: http://www.opticsinfobase.org/abstract.cfm?URI=josaa-14-1-192

[82] L. Cipelletti and D. A. Weitz, "Ultralow-angle dynamic light scattering with a charge coupled device camera based multispeckle, multitau correlator," *Review of Scientific Instruments*, vol. 70, no. 8, p. 3214, 1999. [Online]. Available: http://scitation.aip.org/content/aip/journal/rsi/70/8/10.1063/1.1149894

[83] R. Bandyopadhyay, A. S. Gittings, S. S. Suh, P. K. Dixon, and D. J. Durian, "Speckle-visibility spectroscopy: A tool to study time-varying dynamics," *Review of Scientific Instruments*, vol. 76, no. 9, p. 093110, 2005. [Online]. Available: http://link.aip.org/link/RSINAK/v76/i9/p093110/s1&Agg=doi

[84] D. D. Duncan and S. J. Kirkpatrick, "Can laser speckle flowmetry be made a quantitative tool?" *Journal of the Optical Society of America. A, Optics, image science, and vision*, vol. 25, no. 8, pp. 2088–94, Aug. 2008. [Online]. Available: http://www.pubmedcentral.nih.gov/articlerender.fcgi?artid=2572153&tool=pmcentrez&rendertype=abstract

[85] V. Rajan, B. Varghese, T. G. van Leeuwen, and W. Steenbergen, "Review of methodological developments in laser doppler flowmetry," *Lasers in Medical Science*, vol. 24, no. 2, pp. 269–83, Mar. 2009. [Online]. Available: http://www.ncbi.nlm.nih.gov/pubmed/18236103

[86] S. Guyot, M. C. Peron, and E. Delechelle, "Spatial speckle characterization by brownian motion analysis," *Physical Review E*, vol. 70, no. 4, p. 046618, Oct. 2004. [Online]. Available: http://link.aps.org/doi/10.1103/PhysRevE.70.046618

[87] R. Correa, J. Meireles, J. Huguenin, D. Caetano, and L. daSilva, "Fractal structure of digital speckle patterns produced by rough surfaces," *Physica A: Statistical Mechanics and its Applications*, vol. 392, no. 4, pp. 869 – 874, 2013. [Online]. Available: http://www.sciencedirect.com/science/article/pii/S0378437112009193

[88] B. Kaye, *A random walk through fractal dimensions*. VCH, 1989. [Online]. Available: https://books.google.nl/books?id=xHYpAQAAMAAJ

[89] M. Varma and R. Garg, "Locally invariant fractal features for statistical texture classification," *Proceedings of the IEEE International Conference on Computer Vision*, 2007. [Online]. Available: http://ieeexplore.ieee.org/xpls/abs_all.jsp?arnumber=4408876

[90] J. Feder, "The fractal dimension," in *Fractals*, ser. Physics of Solids and Liquids. Springer US, 1988, pp. 6–30. [Online]. Available: http://dx.doi.org/10.1007/978-1-4899-2124-6_2

[91] D. Schleicher, "Hausdorff dimension, its properties, and its surprises," *The American Mathematical Monthly*, pp. 1–28, 2007. [Online]. Available: http://www.jstor.org/stable/27642249

[92] B. Klinkenberg, "A review of methods used to determine the fractal dimension of linear features," *Mathematical Geology*, vol. 26, no. 1, pp. 23–46, 1994. [Online]. Available: http://dx.doi.org/10.1007/BF02065874

[93] M. Barnsley, *Fractals Everywhere*. San Diego, CA, USA: Academic Press Professional, Inc., 1988.

[94] J. Briers and S. Webster, "Quasi real-time digital version of single-exposure speckle photography for full-field monitoring of velocity or flow fields," *Optics Communications*, vol. 116, no. April, 1995. [Online]. Available: http://www.sciencedirect.com/science/article/pii/0030401895000427

[95] M. Draijer, E. Hondebrink, T. van Leeuwen, and W. Steenbergen, "Review of laser speckle contrast techniques for visualizing tissue perfusion," *Lasers in Medical Science*, vol. 24, no. 4, pp. 639–651, 2009. [Online]. Available: http://dx.doi.org/10.1007/s10103-008-0626-3

[96] P. A. Bandettini, A. Jesmanowicz, E. C. Wong, and J. S. Hyde, "Processing strategies for time-course data sets in functional mri of the human brain," *Society of Magnetic Resonance in Medicine*, vol. 30, no. 2, pp. 161–73, Aug. 1993. [Online]. Available: http://www.ncbi.nlm.nih.gov/pubmed/8366797

[97] M. Biswas, T. Ghose, S. Guha, and P. Biswas, "Fractal dimension estimation for texture images: a parallel approach," *Pattern Recognition Letters*, pp. 309–313, 1998. [Online]. Available: http://www.sciencedirect.com/science/article/pii/S0167865598000026

[98] A. K. Bisoi and J. Mishra, "On calculation of fractal dimension of images," *Pattern Recognition Letters*, vol. 22, pp. 631–637, 2001. [Online]. Available: http://www.sciencedirect.com/science/article/pii/S016786550000132X

[99] N. Sarkar and B. Chaudhuri, "An efficient differential box-counting approach to compute fractal dimension of image," *IEEE Transactions on Systems, Man and Cybernetics*, vol. 24, no. I, 1994. [Online]. Available: http://ieeexplore.ieee.org/xpls/abs_all.jsp?arnumber=259692

[100] C. Chen, J. S. DaPonte, and M. D. Fox, "Fractal feature analysis and classification in medical imaging," *IEEE Transaction on Medical Imaging*, vol. 8, pp. 133 – 142, 1989. [Online]. Available: http://ieeexplore.ieee.org/stamp/stamp.jsp?tp=&arnumber=24861&isnumber=942

[101] S. E. Charm and G. S. Kurland, *Blood flow and microcirculation.* Wiley New York, 1974. [Online]. Available: https://books.google.nl/books?id=kclqAAAAMAAJ

[102] S. J. Sherwin and H. M. Blackburn, "Three-dimensional instabilities and transition of steady and pulsatile axisymmetric stenotic flows," *Journal of Fluid Mechanics*, vol. 533, pp. 297–327, Jun. 2005. [Online]. Available: http://www.journals.cambridge.org/abstract_S0022112005004271

[103] C. G. Caro, *The Mechanics of the Circulation.* Cambridge University Press, 2012. [Online]. Available: http://books.google.nl/books?id=UY9qsam9Oi4C

[104] A. Gilman, "G proteins: transducers of receptor-generated signals," *Annual Review of Biochemistry*, vol. 56, no. 1, pp. 615–649, Aug. 1987. [Online]. Available: http://www.ncbi.nlm.nih.gov/pubmed/21894372http://www.annualreviews.org/doi/abs/10.1146/annurev.bi.56.070187.003151

[105] M. C. Michalski, V. Briard, and F. Michel, "Optical parameters of milk fat globules for laser light scattering measurements," *Physiological Measurement*, vol. 81, pp. 787–796, 2001. [Online]. Available: http://lait.dairy-journal.org/articles/lait/abs/2001/06/michalski/michalski.html

[106] M. Vegfors and L. Lindberg, "Accuracy of pulse oximetry at various haematocrits and during haemolysis in anin vitro model," *Medical Biological Engineering and Computing*, vol. 31, no. March, pp. 135–141, 1993. [Online]. Available: http://link.springer.com/article/10.1007/BF02446671

[107] T. Yoshimura, "Statistical properties of dynamic speckles," *Journal of the Optical Society of America A*, vol. 3, no. 7, pp. 1032–1054, 1986. [Online]. Available: http://www.opticsinfobase.org/josaa/fulltext.cfm?uri=josaa-3-7-1032

[108] A. B. Parthasarathy, W. J. Tom, A. Gopal, X. Zhang, and A. K. Dunn, "Robust flow measurement with multi-exposure speckle imaging," *Optics Express*, vol. 16, no. 3, pp. 1975–1989, Feb 2008. [Online]. Available: http://www.opticsexpress.org/abstract.cfm?URI=oe-16-3-1975

[109] P. Sobieszczyk and J. Beckman, "Carotid artery disease," *Circulation*, vol. 114, no. 7, pp. e244–7, Aug. 2006. [Online]. Available: http://www.ncbi.nlm.nih.gov/pubmed/16908775

[110] J. G. Terry, "Carotid arterial structure in patients with documented coronary artery disease and disease-free control subjects," *Circulation*, vol. 107, no. 8, pp. 1146–1151, Feb. 2003. [Online]. Available: http://www.ncbi.nlm.nih.gov/pubmed/12615793

[111] S. Kenjeres, "Modeling and simulation of multi-physics multi-scale transport phenomenain bio-medical applications," *Journal of Physics: Conference Series*, vol. 530, p. 012006, Aug. 2014. [Online]. Available: http://stacks.iop.org/1742-6596/530/i=1/a=012006?key=crossref.ab66c434606bc6c5f22b9f828130079c

[112] D. P. Giddens, "The role of fluid mechanics in the localization and detection of atherosclerosis," *Journal of Biomedical Engineering*, vol. 115, no. November 1993, 1993. [Online]. Available: http://biomechanical.asmedigitalcollection.asme.org/article.aspx?articleid=1399670

[113] Y. T. Chew, T. C. Chew, and H. T. Low, "Particle image velocimetry in the investigation of flow past artificial heart valves," *Annals of Biomedical Engineering*, vol. 22, no. 20, 1994. [Online]. Available: http://link.springer.com/article/10.1007/BF02368237

[114] J. Westerweel, G. E. Elsinga, and R. J. Adrian, "Particle image velocimetry for complex and turbulent flows," *Annual Review of Fluid Mechanics*, vol. 45, no. 1, pp. 409–436, Jan. 2013. [Online]. Available: http://www.annualreviews.org/doi/abs/10.1146/annurev-fluid-120710-101204?journalCode=fluid

[115] M. Raffel, C. E. Willert, S. T. Wereley, and J. Kompenhans, *Particle Image Velocimetry: A Practical Guide*, ser. Experimental Fluid Mechanics. Springer Berlin Heidelberg, 2007. [Online]. Available: http://books.google.nl/books?id=fdKd50rzfuMC

[116] J. Bassingthwaighte, L. Liebovitch, and B. West, *Fractal Physiology*, ser. American Physiological Society: The American Physiological Society methods in physiology series. American Physiological Society, 1994. [Online]. Available: http://books.google.nl/books?id=vL3zeVedDVcC

[117] A. Goldberger, "Fractal dynamics in physiology: alterations with disease and aging," *Proceedings of the National Academy of Sciences*, vol. 99, 2002. [Online]. Available: http://www.pnas.org/content/99/suppl_1/2466.short

[118] O. Carvalho, M. Benderitter, and L. Roy, "Noninvasive radiation burn diagnosis using speckle phenomenon with a fractal approach to processing," *Journal of Biomedical Optics*, vol. 15, no. 2, pp. 027 013–027 013–13, 2010. [Online]. Available: http://dx.doi.org/10.1117/1.3394261

[119] C. Lal, A. Banerjee, and N. U. Sujatha, "Role of contrast and fractality of laser speckle image in assessing flow velocity and scatterer concentration in phantom body fluids," *Journal of Biomedical Optics*, vol. 18, no. 11, pp. 111 419–111 419, 2013. [Online]. Available: http://dx.doi.org/10.1117/1.JBO.18.11.111419

[120] G. J. Noordergraaf, T. J. Dijkema, W. J. P. M. Kortsmit, W. H. a. Schilders, G. J. Scheffer, and A. Noordergraaf, "Modeling in cardiopulmonary resuscitation: Pumping the heart," *Cardiovascular Engineering*, vol. 5, no. 3, pp. 105–118, Sep. 2005. [Online]. Available: http://link.springer.com/10.1007/s10558-005-7671-3. DOI:10.1007/s10558-005-7671-3

[121] M. J. Hayes and P. R. Smith, "Artifact reduction in photoplethysmography," *Appl. Opt.*, vol. 37, no. 31, pp. 7437–7446, Nov 1998. [Online]. Available: http://ao.osa.org/abstract.cfm?URI=ao-37-31-7437. DOI:10.1364/AO.37.007437

[122] I. Korhonen and A. Yli-Hankala, "Photoplethysmography and nociception," *Acta Anaesthesiologica Scandinavica*, vol. 53, no. 8, pp. 975–985, 2009. [Online]. Available: http://dx.doi.org/10.1111/j.1399-6576.2009.02026.x. DOI:10.1111/j.1399-6576.2009.02026.x

[123] D. L. Fried, "Laser eye safety: the implications of ordinary speckle statistics and of speckled-speckle statistics," *Journal of the Optical Society of America*, vol. 71, no. 7, pp. 914–916, 1981. [Online]. Available: http://www.opticsinfobase.org/abstract.cfm?uri=josa-71-7-914

[124] K. A. ODonnell, "Speckle statistics of doubly scattered light," *Journal of the Optical Society of America*, vol. 72, no. 11, pp. 1459–1463, 1982. [Online]. Available: http://www.opticsinfobase.org/abstract.cfm?uri=josa-72-11-1459

[125] A. Papoulis and S. Pillai, *Probability, Random Variables, and Stochastic Processes*, ser. McGraw-Hill series in electrical engineering: Communications and signal processing. Tata McGraw-Hill, 2002. [Online]. Available: https://books.google.nl/books?id=g6eUoWOlcQMC

[126] D. Newman, "K distributions from doubly scattered light," *Journal of the Optical Society of America A*, vol. 2, no. 1, pp. 22–26, 1985. [Online]. Available: http://www.opticsinfobase.org/abstract.cfm?uri=josaa-2-1-22

[127] T. Yoshimura and K. Fujiwara, "Statistical properties of doubly scattered image speckle," *Journal of the Optical Society of America A*, vol. 9, no. 1, pp. 91–95, Jan 1992. [Online]. Available: http://josaa.osa.org/abstract.cfm?URI=josaa-9-1-91

[128] D. Li, D. P. Kelly, and J. T. Sheridan, "K speckle space time correlation function of doubly scattered light in an imaging system," *Journal of the Optical Society of America A*, vol. 30, no. 5, pp. 969–978, May 2013. [Online]. Available: http://josaa.osa.org/abstract.cfm?URI=josaa-30-5-969

[129] L. Dayan, P. K. Damien, and J. T. Sheridan, "Speckle suppression by doubly scattering systems," *Applied Optics*, vol. 52, no. 35, pp. 8617–8626, Dec 2013. [Online]. Available: http://ao.osa.org/abstract.cfm?URI=ao-52-35-8617

[130] L. G. Shirley and N. George, "Speckle from a cascade of two thin diffusers," *Journal of the Optical Society of America A*, vol. 6, no. 6, pp. 765–781, Jun 1989. [Online]. Available: http://josaa.osa.org/abstract.cfm?URI=josaa-6-6-765

[131] D. Briers, D. D. Duncan, E. Hirst, S. J. Kirkpatrick, M. Larsson, W. Steenbergen, T. Stromberg, and O. B. Thompson, "Laser speckle contrast imaging: theoretical and practical limitations," *Journal of Biomedical Optics*, vol. 18, no. 6, p. 66018, 2013. [Online]. Available: http://dx.doi.org/10.1117/1.JBO.18.6.066018

[132] T. Namita, Y. Kato, and K. Shimizu, "Ct imaging of diffuse medium by time-resolved measurement of backscattered light," *Applied Optics*, 2009. [Online]. Available: http://www.osapublishing.org/vjbo/fulltext.cfm?uri=ao-48-10-D208

[133] H. W. Lee, J. W. Lee, W. G. Jung, and G. K. Lee, "The periodic moving average filter for removing motion artifacts from ppg signals," *International Journal of Control, Automation, and Systems*, vol. 5, no. 6, pp. 701–706, 2007. [Online]. Available: http://www.ijcas.com/admin/paper/files/ijcas_v5_n6_pp.701-706.pdf

[134] K. V. Madhav, M. R. Ram, E. H. Krishna, N. R. Komalla, and K. A. Reddy, "Robust extraction of respiratory activity from ppg signals using modified mspca," *IEEE Transaction on Instrumentation and Measurement*, vol. 62, no. 5, pp. 1094–1106, May 2013. [Online]. Available: http://ieeexplore.ieee.org/lpdocs/epic03/wrapper.htm?arnumber=6412799

Acknowledgments

Sometimes our light goes out but is blown into flame by another human being. Each of us owes deepest thanks to those who have rekindled this light.

Albert Einstein

By reaching this stage of the Ph.D. journey, several people have been a part of it, which I would like to acknowledge. Although my name may be alone on the front cover of this thesis, I am not definitely the only contributor and this would have not been possible without help of many who I can briefly address here.

First of all, I would like to express my special appreciation to my supervisor Prof. H.P. Urbach for his guidance, insightful discussions and allowing me to grow as an independent research scientist. My sincere gratitude to my daily supervisor, Dr. N. Bhattacharya, for her open-door attitude whenever I needed. You have been a tremendous adviser on both professional and personal level. Thank you both of you for the opportunity to work together on such an interesting project and for all your encouragement during these years.

I would also like to thank all the committee members, for your interest in this research and reviews of my thesis. Thank you for your time and availability.

During this project, we had many periodic project meetings and I would like to thank all people for being continuously present and involved in the project progress. Thank you for all your input, influence and expert knowledge which have helped me bring this project to its currents state. I have learned a lot from our meetings and discussions which always helped me consider different viewpoints in my research, and ultimately led to the project to grow. My special thanks to Marco, Sjoerd, Luca from LifeTec Group. You never stop supporting this project and your support made it possible to cope with the upcoming challenges. Some of the work has been done with Ralph Wijshoff. Thank you for the time that we worked together and specially for supporting each other labs with the experimental components.

I also would like to thank Cristian Presura as an initiator of this project. Thank you for all your inputs and considerable amount of time that you have spent. It

is always a learning opportunity working with you and thanks for being always so enthusiastic and not delaying experimenting any new ideas.

I would like to extend my sincerest thanks and appreciation to the Optica support team, Yvonne van Aalst, Roland Horsten, Rob Pols and Thim Zuidwijk. It is hard to express it in words, but there is no doubt that this project would not be possible without your support. I can say from my personal experience how simple documents and bureaucracy can sometimes be a big deal in life and how peaceful a day can become by having Yvonne around. I feel a debt of gratitude for all the help and effort you have done for me. An experiment could not be realized more efficient without Thim. He always surprised me by having an immediate solution when we have been struggling to find a missing component in our setup. Thank to Rob, for turning a simple drawing with a short discussion over a setup, to a masterpiece which has the precision and robustness which you could only wish for. Roland, all the respect from the first moment I stepped into this group.

I would like to thank all the people with our group, for making this time as enjoyable as could be imagined. Prof. Joseph Braat for enjoyable discussion and helpful inputs. Thanks to Dr. Florian Bociort for all the encouragement and learning opportunities. I also would like to acknowledge Dr. Aurele Adam, Prof. Paul Planken and Dr. Silvania Pereira for their help during these years.

A special Thanks to Peter Somers and Willeke, for all the great times we had inside and outside Optica. A big thank you to Peter for all the amazing discussion and openly sharing his knowledge and experiences which can not be experienced from books. Not to forget the effort of double checking the translation of my summary.

I would like to thank all my former and current colleagues at Optica over these years for their good company and wonderful time: Wouter, Sven, Alberto, Nishant, Nitish, Gopika, Man , Gopakumar, Kate, Thomas, Omar, Alessandro, Lei, Andreas, Adonis, Luca, Sarathi, Jeffrey, Wim, Vincent, Joost, Diego, Priya, Fellipe, Anna, Marco, Zhe, Ying, Hamed, Yifeng, Danniel, Matthias, Lisa and all others. I would also like to thank the two dedicated master students whom I worked with, Gyllion and Kevin, for the interesting discussions and for their contributions to several parts of my research. There has been a lot of interactions with Mounir during this project, thank for being so supportive in all the times. Special thanks to Pascal for all the support in the first years. I am happy to have found a good friend, although we have been introduced with a 'tragedy' of having my laptop stolen. Thank to you, I have now my story of shaking hands with a police officer in my office.

I would like to leave a special thank you to Janny and Ted, for their friendship during this period and for their decisive support in integrating myself in the Dutch society.

I would like to thank to my family for your unconditional caring and support. In-spite of the challenging and stressful times they have been going through in the last years, they have always been there to support me. A very special Thank you

to my mom, for giving me the confidence to always fly. Mom, you lead me here and I never can express how grateful I am for all the efforts that you have faced on my behalf.

Finally, my appreciation to my love of my life, Jacek. You have been always present and supportive in striving towards my goals. Thank you for being an inspiration and showing me how challenges can be overcome, no matter under which circumstances. Thank you for your unremitting support and for making each day memorable which keeps reminding me why I need to keep on going. I am look forward to continuing our lifelong journey.

Biography

About Author

Mahsa Nemati was born in Ahvaz, Iran in 1985. After completing her high school, she moved to Budapest, Hungary. In 2008 she graduated with a BS.c degree in Electrical Engineering from Budapest University of Technology and Economics, with honors. She moved to the Netherlands where she followed her studies at Delft University of Technology. In 2010, she graduated with MS.c degree in Biomedical Engineering with biomedical instrumentation major. Her master thesis was followed by an internship in Philips Applied Technology in Eindhoven. This project was focused on a wearable optical sensor design for heart beat detection. This work has been integrated into market as the Mio Alpha sport watch. In 2011, she joined the Optics Research Group in Delft, where she further explored the application of portable health monitoring devices in her PhD research. This project was founded by IOP and STW and has been in collaboration with Philips research, TU/E and LifeTec Group in Eindhoven. Her research has been presented at several international conferences and published in several articles (press release) and peer reviewed journals.

List of Publications

Journal papers

- **M.Nemati**, H. P. Urbach, N. Bhattacharya *Laser speckle and double frequency*, (manuscript in preparation).
- **M.Nemati**, H. P. Urbach, N. Bhattacharya *Studying pulsatile flow with fractal analysis of speckle images*, Sensors and Transducers Journal **197** 52-57 (2016).
- **M.Nemati**, S.Kenjeres, H. P. Urbach, N. Bhattacharya *Fractality of pulsatile flow in speckle images*, Journal of Applied Physics **119** 174902 (2016).
- **M.Nemati**, G.B.Loozen, N. van der Wekken, G. van de Belt, H. P. Urbach, N. Bhattacharya, S.Kenjeres *Application of full field optical studies for pulsatile flow in a carotid artery phantom*, Biomedical Optics Express **6**, 40317-4050 (2015).

- **M.Nemati**, C. N. Presura, H. P. Urbach, and N. Bhattacharya *Dynamic light scattering from pulsatile flow in the presence of induced motion artifacts*, Biomedical Optics Express **5**, 145-2156 (2014).

- **M. Nemati**, L. G. Paroni, N. Bhattacharya and H. P. Urbach *Fluid pulsation detection in presence of induced motion artifacts using speckle techniques*, AIP Confrence Proceeding (2014).

- **M.Nemati**, R.W. C. G. R.Wijshoff, J. M. a. Stijnen, S. van Tuijl, J.W. M. Bergmans, N. Bhattacharya, and H. P. Urbach *Laser-speckle-based detection of fluid pulsation in the presence of motion artifacts: in vitro and in vivo study*, Optics Letters **38**, 5334-5337 (2013).
  Paper has been selected by editors and being also published in the special feature of OSA's Optics InfoBase, Virtual Journal for Biomedical Optics (VJBO).

- **M. Nemati**, L. Wei, M. G. Zeitouny, M. Stijnen, S. van Tuijl, N. Bhattacharya, and H. P. Urbach *Laser speckle analysis of flow in presence of static scatterers*,Proceeding of SPIE (2012).

Conferences

- **M. Nemati**, N. Bhattacharya, H. P. Urbach *Monitoring Pulsatile Flow Using Dynamic Speckle Patterns*, Measuring by Light, Rijswijk, The Netherlands 2015 (Oral Presentation).

- **M. Nemati**, G B Loozen, N van der Wekken, H P Urbach, S Kenjeres, N. Bhattacharya *Quantitative monitoring of pulsatile flow using of particle image velocimtery and laser speckle*, The 10th Pacific Symposium on Flow Visualization and Image Processing, Naples, Italy , june 2015 (Oral Presentation).

- **M. Nemati**, N. Bhattacharya, H. P. Urbach, 7th International Graduate summer school - Biophotonics '15, (Poster Presentation).

- **M. Nemati**, N. Bhattacharya, H. P. Urbach *Heart rate monitoring in presence of induced motion artifacts*,PhotoMechanics, Delft, The Netherlands 2015 (Oral Presentation).

- **M. Nemati**, N. Bhattacharya, H. P. Urbach *Laser speckle study of pulsatile flow in presence of induced motion artifact*, Frontiers in Optics/Laser Science Conference (OSA), Tucson, Arizona, USA 2014 (Oral Presentation).

- **M. Nemati**, N. Bhattacharya, H. P. Urbach, R. Wijshoff, M. Mischi, R. Aarts, M. Stijnen, L. Paroni *Hemodynamics by Interferometric Photonics*, IOP Photonic Devices symposium, Amsterdam, The Netherlands 2014 (Poster presentation).

- **M. Nemati**, L. G. Paroni, N. Bhattacharya and H. P. Urbach *Fluid pulsation detection in presence of induced motion artifacts using speckle techniques*,International Conference on Vibration Measurements by Laser Techniques (AIVELA),Ancona, Italy 2014 (Oral Presentation).

- **M. Nemati**, N. Bhattacharya, H. P. Urbach *Laser speckle based pulsation rate measurement in presence of induced motion artifacts*, Physics FOM Veldhoven Conference, Veldhoven, The Netherlands 2014 (Poster presentation).
- **M. Nemati**, N. Bhattacharya, H. P. Urbach, R. Wijshoff, M. Mischi, R. Aarts, M. Stijnen, L. Paroni *Hemodynamics by Interferometric Photonics*, IOP Photonic Devices symposium, Leiden, The Netherlands 2013 (Poster presentation).
- **M. Nemati**, L. Wei, M. G. Zeitouny, M. Stijnen, S. van Tuijl, N. Bhattacharya, and H. P. Urbach *Laser speckle analysis of flow in presence of static scatterers*, V International Conference on Speckle Metrology, Vigo, Spain 2012 (Oral presentation).